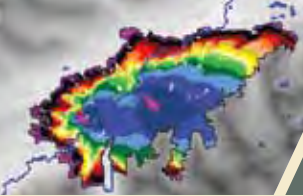




Natural Resources  
Canada

Ressources naturelles  
Canada



# Development and Structure of Prometheus: the Canadian Wildland Fire Growth Simulation Model



C. Tymstra, R.W. Bryce, B.M. Wotton, S.W. Taylor, and O.B. Armitage

Information Report NOR-X-417

Northern Forestry Centre

Canadian Forest Service

Canada 

---

The Northern Forestry Centre is one of five centres of the Canadian Forest Service, which has its headquarters in Ottawa, Ontario. This centre undertakes the regional delivery of national projects.

The Canadian Forest Service's main objective is research in support of improved forest management for economic, social, and environmental benefits to all Canadians.

Le Centre de foresterie du Nord constitue l'un des cinq établissements du Service canadien des forêts, dont l'administration centrale est à Ottawa (Ontario). Le Centre entreprend la réalisation régionale de projets nationaux.

Le Service canadien des forêts s'intéresse surtout à la recherche en vue d'améliorer l'aménagement forestier afin que tous les Canadiens puissent en profiter aux points de vue économique, social et environnemental.

Cover images: Jackpine fire in Willmore Wilderness Park, Alberta, 2006 and Prometheus simulation of the fire. Courtesy of Cordy Tymstra, Alberta Sustainable Resource Development.

Information contained in this publication or product may be reproduced, in part or in whole, and by any means, for personal or public non-commercial purposes, without charge or further permission, unless otherwise specified.

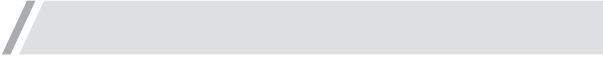
You are asked to:

- Exercise due diligence in ensuring the accuracy of the materials reproduced;
- Indicate both the complete title of the materials reproduced, as well as the author organization; and
- Indicate that the reproduction is a copy of an official work that is published by the Government of Canada and that the reproduction has not been produced in affiliation with, or with the endorsement of the Government of Canada.

Commercial reproduction and distribution is prohibited except with written permission from the Government of Canada's copyright administrator, Public Works and Government Services of Canada (PWGSC). For more information, please contact PWGSC at: 613-996-6886 or at: [droitdauteur.copyright@tpwgs-pwgsc.gc.ca](mailto:droitdauteur.copyright@tpwgs-pwgsc.gc.ca).

**DISCLAIMER**

Her Majesty is not responsible for the accuracy or completeness of the information contained in the reproduced material. Her Majesty shall at all times be indemnified and held harmless against any and all claims whatsoever arising out of negligence or other fault in the use of the information contained in this publication or product.



# DEVELOPMENT AND STRUCTURE OF PROMETHEUS: THE CANADIAN WILDLAND FIRE GROWTH SIMULATION MODEL

C. Tymstra<sup>1</sup>, R.W. Bryce<sup>2</sup>, B.M. Wotton<sup>3</sup>, S.W. Taylor<sup>4</sup>, and O.B. Armitage<sup>5</sup>

INFORMATION REPORT NOR-X-417

Canadian Forest Service  
Northern Forestry Centre  
2010

---

<sup>1</sup>Wildfire Science Unit, Forestry Division, Alberta Sustainable Resource Development, 9th Floor, 9920–108 Street, Edmonton, AB T5K 2M4

<sup>2</sup>Heartland Software Solutions Inc., Box 333, Austin, MB R0H 0C0

<sup>3</sup>Natural Resources Canada, Canadian Forest Service, Great Lakes Forestry Centre, 1219 Queen Street East, Sault Ste. Marie, ON P6A 2E5

<sup>4</sup>Natural Resources Canada, Canadian Forest Service, Pacific Forestry Centre, 506 West Burnside Road, Victoria, BC V8Z 1M5

<sup>5</sup>Ember Research Services Ltd., 4345 Northridge Crescent, Victoria, BC V8Z 4Z4

© Her Majesty the Queen in Right of Canada, 2010

Natural Resources Canada  
Canadian Forest Service  
Northern Forestry Centre  
5320-122 Street  
Edmonton, Alberta T6H 3S5

Catalogue No. Fo134-10/2010E-PDF  
ISBN 978-1-100-14674-4  
ISSN 0831-8247

For an electronic version of this report, visit the Canadian Forest Service Bookstore at <http://bookstore.cfs.nrcan.gc.ca/>

TTY: 613-996-4397 (Teletype for the hearing-impaired)  
ATS: 613-996-4397 (appareil de télécommunication pour sourds)

### **Library and Archives Canada Cataloguing in Publication**

Development and structure of Prometheus [electronic resource] : the Canadian Wildland Fire Growth Simulation Model / C. Tymstra ... [et al.].

(Information report ; NOR-X-417)

Type of computer file: Electronic monograph in PDF format.

Issued also in printed form.

Includes bibliographical references.

ISBN 978-1-100-14674-4  
Cat. no.: Fo134-10/2010E-PDF

1. Prometheus (Computer file).
2. Wildfires--Canada--Computer simulation.
3. Wildfire forecasting--Canada--Computer programs.
  - I. Tymstra, Cordy, 1955-
  - II. Northern Forestry Centre (Canada)
  - III. Series: Information report (Northern Forestry Centre (Canada): Online) NOR-X-417

SD421.36 D47 2010

634.9'618097101

C2010-980030-3

---

## DEDICATION

---

This publication is a tribute to the memory of Bernie Todd, who was a dedicated member of the Canadian fire research community for over 30 years and a driving force in the development of Prometheus. Bernie's tenacity, commitment to excellence, and passion for fire research will be fondly remembered.



---

## ABSTRACT

---

Accurate, high-resolution fire behavior prediction is a critical component of fire management decision-making before and during fires. Prometheus is a deterministic fire growth simulation model that was developed to help fire managers to understand the probable consequences of their decisions. It uses spatial input data on topography (slope, aspect, and elevation), fuel types, and weather to simulate fire growth by applying Huygens' principle of wave propagation to the rate-of-spread predictions from the Canadian Forest Fire Behavior Prediction System of the Canadian Forest Fire Danger Rating System. This approach produces detailed fire perimeters at user-specified display time step intervals. Each active vertex along the perimeter has corresponding fire behavior output. Exported fire perimeters are compatible with geographic information systems. Additionally, three interpolation techniques are available to produce optional raster fire behavior outputs. This report documents the structure of the Prometheus model and an assessment of its performance. The report includes a general discussion of approaches to the modeling of fire growth simulation and explains the vector propagation technique used in Prometheus. The limitations and assumptions of applying the model, as well as the most appropriate directions for future research, are also discussed.

---

## RÉSUMÉ

---

La prévision précise et à haute résolution du comportement des feux de forêt est un élément essentiel du processus décisionnel de gestion avant et pendant les incendies. Le modèle de simulation déterministe de la croissance des feux Prometheus a été élaboré pour aider les gestionnaires des incendies à comprendre les conséquences probables de leurs décisions. À l'aide de données spatiales sur la topographie (pente, aspect et élévation), les types de combustible et les conditions météorologiques, le modèle simule la croissance des feux au moyen du principe de Huygens de propagation des ondes aux prévisions de la vitesse de propagation, obtenues à l'aide de la Méthode canadienne de prévision du comportement des incendies de forêt (Méthode canadienne d'évaluation des dangers d'incendie de forêt). Cette approche permet d'obtenir des périmètres d'incendie détaillés selon les intervalles de temps sélectionnés par l'utilisateur. À chaque point actif le long du périmètre correspond un comportement du feu. Les données exportées relatives aux périmètres d'incendie sont compatibles avec les systèmes d'information géographique. De plus, on dispose de trois techniques d'interpolation pour produire des données de trame optionnelles sur le comportement des

incendies. Le présent document explique la structure du modèle Prometheus et évalue son rendement. Le rapport comprend également un examen général des méthodes de modélisation de la croissance des incendies et précise la technique de propagation du vecteur utilisée dans le modèle Prometheus. On y analyse aussi les limites et les hypothèses touchant le modèle, de même que les avenues de recherche les plus appropriées.

---

# CONTENTS

---

|                                                                                         |    |
|-----------------------------------------------------------------------------------------|----|
| INTRODUCTION . . . . .                                                                  | 1  |
| DEVELOPMENT OF FIRE GROWTH SIMULATION MODELING . . . . .                                | 3  |
| Fire Growth Simulation under Homogeneous Conditions . . . . .                           | 3  |
| Fire Growth Simulation under Heterogeneous Conditions . . . . .                         | 6  |
| Cellular Propagation . . . . .                                                          | 6  |
| Wave Propagation . . . . .                                                              | 11 |
| STRUCTURE OF PROMETHEUS: THE CANADIAN WILDLAND FIRE GROWTH<br>SIMULATION MODEL. . . . . | 15 |
| Prometheus Project File . . . . .                                                       | 15 |
| Fire Growth Simulation Scenarios . . . . .                                              | 15 |
| Model Structure. . . . .                                                                | 16 |
| LANDSCAPE DATA . . . . .                                                                | 18 |
| FBP Fuel-Type Grids and Lookup Tables. . . . .                                          | 18 |
| FBP Fuel-Type Modifier Grids. . . . .                                                   | 20 |
| Green-up and Grass Curing . . . . .                                                     | 20 |
| Percent Conifer and Percent Dead Fir . . . . .                                          | 20 |
| Crown Base Height . . . . .                                                             | 20 |
| Landscape and Polygon Fuel-Type Patches and Layering . . . . .                          | 22 |
| Slope, Aspect, and Elevation Grids . . . . .                                            | 22 |
| Geographic Vector Data . . . . .                                                        | 22 |
| WEATHER AND FWI SYSTEM DATA . . . . .                                                   | 22 |
| Weather Stations . . . . .                                                              | 22 |
| Hourly Weather Streams . . . . .                                                        | 23 |
| Interpolating Diurnal Hourly Temperature and Wind Speed. . . . .                        | 24 |
| Calculating Hourly <i>FFMC</i> and <i>ISI</i> . . . . .                                 | 26 |
| Creating Weather Streams. . . . .                                                       | 28 |
| Hourly Weather Data with FWI System Values . . . . .                                    | 28 |
| Hourly Weather Data without FWI System Values . . . . .                                 | 29 |
| Daily Weather Data. . . . .                                                             | 29 |
| Weather Grids and Patches . . . . .                                                     | 29 |
| Temporal Interpolation of Weather and FWI System Values . . . . .                       | 30 |
| Spatial Interpolation . . . . .                                                         | 32 |
| FIRE GROWTH SIMULATION . . . . .                                                        | 33 |
| Scenario Settings and Parameters . . . . .                                              | 33 |
| Buildup Effect . . . . .                                                                | 33 |
| Terrain Effect. . . . .                                                                 | 33 |

|                                                                            |    |
|----------------------------------------------------------------------------|----|
| <i>FMC</i> Override . . . . .                                              | 33 |
| FBP System Equation Parameters . . . . .                                   | 34 |
| Fire Growth at the Landscape Extent. . . . .                               | 34 |
| Daily Burning Period . . . . .                                             | 34 |
| Spatial and Temporal Resolution. . . . .                                   | 34 |
| Fire Initiation . . . . .                                                  | 34 |
| Point Ignition. . . . .                                                    | 35 |
| Line Ignition . . . . .                                                    | 36 |
| Polygon Ignition . . . . .                                                 | 36 |
| Fire Behavior at Vertices and Fire Statistics . . . . .                    | 36 |
| Acceleration and Use of $ROS_r$ . . . . .                                  | 36 |
| Fire Perimeter Behavior and Management . . . . .                           | 37 |
| Propagation of the Fire Perimeter . . . . .                                | 37 |
| Two-dimensional Transformations . . . . .                                  | 38 |
| Transformations for Sloping Terrain . . . . .                              | 39 |
| Smoothing the Perimeter . . . . .                                          | 40 |
| Perimeter Adjustment for Fuel Breaks and Landscape<br>Boundaries . . . . . | 40 |
| Gridded Fuel Breaks . . . . .                                              | 41 |
| Vector Fuel Breaks. . . . .                                                | 41 |
| Breaching of Nonfuel Areas . . . . .                                       | 42 |
| Polygon Untangling and Rationalization . . . . .                           | 45 |
| Polygon Intersections and Unions . . . . .                                 | 46 |
| Rediscretization of the Fire Perimeter . . . . .                           | 47 |
| Adding Vertices . . . . .                                                  | 47 |
| Inter-vertex Weighted Distance Threshold. . . . .                          | 47 |
| Vertex Fire Behavior and Fire Polygon Statistics . . . . .                 | 49 |
| FIRE GROWTH SIMULATION OUTPUTS. . . . .                                    | 49 |
| Statistics View . . . . .                                                  | 49 |
| Map View. . . . .                                                          | 49 |
| Vector Output . . . . .                                                    | 51 |
| Raster Output . . . . .                                                    | 51 |
| Nearest Vertex to Center of Grid Cell . . . . .                            | 52 |
| Inverse Distance Weighting . . . . .                                       | 52 |
| Voronoi Area Weighting . . . . .                                           | 53 |
| MODEL VALIDATION, LIMITATIONS, AND CALIBRATION . . . . .                   | 54 |
| Validation . . . . .                                                       | 54 |
| Prometheus Tester Suite . . . . .                                          | 54 |
| Case Studies. . . . .                                                      | 55 |
| Limitations and Assumptions. . . . .                                       | 55 |
| Model Error . . . . .                                                      | 55 |
| User Error . . . . .                                                       | 56 |

|                            |    |
|----------------------------|----|
| Data Error . . . . .       | 56 |
| Calibration . . . . .      | 58 |
| CONCLUSIONS . . . . .      | 59 |
| ACKNOWLEDGMENTS . . . . .  | 60 |
| LITERATURE CITED . . . . . | 61 |

---

## APPENDIXES

---

|                                                                              |    |
|------------------------------------------------------------------------------|----|
| 1. LIST OF SYMBOLS . . . . .                                                 | 67 |
| 2. PROMETHEUS CASE STUDY: SHARPSAND PRESCRIBED<br>BURN (2007) . . . . .      | 73 |
| 3. ORDER AND SET OF PROMETHEUS FIRE GROWTH<br>SIMULATION OPERATIONS. . . . . | 83 |

---

## FIGURES

---

|                                                                                                                                                                                     |    |
|-------------------------------------------------------------------------------------------------------------------------------------------------------------------------------------|----|
| 1. Dimensions for a simple elliptical fire growth model. . . . .                                                                                                                    | 4  |
| 2. Elliptical fire spread. . . . .                                                                                                                                                  | 4  |
| 3. Four geometric shapes that have been used to model fire growth<br>in homogenous environments. . . . .                                                                            | 5  |
| 4. Adjacency templates for symmetric 8-point, 16-point, and<br>32-point cellular automata models. . . . .                                                                           | 6  |
| 5. Adjacency templates for asymmetric 8-2-4 and 8-12-8 cellular<br>automata models. . . . .                                                                                         | 7  |
| 6. Fire growth in three symmetric cellular automata models layered<br>over the simple elliptical fire growth model, according to length-to-<br>breadth ratio. . . . .               | 8  |
| 7. An eight-point cellular automata method to calculate directional<br>rate of spread. . . . .                                                                                      | 8  |
| 8. Propagation of light waves, as proposed by Huygens (1912/1962). . . . .                                                                                                          | 11 |
| 9. Formation of a new wave front using Huygens' principle. . . . .                                                                                                                  | 12 |
| 10. Application of Huygens' principle to simulate fire growth. . . . .                                                                                                              | 12 |
| 11. Propagation of an elliptical fire from an ignition point with a<br>uniform wind speed in the $x$ direction ( $\theta = 0$ ), as described by<br>Anderson et al. (1982). . . . . | 13 |
| 12. Prometheus Common Object Model (COM) architecture. . . . .                                                                                                                      | 17 |
| 13. Annotated example of an ASCII fuel-type grid used in<br>Prometheus. . . . .                                                                                                     | 19 |

|     |                                                                                                                                                                                                        |    |
|-----|--------------------------------------------------------------------------------------------------------------------------------------------------------------------------------------------------------|----|
| 14. | Variation in hourly Fine Fuel Moisture Code over three 24-h periods, as calculated by the Van Wagner (1977) and Lawson et al. (1996) algorithms, with rain in the afternoon of the second day. . . . . | 27 |
| 15. | Variation in hourly Fine Fuel Moisture Code over two 24-h periods, as calculated by the Van Wagner (1977) and Lawson et al. (1996) algorithms in the absence of rain. . . . .                          | 28 |
| 16. | Effects of temporal (subhourly) interpolation on hourly Fine Fuel Moisture Code ( <i>FFMC</i> ) values. . . . .                                                                                        | 31 |
| 17. | Simulation of ignition in Prometheus: (a) Ignition from a pseudo-point. (b) Ignition from a pseudo-line. (c) Ignition from a polygon. . . . .                                                          | 35 |
| 18. | Formation of a new fire perimeter using the tangential envelope of the theoretical firelets projected from vertices along the existing fire perimeter. . . . .                                         | 39 |
| 19. | Integration of a fire perimeter defined by $n$ vertices and a fuel break in Prometheus. . . . .                                                                                                        | 42 |
| 20. | Breaching a vector fuel break. . . . .                                                                                                                                                                 | 44 |
| 21. | Progression of steps during the breaching of a fuel break. . . . .                                                                                                                                     | 44 |
| 22. | Untangling of a fire perimeter. . . . .                                                                                                                                                                | 45 |
| 23. | Intersection of two fires associated with different ignitions. . . . .                                                                                                                                 | 46 |
| 24. | Interior angle $\beta_j^i$ of the fire front at vertex $P_j^i$ , defined by three vertices. . . . .                                                                                                    | 47 |
| 25. | Relationship between the maximum allowable distance between $L_j^i/L_x$ neighboring vertices and the threshold angle $\beta_j^i$ . . . . .                                                             | 48 |
| 26. | Thirty-five-minute simulation output in the Prometheus Map View using a distance resolution of one grid cell (25 m) and a display interval of 5 min. . . . .                                           | 50 |
| 27. | Propagation of a fire perimeter over three time steps. . . . .                                                                                                                                         | 52 |
| 28. | Interpolation of fire characteristics associated with the vertices along the fire perimeters to a grid cell. . . . .                                                                                   | 52 |

---

## TABLES

---

|     |                                                                                                                           |    |
|-----|---------------------------------------------------------------------------------------------------------------------------|----|
| 1.  | Fuel types in the Canadian Forest Fire Behavior Prediction System . . . . .                                               | 19 |
| 2.  | Canadian Forest Fire Behavior Prediction System fuel-type parameters that can be modified for use in Prometheus . . . . . | 21 |
| 3.  | Example of an hourly weather stream exported from Prometheus, with header information . . . . .                           | 23 |
| 4.  | User-tunable parameters for temperature for forecasting diurnal weather conditions . . . . .                              | 25 |
| 5.  | Example of an input hourly weather stream (over 3 h) with the calculated fuel moisture codes . . . . .                    | 29 |
| 6.  | Example of an input daily weather stream (3 days) . . . . .                                                               | 30 |
| 7.  | Fire Behavior Prediction Calculator and FireEngine Calculator outputs . . . . .                                           | 51 |
| 8.  | Area and perimeter calculations for the 2001 Dogrib fire. . . . .                                                         | 57 |
| 9.  | Area and perimeter calculations for the 2004 Myers Lake fire . . . . .                                                    | 58 |
| 10. | Area and perimeter calculations for the 2006 Willmore fire. . . . .                                                       | 58 |



---

## INTRODUCTION

---

*The ultimate dream of forest fire control officers is to be able to predict for any set of conditions how fast a fire will spread and how much manpower and equipment would be needed for control at any time after ignition.*

—Van Wagner (1963)

The development of contemporary fire behavior prediction systems, including the Canadian Forest Fire Behavior Prediction (FBP) System (Forestry Canada Fire Danger Group 1992) and the United States Department of Agriculture (USDA) Forest Service BEHAVE Fire Modeling System (Burgan and Rothermel 1984), has been motivated by the need to accurately predict the rate of spread, intensity, area, and perimeter growth of wildland fires—information that is needed to support a wide variety of fire management decisions. The FBP System, for example, comprises a series of mathematical equations relating fire characteristics to wind, fuel moisture, and topographic conditions for 16 benchmark fuel (vegetation) types. This system can be used to predict the behavior, during a single burning period, of a fire spreading from a single point or line, assuming that fuels are uniform and continuous, that topography is simple and homogeneous, and that wind is constant and unidirectional. Although the FBP System constitutes an important foundation, forecasting fire behavior at many points along the perimeter of a large fire burning across a landscape composed of complex fuels and topography and predicting the fire's ultimate spread over periods of many hours or days are formidable computational tasks beyond the scope of the FBP System and other contemporary fire behavior models.

In the 1970s, researchers began to apply computer simulation techniques to the modeling of fire growth at a landscape scale (e.g., Kourtz and O'Regan 1971). Since that time, developments in mathematics and in fire behavior prediction have resulted in more realistic fire growth simulation models, while the

ready availability of spatial fuel and topographic databases and advances in computing have made the use of such models operationally feasible. In 1999, the Prometheus project was initiated with the goal of developing a state-of-the-art, deterministic fire growth simulation model based on the FBP System and the wave propagation equations developed by Richards (1990, 1993, 1995, 1999), thus allowing for operational and strategic assessments of spatial fire behavior potential in Canadian fuel complexes. The project was named for a Greek god whose name means "forethought" (Cotterell 1986).

The Prometheus project (Prometheus Project Steering Committee 1999) had the following objectives:

- to review and evaluate existing models;
- to use and enhance key features from a number of existing models in the development of a spatially explicit wave propagation fire growth model to simulate fire spread over a landscape on an hourly or daily basis;
- to demonstrate the application of the fire growth model to predict, in real time, the growth of escaped fires (for operational purposes);
- to strategically apply the fire growth model to determine the potential threat that an individual wildfire, or multiple wildfires, might pose to selected values at risk and also to determine the effectiveness of possible mitigative strategies such as fuel management; and
- to ensure that the fire growth model would function as a stand-alone application that could be easily used and integrated with other applications.

The project was guided by the Prometheus Project Steering Committee,<sup>1</sup> which recognized the importance of developing a stand-alone model with a highly interactive graphical user

---

<sup>1</sup>Original members and their affiliations at that time included Don Harrison, Cordy Tymstra, and Karl Peck, Alberta Land and Forest Service; Kelvin Hirsch and Bernie Todd, Canadian Forest Service; Gwynfor Richards, Brandon University; and Robert Bryce, RamSoft Systems Ltd.

interface and of offering users extensive flexibility to modify both input parameters and output format. An integrated, multidisciplinary team of researchers and managers from governments, universities, and the private sector began the software engineering of Prometheus in February 2000. This broad-based approach ensured consideration of other potential applications of the model, such as modeling of biodiversity, timber supply, carbon budgets, emissions, and landscape disturbance, and allowed increased understanding of the ecological function of fire at the stand and landscape levels.

Prometheus integrates fire science, mathematics, and computer software engineering. The FBP System is used to predict the physical characteristics of a wildfire at many points around the fire perimeter, including the underlying rates of spread for the spatial simulation of fire-front propagation. Wave propagation equations provide a mathematically tractable approach to simulate the complex geometry of an expanding fire perimeter over a long period of time in a heterogeneous environment. Computer programming and simulation modeling allow the model to be implemented at high spatial and temporal resolution through the performance and management of millions of calculations.

In May 2002, version 1.0 of the Prometheus model was released, and the software was used operationally for the first time to provide fire management decision support for the 248 243 ha House River fire in Alberta. This classic boreal wind-driven fire started on 17 May 2002 and became the second-largest fire in Alberta since 1961 (Tymstra et al. 2005). The House River fire provided an opportunity to evaluate the model and its limitations in an operational setting. This evaluation resulted in the addition of new functionalities, such as the ability to specify burn periods, export simulated data for GIS systems, and import ignitions in different cartographic projections.

Since the 2002 House River fire, the Prometheus model has been used for many other applications:

- providing forensic support for wildfire investigations (by applying the model in reverse);
- fire behavior training;
- assessing the impact of climate change on area burned (Tymstra et al. 2007);
- planning prescribed burns;
- assessing the efficacy of fuel isolation and fuel conversion to reduce the area burned in protected areas (Suffling et al. 2008);
- assessing the efficacy of fuel management strategies to protect values at risk;
- evaluating fire management alternatives and costs; and
- providing spatial and temporal estimates of smoke emissions.

This report reviews the development of fire growth simulation and documents the structure of Prometheus, the Canadian Wildland Fire Growth Simulation Model, to version 5.3 (current at the time of publication in 2009). Readers will benefit from prior familiarity with, and understanding of, the structure and application of the Canadian Forest Fire Weather Index (FWI) System (Van Wagner 1987) and the Canadian FBP System (Forestry Canada Fire Danger Group 1992; Hirsch 1996; Wotton et al. 2009). Lawson and Armitage (2008) provide a thorough overview of the weather component of the Canadian Forest Fire Danger Rating System. A user's manual, a Common Object Model (COM) programmer's manual, and a data input/output standards manual for Prometheus are also available from the Prometheus website (<http://www.firegrowthmodel.com>). A list of the symbols used in this report appears in Appendix 1.

## DEVELOPMENT OF FIRE GROWTH SIMULATION MODELING

The theory, application, and limitations of previous fire growth simulation models and approaches were reviewed to inform the development of Prometheus. A number of simulation approaches have been developed to extend mathematical models of fire behavior and thus to allow projection of the growth of large wildfires burning in complex environments. However, our ability to mathematically model all aspects of fire behavior, including quantification of fire spread in complex terrain and fuel conditions, of interactions between fires and with the upper atmosphere, and of long-range ember transport, is incomplete. Therefore, several simplifications and assumptions are still necessary in fire growth simulation models.

### Fire Growth Simulation under Homogeneous Conditions

Forest fire behavior research has advanced from early quantitative observations of fire growth (Gisborne 1927; Kay 1927), observations of the rate of fire spread in field trials (Curry 1936; Curry and Fons 1938), case studies (Olsen 1941), and fire reports (Abell 1940) to mathematical modeling of fire spread and intensity informed

by laboratory work (Fons 1946; Rothermel and Anderson 1966) and field experiments (Van Wagner 1966, 1973). Mathematical models of fire spread and of spread distance over a particular time period can be used, along with assumptions about geometric shape, to predict a fire's area and perimeter under uniform conditions.

In a homogeneous environment with constant, uniform wind, the shape of a fire growing from a point ignition is assumed to be elliptical (McArthur 1966; Van Wagner 1969; Anderson 1983), whereas under conditions of no wind and topography, the shape of a fire growing from a point ignition is assumed to be circular. The simplicity of the mathematical representation of the basic ellipse and its ease of use with respect to data inputs have resulted in the general adoption of this shape for computerized fire growth simulation models. Important dimensions of the ellipse used in models of fire spread and growth are shown in Figure 1. Using a simple ellipse, Catchpole et al. (1982) calculated the rate of spread for any Cartesian angle diverging from 0° (Equation 1).

$$ROS = \frac{b_e (c_e \cos \phi + a_e)}{\sqrt{b_e^2 \cos^2 \phi + a_e^2 \sin^2 \phi}} \quad [1]$$

where  $ROS$  is the rate of spread associated with the spread direction, defined by the angle  $\theta$  (Figure 2), which can be obtained using equation 2:

$$\phi = \cos^{-1} \frac{\left( b_e \cos \theta \left( b_e^2 \cos^2 \theta + (a_e^2 - c_e^2) \sin^2 \theta \right)^{0.5} - a_e c_e \sin^2 \theta \right)}{b_e^2 \cos^2 \theta + a_e^2 \sin^2 \theta} \quad [2]$$

where  $a_e$ ,  $b_e$ , and  $c_e$  are the parameters defining the dimensions of the ellipse,  $\theta$  is the net effective spread direction measured as the Cartesian angle from the positive  $x$  axis, and  $\phi$  is the angle from the positive  $x$  axis to the vector from the center of the ellipse to the subtending circle at point  $K$  (Figure 2).

Equation 1 does not require the ignition point, or point of propagation, to coincide with either of the

two foci of the ellipse. Parameter  $c_e$ , the distance from the center of the ellipse to the ignition point (Figure 2), translates the ellipse relative to the point of ignition but does not influence the shape or size of the ellipse. As such, small differences between the point of ignition and the focus of the ellipse (which would alter  $c_e$ ) do not change the results (Richards 1993).

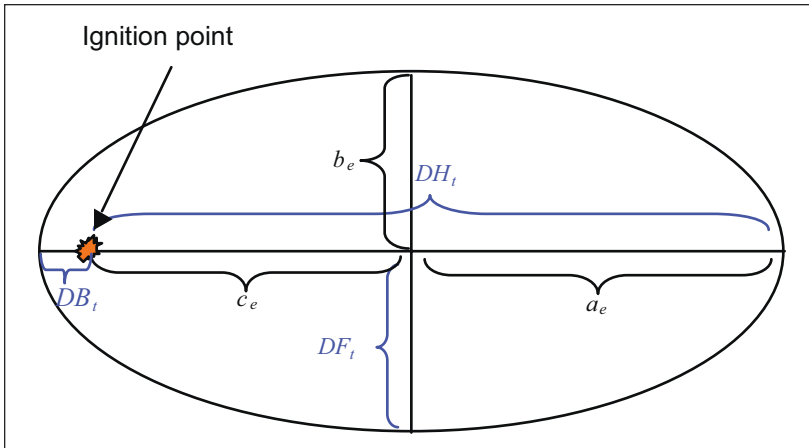


**Figure 1.** Dimensions for a simple elliptical fire growth model.  $DH_t$  = head fire spread distance at elapsed time  $t$ ,  $DB_t$  = back fire spread distance at time  $t$ ,  $DF_t$  = flank fire spread distance at time  $t$ ,  $a_e$  = forward spread distance from the center of the ellipse,  $b_e$  = flank spread distance,  $c_e$  = forward spread distance from the ignition point to the center of the ellipse.

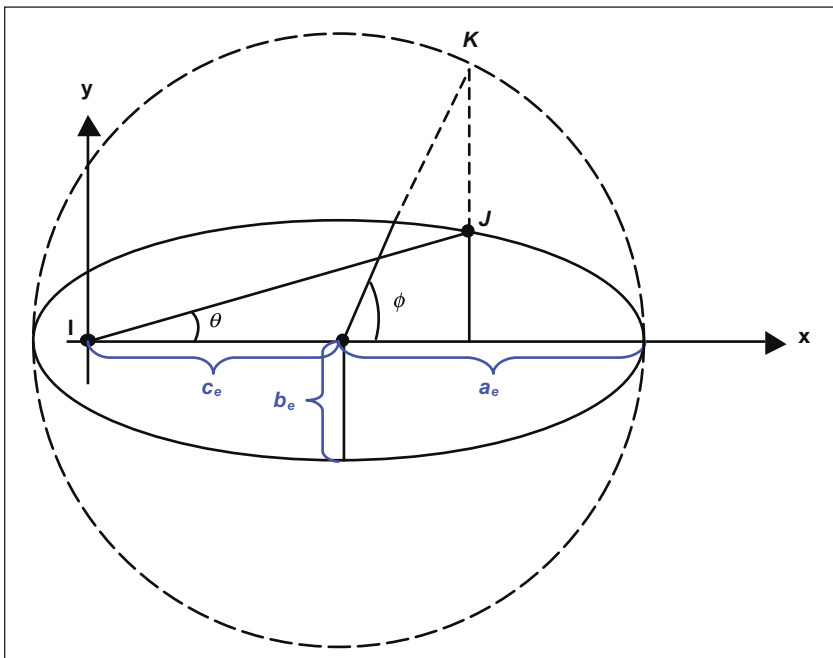


**Figure 2.** Elliptical fire spread.  $I$  = ignition point,  $a_e$  = forward spread distance from the center of the ellipse,  $b_e$  = flank spread distance,  $c_e$  = forward spread distance from the ignition point to the center of the ellipse,  $\theta$  = counterclockwise angle from the positive  $x$  axis to the spread direction vector,  $J$  = point where the spread direction vector intersects the ellipse,  $\phi$  = angle from the positive  $x$  axis to the vector from the center of the ellipse to the subtending circle at point  $K$ . Reproduced from Catchpole et al. (1982), with the permission of CSIRO Publishing.

Rather than assuming that the ignition point is one of the ellipse foci, the FBP System calculates an explicit back fire spread rate (BROS) (Forestry Canada Fire Danger Group 1992).

Other geometric shapes have been examined for their suitability to represent fires (see Figure 3). Data from experimental burns conducted in a wind tunnel (Fons 1946) were best fit with the double-ellipse model. The laboratory fires generated by Fons were constrained to a maximum width of about 45 cm, and equilibrium rates of spread were not attained. After comparing those data with field observations, however, Anderson (1983) concluded that there was little difference in final fire area, perimeter, or shape between double and simple ellipses.

Peet (1967) described the shape of low-intensity fires in western Australia's eucalyptus forest as egg-shaped (i.e., ovoid). This shape accounts for a faster flank rate of spread, whereas the double-ellipse model produces a shape that can account for a faster back rate of spread. The double ellipse, represented by two semi-ellipses, can assume an ovoid or simple elliptical shape depending on

the rate of spread associated with each semi-ellipse. Green (1983) was able to produce fires with ovoid and lemniscate (teardrop) shapes by running simulations in patchy, heterogeneous fuels. In continuous fuels, however, the shapes obtained were nearly elliptical.

Green et al. (1983) tested the adequacy of five shape representations to fit fire perimeters mapped from experimental fires in eucalyptus and grass fuels: ellipse, double ellipse, ovoid, rectangle, and output from a simulation model. All five models produced reasonable approximations of the test fire perimeters, but the ellipse produced the best results. Some of the experimental fires assumed an ovoid shape during the acceleration phase, but changed to an elliptical shape once equilibrium spread rates were attained. Nonetheless, under the influence of high winds and patchy fuels, lemniscate shapes were simulated by Green (1983) during the acceleration phase of growth. This fire shape, he noted, was common in the Australian heath fuel type.

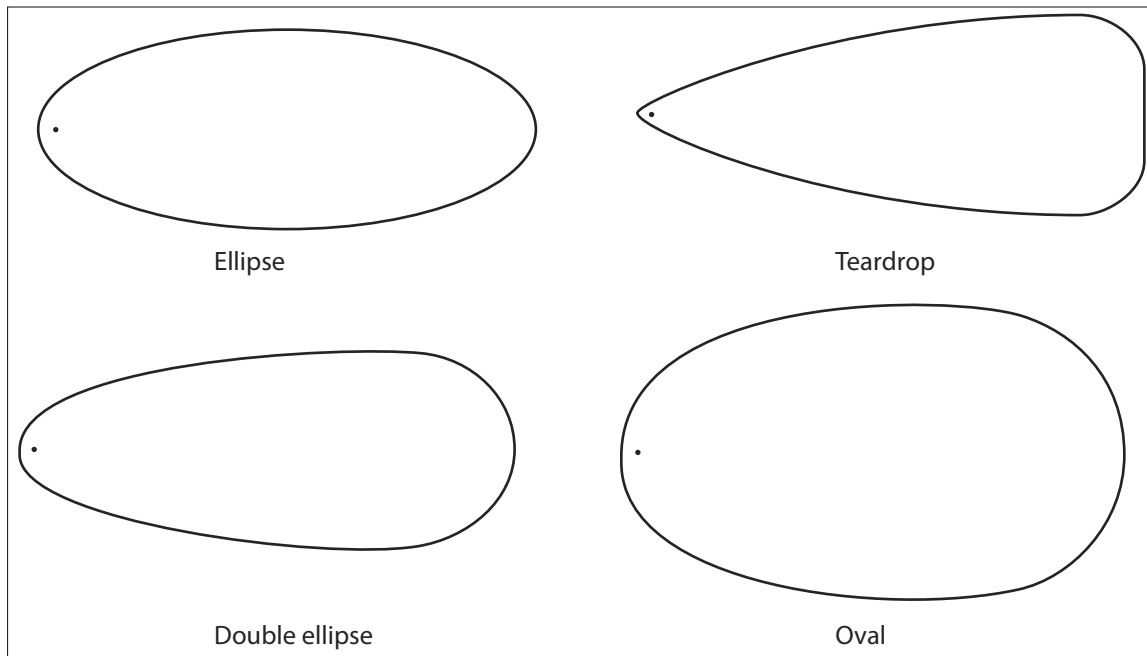


**Figure 3.** Four geometric shapes that have been used to model fire growth in homogenous environments. The small dot in each shape represents the point of ignition.

Richards (1993) applied symmetric variations in wind direction and variations in wind speed but was unable to change the shape of the fire from an ellipse to a teardrop or double ellipse. He concluded that other factors, such as fuel type and pattern, spotting, and asymmetric variations, influenced fire shape.

As a fire transitions from ignition to its equilibrium rate of spread, it is reasonable to assume a corresponding transition in fire shape. McAlpine (1989) showed that the length-to-breadth ratio is not static during the acceleration phase; rather, the fire initially approximates the shape of a circle and then becomes elliptical. The timing of this transition is assumed to coincide with the point at which the equilibrium rate of spread is reached.

Despite this additional research, both the Canadian FBP System and the USDA Forest Service BEHAVE Fire Modeling System currently use the simple ellipse to model fire shape because of its ease of use. Fire growth models employing a simple geometric shape assume a uniform rate of spread, and thus uniform fuel, weather, and topographic conditions; as such, they are most suited to projections over relatively short burning periods, and their application becomes limited under heterogeneous conditions.

### Fire Growth Simulation under Heterogeneous Conditions

As fires grow in size over many hours to days, they are more likely to encounter variation in weather, fuel, and terrain conditions, which will result in variation in fire spread rates and

directions. The two principal methods that have been used to simulate fire spread rates and fire growth in complex environments are the cellular automata and wave propagation approaches.

### Cellular Propagation

Cellular automata models, which employ a grid of square or hexagonal cells, are widely used to simulate natural phenomena. In fire spread applications, fuel and terrain conditions are assumed to be homogeneous within each cell. The fire propagates through the grid on a per-cell basis, typically from cell center to cell center. Each ignited cell behaves as an ignition source and is independent of any adjacent burning cells. To spread the fire from one cell to another, a search mechanism such as an adjacency or spread template is required.

Figure 4 illustrates the adjacency templates for 8-, 16-, and 32-point models. O'Regan et al. (1976) quantified the relative theoretical errors associated with using 8-, 16-, 32-, and 64-point spread templates as a function of time since ignition, eccentricity, and the semi-major axis. They concluded that the 8-point spread template produced unsatisfactory shapes, whereas the 32- and 64-point spread templates produced reasonably satisfactory shapes. They also suggested that an asymmetric spread template be used to reduce the error associated with wind-driven fires starting from an ignition point. Although they gave no further details of the asymmetric spread template, O'Regan et al. (1976) were the first to discuss the use of such a template to improve the accuracy of a cellular automata model.

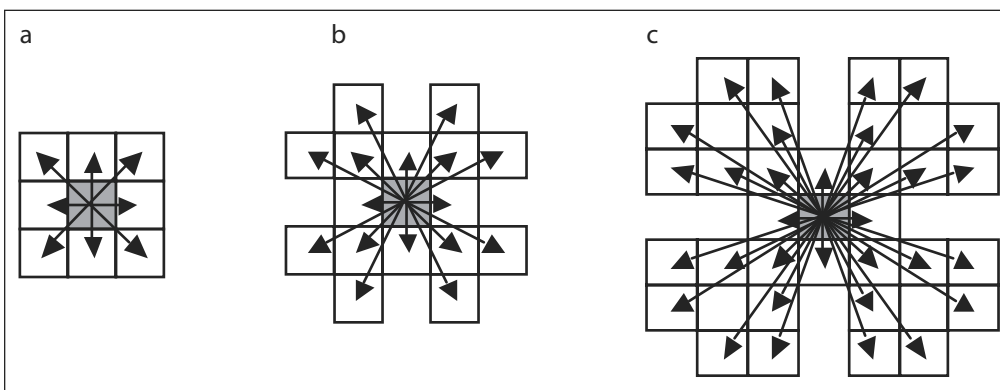


**Figure 4.** Adjacency templates for symmetric 8-point (a), 16-point (b), and 32-point (c) cellular automata models. A fire (or other process) can spread to the unshaded cells from the central shaded cell in the 8, 16, and 32 directions, respectively, represented by the arrows.

The notation for describing asymmetric templates consists of three numbers (separated by hyphens): the first represents the number of spread directions in the base symmetric template, the second is the number of additional spread vectors assigned to the head of the fire, and the third is the farthest-neighbor distance measured in number of cells. For example, the notation 8-2-4 indicates that the asymmetric model is based on an 8-point symmetric model with an additional 2 adjacent cells (i.e., spread directions) located no more than 4 cells from the ignition source.

Feunekes (1991) analyzed in detail the errors between symmetric and asymmetric fire growth simulation models using various simulation variables (definition of adjacency, number of spread directions, wind speed, wind direction, and fuel complexity). He defined simulation error as the difference between the expected shape (e.g., a simple ellipse under homogeneous conditions) and the simulated shape. The asymmetric models produced significantly more accurate projections than the symmetric models. The 8-2-4 asymmetric model (Figure 5a), for example, produced less error than a 32-point

symmetric model, and the 8-12-8 asymmetric model (Figure 5b) produced less error than a 96-point symmetric model.

Spread templates often approximate an elliptical shape. Figure 6 illustrates how the symmetric models increasingly underestimate the area burned as the length-to-breadth ratio increases. These errors can be reduced by extending the definition of adjacency or by using asymmetric spread templates. A more accurate perimeter location for the head of the fire can be obtained by applying additional spread vectors in the direction of spread.

Percolation theory, which uses probability functions, has also been applied in cellular automata models to simulate fire spread as a diffusion process (MacKay and Jan 1984; Green and Tridgell 1990). The use of transition functions allows the modeling of probabilistic processes such as spotting. Still, the ability to model realistic perimeters for individual fires remains a challenge (Beer and Enting 1990). Modeling fire as a diffusion process requires the use of a defined connectivity, or path, for the fire to spread from cell to cell, and nearest-neighbor percolation is commonly used.

Kourtz and O'Regan (1971) developed the first computer simulation model to spatially simulate the growth of a small fire. Their model was based on a heterogeneous and discontinuous fuel-type grid but did not account for the effects of terrain and wind. This deterministic model predicted how long it would take a fire to burn through one square area or cell within a fuel grid when the location of the fire, the starting time, and the grid resolution were known. Travel times were calculated using fixed rates of spread (based on the fuel type and the spread index for the day) and fixed spread directions (i.e., the spread template) from the burning cell (Figure 7).

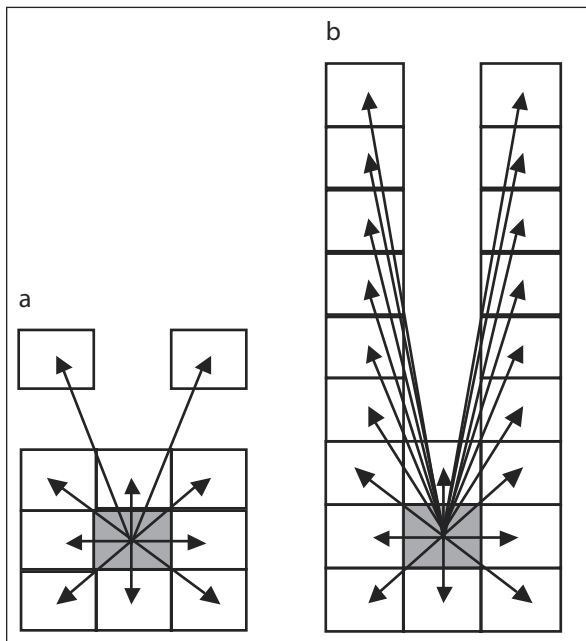


**Figure 5.** Adjacency templates for asymmetric 8-2-4 (a) and 8-12-8 (b) cellular automata models. A fire (or other process) can spread to the unshaded cells from the central shaded cell in the 10 and 20 directions, respectively, represented by the arrows.

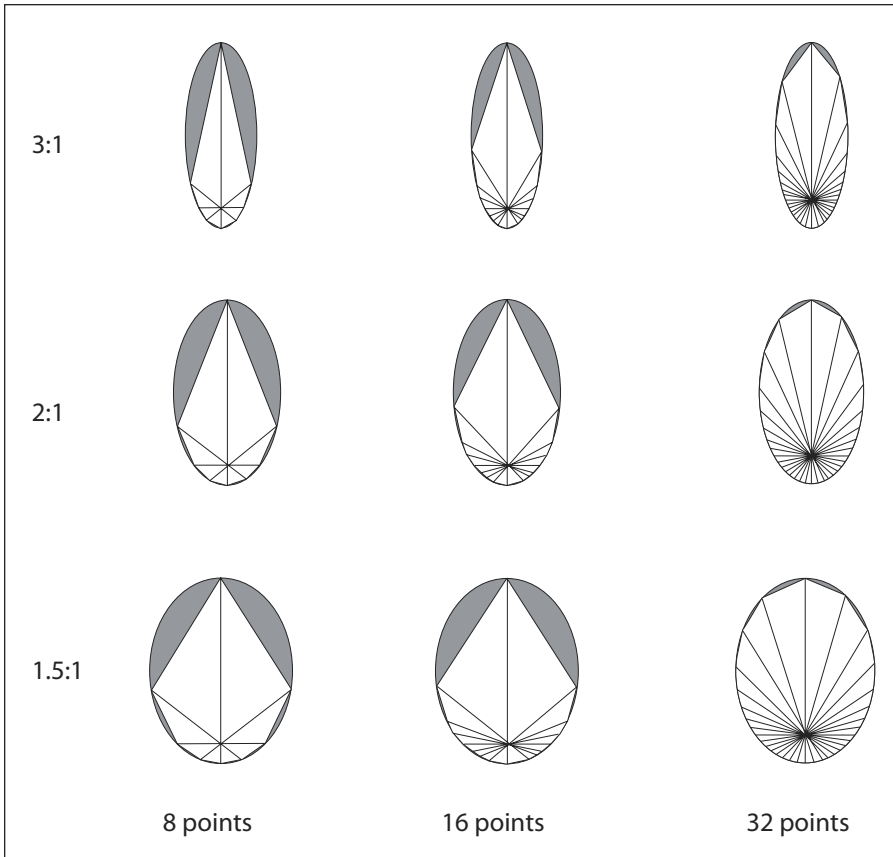


**Figure 6.** Fire growth (white polygons) in three symmetric cellular automata models layered over the simple elliptical fire growth model, according to length-to-breadth ratio (shown at left). The gray shaded areas within the ellipses represent the error or underestimation of fire growth.

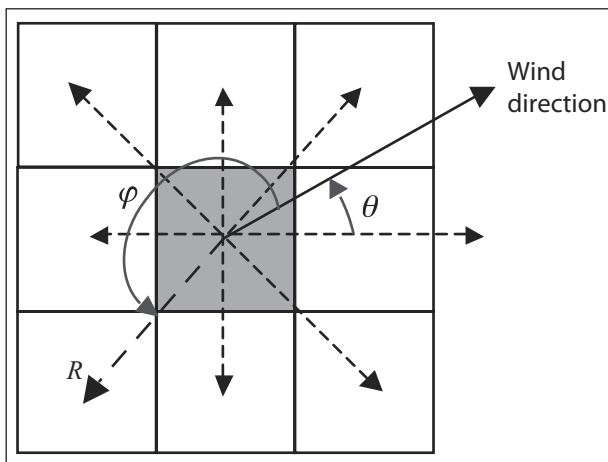


**Figure 7.** An eight-point cellular automata method to calculate directional rate of spread.  $\varphi$  = angle from the wind direction vector to the vector from the burning cell to an adjacent cell,  $R$  = rate of spread in the southwest direction,  $\theta$  = angle of the wind direction vector. The dashed arrows represent the eight spread directions. The difference between the modeled and actual spread direction can be up to  $22.5^\circ$ ,  $11.25^\circ$ , or  $5.6^\circ$  for models with 8-, 16-, and 32-point symmetric adjacency templates, respectively.

Kourtz and O'Regan (1971) concluded that because many fuel types may occur in a small landscape extent, it would be impossible to develop a fuel-type grid to accurately reflect reality. Therefore, they applied their model many times, using different hypothetical fuel-type grids, which were generated by Monte Carlo sampling of probability distributions derived from data on fuel-type patterns collected in the field.

Initially, the problem of spreading a fire from cell to cell seemed relatively easy to solve. However, a fire can take any of several paths to reach and burn each cell in the grid. Kourtz and O'Regan (1971) applied Dijkstra's (1959) algorithm to compute minimum travel times and hence to identify actively burning cells and those already burned. Dijkstra's algorithm maps the path of least resistance for a fire in an ignited cell to spread to neighboring cells. This approach continues to have merit: for example, Finney (2002) applied the concept of minimum travel time using constant weather conditions and a two-dimensional lattice to generate fire perimeter positions identical with those produced by elliptical propagation.

O'Regan et al. (1973) developed a method for using directional rates of spread to predict fire growth. They also rewrote the original model (Kourtz and O'Regan 1971) for use on a large computer to simulate fires of up to 15 000 ha. O'Regan et al. (1976) calculated average directional rates of spread using equation 3a and 3b (Figure 7).

$$ROS = \frac{a_e (1 - E^2)}{1 - E \cos \varphi} \text{ for } 270^\circ < \varphi < 90^\circ \quad [3a]$$

$$ROS = a_e (1 - E^2) \text{ for } 90^\circ \leq \varphi \leq 270^\circ \quad [3b]$$

where *ROS* is the rate of spread, *E* is the eccentricity ( $c_e/a_e$ ),  $a_e$  and  $c_e$  are ellipse parameters, and  $\varphi$  is the angle from the wind direction vector to the vector from the burning cell to an adjacent cell (see Figures 1 and 7).

Kourtz et al. (1977) further modified this model to accommodate hourly wind conditions. Although the operational application of this model assumed homogeneous fuel conditions, it was designed to use rate-of-spread equations for eight fuel types from eastern Canada (Van Wagner 1973) and nine fuel models from the United States (Rothermel 1972).

Kourtz et al. (1977), recognizing the need to provide operational forecasts of fire growth, adapted the program to run on a minicomputer and successfully modeled fires of up to 7 000 ha with a grid resolution of either 71 m or 142 m. Although Kourtz et al. (1977) developed a method to derive and map fuel types using Landsat imagery, the lack of availability of a digital fuel-type database was a continuing limitation (Kourtz 1977).

O'Regan et al. (1976) noted that the ignition type influenced fire spread and found that simulating fire growth with an ignition line produced less error than using an ignition point. The spread template, which they referred to as the "definition of adjacency," was another important variable because it influences the size and shape of the fire.

Frandsen and Andrews (1979) simulated the spread of fire using a hexagonal network of fuel cells. The fuel parameters and the corresponding spread rates associated with each hexagonal cell determined how fast the fire would spread. This approach captured nonuniformities in fuel type and the resulting spatial variability in fire behavior. Frandsen and Andrews (1979) applied their model using no slope and no wind, then using no slope and 3.2 km/h winds (normal for the ignition line) for the slash fuel type, and finally using no slope and no wind for the grass/sagebrush fuel type. However, this research model was not intended for operational use, nor could it model dynamic spread in all hexagonal directions.

Todd (1999) adapted the Kourtz et al. (1977) model to create an eight-point symmetric model called Wildfire. Because Wildfire incorporated the spread rates of the Canadian FBP System, it became the default national fire growth simulation model in Canada. The features and functionalities of the Wildfire model were assessed and considered during the design of the Prometheus model.

Boyчук et al. (2009) developed a stochastic model of fire spread using a lattice Markov chain model, in which they associated transition functions with each cell. Each of these cells interacts with its four nearest neighbors, and a cell transitions from unburned to burning depending on the state of the neighboring cells.

Models simulating landscape disturbance typically use cellular automata models to simulate probabilistic fire spread. Keane et al. (2004) evaluated and classified 44 landscape fire simulation models. They identified three approaches for simulating fire spread in these models: shape (use of predetermined fire perimeters and areas), lattice (spread of fire from one pixel or cell to another), and vector (expanding fire polygon). In Canada, these models include FEENIX and TARDIS (Cumming 2000; Messier et al. 2003), LANDMINE (Andison 2000a, 2000b), SELES (Spatially Explicit Landscape Event Simulator) (Fall and Fall 1996), STANDOR (Rogeanu et al. 1998), and BFOLDS (Boreal Forest Landscape Dynamics Simulator) (Perera et al. 2002). FEENIX uses spread probabilities specific to vegetation types and an eight-neighbor percolation model to simulate fire spread. In LANDMINE, conditional probabilities based on input layers such as fuel type, topography, and wind are used to spread fire to one of eight neighbors; however, size and area burned are predetermined. In SELES, probability distributions specify the time interval between fire events, fire intensity, burning period, and how the fire spreads from a cell to each of its four neighboring cells. STANDOR incorporates the FBP System and a 16-5-7 asymmetric model developed by Feunekes (1995). Fire spread in this model depends on the availability of fuel and the probability of burning, which is based on topography. BFOLDS uses a 16-point symmetric cellular spread model and the FBP System equations. None of these landscape disturbance models are intended to accurately predict individual fire events, and therefore they are not used to provide decision support for fire management operations.

Simulation models based on the physical mechanisms of fire spread form a separate class of models requiring an understanding of complex processes such as convection, radiation, and turbulence (Stewart 1971; Baines 1990). These complex processes are usually studied in laboratories, where the fire environment can be controlled. The challenge of scaling from homogeneous microscale laboratory experiments to heterogeneous mesoscale landscapes has been one reason for the limited operational use of physical models. They are also data intensive and computationally demanding.

The heat simulation model developed by Johnston et al. (2006) propagates fire from hot polygons to neighboring cooler polygons by heat transfer (conduction) events. These authors used effective conductivity rules to influence the rate of heat transfer to adjacent unburned polygons.

The objective of three-dimensional transport models called coupled atmosphere–fire models is to incorporate the interaction between a fire and its atmospheric environment. Researchers at the National Center for Atmospheric Research in Boulder, Colorado, developed an atmospheric prediction model, in which the heat and moisture generated by a fire are input back into the model (Clark et al. 1996, 2004; Coen 2005). This feedback allows for the simulation of local winds around and influencing the fire, thereby providing more accurate predictions of fire behavior than with the empirical fire spread model. The coupled atmosphere–fire model can predict small-scale, erratic, intense fire behavior resulting from sudden increases in spread rates not generated by the use of observed winds only. However, these simulations cannot be completed in real time with the required high-resolution grids (10–20 m). Additionally, Coen (2005) concluded that although simulations using 100- to 500-m resolution grids provide faster-than-real-time predictions of the overall spread of the fire, their coarser resolution does not adequately capture the behavior of small-scale fires.

Researchers at the Los Alamos National Laboratory developed another coupled atmosphere–fire model called HIGRAD/FIRETEC. The FIRETEC component models the important physical processes that influence fire behavior, such as combustion, heat transfer (radiation and convection), and turbulence. It is coupled with HIGRAD, a high-gradient flow model that yields accurate atmospheric simulations (Linn 1997; Linn and Cunningham 2005).

The National Institute of Standards and Technology of the United States Department of Commerce, in cooperation with the VTT<sup>2</sup> Technical Research Centre of Finland, extended the structural fire dynamics simulator to include fuels within the wildland–urban interface. The resulting community-scale model (approximately 1 × 1 km), called WFDS (for Wildland–Urban Interface Fire Dynamics Simulator), is a fire-driven computational fluid dynamic model

that solves equations governing the flow of fire (Mell et al. 2006). Physics-based and coupled atmosphere–fire models allow a better understanding of the physical processes that control fire behavior.

The grid geometry used in cellular automata models can influence the shape of a fire, a phenomenon that Richards (1995) referred to as “coordinate ghosting.” This problem is related to assumptions regarding where changes in fuel type actually take place and to the difference between the direct distance and the distance traveled by the spread algorithm. This difference occurs because the search domain restricts possible travel paths and hence potential solutions. It is particularly evident with cellular automata models that restrict fire spread to eight directions. Caballero (2006) has described this problem as “taxicab geometry,” suggesting that errors associated with this behavior can be reduced by improvements in the algorithms. To

avoid the influence of uniform grid geometry on fire shape, Johnston et al. (2006) used Voronoi polygons.

The limitations common to all cellular automata models, though challenging, can be overcome by applying Fermat’s principle for the determination of travel times and hence the shortest paths for spread of fire between nodes (Finney 2002). However, this method has its own limitations, specifically, the assumption of constant weather conditions.

### Wave Propagation

An entirely different approach to modeling fire spread, based upon Huygens’ important discovery about the propagation of light waves, has also been used. In his *Treatise on Light*, Huygens (1912/1962) concluded, “So it arises that around each particle there is made a wave of which that particle is the centre” (Figure 8).

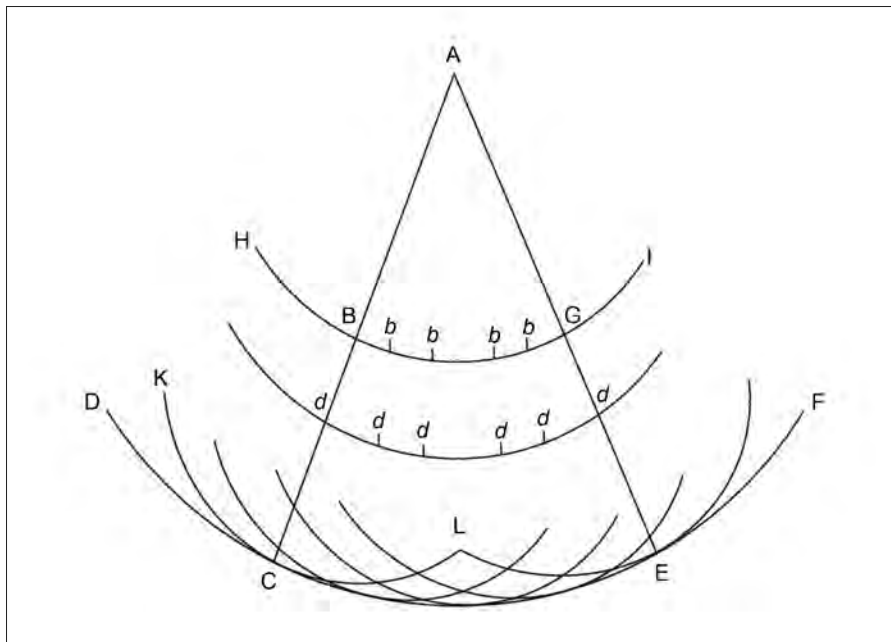


**Figure 8.** Propagation of light waves, as proposed by Huygens (1912/1962). The principal wave DCEF emanates from point source A. Secondary wave KCL emanates from point source B and contacts the wave DCEF at C. Principal wave HBGI also emanates from point source A. Point sources b and d also generate their own individual secondary waves. Source: Huygens (1962).

<sup>2</sup>VTT = Valtion Teknillinen Tutkimuskeskus (Finnish), meaning “governmental technical research center.”

Huygens considered every point on a wave front of light as a source of individual wavelets and described the new wave front as the surface tangential to the circumferences of the secondary waves (Figure 9).

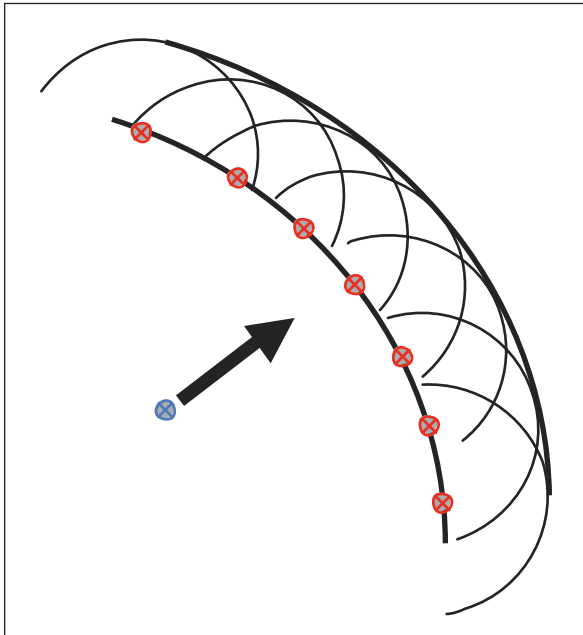


**Figure 9. Formation of a new wave front using Huygens' principle.** The blue crossed circle is the point of origin, the arrow represents the spread direction of the wave, and the red crossed circles represent the origins of secondary waves. Source: Huygens (1962).

The application of Huygens' principle to simulate fire growth assumes that the shape of a fire can be represented by a polygon, a plane figure composed of a sequence of straight-line segments forming a closed path. The points around the perimeter where two line segments meet are the polygon's vertices, and each vertex along the perimeter of a fire polygon propagates as an independent elliptical wavelet, which can be referred to as a "firelet" (Figure 10). The conditions at each vertex (e.g., fuel, weather, topography) are sampled and used to orient the elliptical firelet and define its dimensions; this interface propagation is referred to as the Marker method (Hyman 1984). The connected vertices represent the new fire perimeter at the beginning of the next time step and approximate the tangential envelope of the elliptical firelets. In the Prometheus application, individual firelets are not grown using actual ellipses or firelets. Rather, partial differential equations (Richards 1995, 1999) are used to propagate and locate the vertices. The conceptual ellipses are included in the figures within this report only for illustrative purposes.

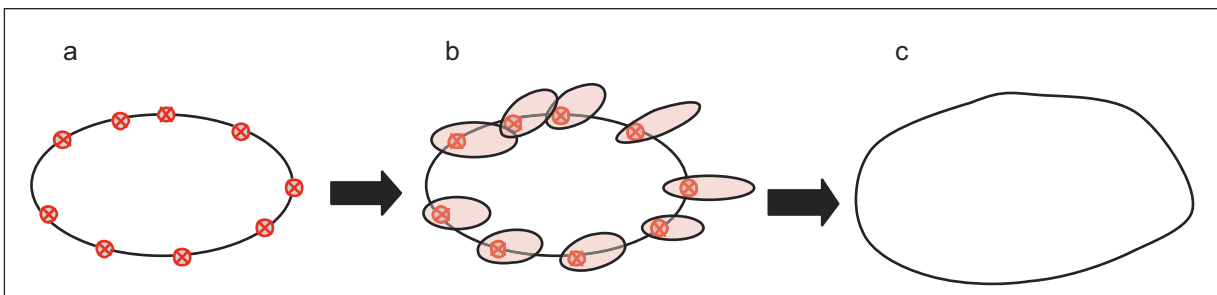


**Figure 10. Application of Huygens' principle to simulate fire growth.** a. Points of origin (vertices) for wave propagation are identified around the fire perimeter (red crossed circles) at time  $t$ . b. Elliptical firelet growth over elapsed time  $\Delta t$  (red shaded ellipses) is projected using spread functions. c. The new fire perimeter at time  $t + \Delta t$  is drawn as the tangential envelope of the firelets in Fig. 10b.

Huygens' principle was first applied to the simulation of fire spread by Sanderlin and Sunderson (1975). Their work was part of a wildland fire behavior research program initiated by the USDA Forest Service following the disastrous 1970 fire season in California (which included a particularly catastrophic 13-day period during which a total of 234 717 ha was burned over, with the loss of 770 homes and 9 lives). The radial fire propagation model developed by Sanderlin and Sunderson (1975) was integrated in an overall real-time decision support system to simulate fire behavior and suppression effectiveness in southern California (Sanderlin and Van Gelder 1977). Each vertex on the fire perimeter is propagated using a local directional spread rate. Vertices are added and deleted to adhere to a specified threshold distance between vertices. Sanderlin and Sunderson (1975) were also the first to document the problem of the undesirable vertex behavior (i.e., the creation of loops) that was produced when Huygens' principle was applied to simulate fire spread. Their model subsequently included the functionality to detect and remove these loops.

Anderson et al. (1982) later developed a simple elliptical model based on Huygens' principle of wave propagation to simulate the spread of grass fires. They concluded that, for an elliptical fire growing in homogeneous fuels under uniform wind conditions, the fire front at a particular time after ignition ( $\Delta t$ ) can be represented in parametric form as follows:

$$x = ROS_0 f \Delta t \cos \phi + ROS_0 g \Delta t \quad [4]$$

$$y = ROS_0 h \Delta t \sin \phi \quad [5]$$

where  $x$  and  $y$  are local point coordinates;  $ROS_0$  is the rate of spread (m/min) with no wind;  $f$ ,  $g$ , and  $h$  are wind-dependent parameters that change the rate of spread ( $ROS_0$ ) to account for the influence of wind;  $\phi$  is the angle from the centroid to the subtending circle of the ellipse (see Figures 2 and 7 and equation 3); and  $\Delta t$  is the change in time from one time step to the subsequent time step. The new location on the fire perimeter is denoted by  $J$  in Figure 11. Also pertinent to these equations is  $\theta$ , the angle from the positive  $x$  axis (see Figure 2), which represents the net effective spread direction.

Using the parameters in Figure 1 and straightforward substitution,  $x$  and  $y$  from equations 4 and 5 can be calculated as follows:

$$x = a_e \cos \phi + c_e \quad [6]$$

$$y = b_e \sin \phi \quad [7]$$

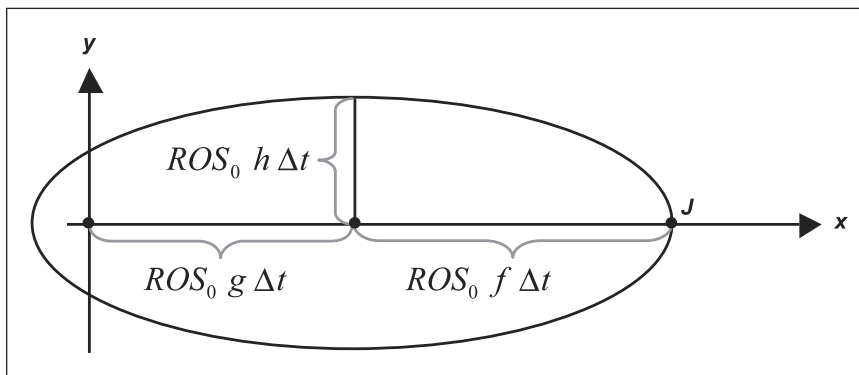


**Figure 11. Propagation of an elliptical fire from an ignition point with a uniform wind speed in the  $x$  direction ( $\theta = 0$ ), as described by Anderson et al. (1982).**  $x$  and  $y$  = local point coordinates;  $ROS_0$  = rate of spread (m/min) with no wind;  $f$ ,  $g$ ,  $h$  = wind-dependent parameters that change the rate of spread to account for the influence of wind;  $J$  = point where the spread direction vector intersects the ellipse when  $\theta = 0$ ;  $\Delta t$  = time duration.

If the net effective spread direction is aligned with the positive  $x$  axis, and the angles  $\theta$  and  $\phi$  are zero, then the resulting forward spread distance is  $a_e + c_e$ , the flank spread distance is  $b_e$ , and the back spread distance is  $a_e - c_e$ . If the net effective spread direction  $\theta$  changes, then the corresponding angle  $\phi$  must be recalculated.

Although Anderson et al. (1982) fitted their model with data from experimental grassland fires in Australia, they did not have measurements allowing them to apply appropriate values for  $ROS_0$ ,  $f$ ,  $g$ , and  $h$  for different fuel and weather conditions.

Disastrous fire seasons in Australia in 1983 and 1985 prompted the development of a fire growth simulation model in that country. In 1987, the National Bushfire Research Unit agreed to develop a fire simulation model for use on a personal computer. The resulting model, the National Bushfire Model (Beer 1990), used a four-point ellipse template as the basis to propagate fire in three fuel types (grass, forest, and nonfuel). An algorithm described by Shimrat (1962) was used to determine the position of the points relative to the perimeter and hence to select the points to be retained to form the next fire perimeter. Knight and Coleman (1993) later incorporated an algorithm for expanding the fire perimeter, which was based on the model described by Anderson et al. (1982). This algorithm included the detection and removal of undesirable internal loops and regions of overlap. To avoid the problems associated with expanding a closed curve by means of Huygens' principle (i.e., the creation of loops and enclosures), Coleman and Sullivan (1996) used only elliptical geometry for propagation in their SiroFire model. Although SiroFire was never used operationally, it has been incorporated in a new model for mapping fire characteristics, called Phoenix, which is under development at the University of Melbourne (Tolhurst et al. 2006).

Richards (1990) extended the work of Anderson et al. (1982) by deriving a set of partial differential equations to model the growth of fires under heterogeneous conditions.

Using test cases, French (1992) compared and verified various techniques for simulating two-dimensional fire growth. These techniques included the eight-point symmetric cellular automata method (Kourtz and O'Regan 1971), Green's contact and heat accumulation methods (Green 1983), percolation modeling (MacKay and Jan 1984), and the application of Huygens' principle (Anderson et al. 1982; Catchpole et al. 1982; Roberts 1989; Richards 1990). French's (1992) simulation test cases used either no wind, constant wind, or variable wind, along with heterogeneous fuel types. With the contact method, intersection points of a square lattice were burned if the points lay within an elliptical template area. In the heat accumulation model, unburned cells absorbed heat from neighboring cells until an ignition threshold was reached. The percolation model propagated fire from burning cells to unburned cells in a square lattice according to defined probabilities. French (1992) concluded that the methods based on Huygens' principle yielded more satisfactory results than the other propagation methods.

Both the Farsite model (Finney 2004) and the Prometheus model use the partial differential equations of Richards (1990) to propagate each vertex along the fire perimeter. However, the models differ in the danger rating system components and fuel models used to model spread rates. Farsite uses the National Fire Danger Rating System and fire behavior prediction fuel models developed by Rothermel (1972) and extended by Anderson (1982) and Scott and Burgan (2005), whereas Prometheus uses the components of the Canadian Forest Fire Danger Rating System. Opperman et al. (2006) compared these two models.

---

## STRUCTURE OF PROMETHEUS: THE CANADIAN WILDLAND FIRE GROWTH SIMULATION MODEL

---

The Prometheus model simulates fire growth over one or many daily burning periods in a complex fire environment where fuel and topographic conditions vary spatially across the landscape and where weather conditions vary both spatially and temporally. Fire environment data and user-defined modeling parameters are managed as scenarios within a project file.

### Prometheus Project File

A Prometheus project file contains all of the fuel, topographic, and weather data needed to describe the fire environment and all of the scenario settings and parameters needed to deterministically run a simulated fire; it is a binary file with an .fgm extension. A project file can be reopened and modified, it can be transferred to other users, and it may include one or more simulation scenarios. Prometheus allows users to compose and assess various “what if” scenarios. Multiple ignitions and different ignition types, landscape and polygon fuel-type patches, wind speed and wind direction patches and grids, and fuel breaks can be easily added to or removed from scenarios.

### Fire Growth Simulation Scenarios

A Prometheus scenario refers to the input data and model parameters for a single fire growth simulation that predicts fire growth from single or multiple ignitions, or fire starting events, in a landscape.

Simulation scenarios for a given time period ( $t_0$  ...  $t_n$ ) are executed by loading the appropriate fuel, topography, and weather data for the landscape extent and simulation period and then defining an ignition event or events. The extent of the modeling space is determined by the geographic extent of the fuel and topographic grids. Weather streams consist of a sequence of time-referenced weather data that are assumed to be uniform across the landscape for a particular scenario, unless the spatial weather interpolation is used (see section entitled “Spatial Interpolation,” below) or weather patches are assigned to the scenario. The duration of the simulation is limited by the length of the weather data file.

The ignition event is described by the start time ( $t_0$ ), start location, and ignition type; a small circular polygon approximates a point, a thin polygon approximates a line, and a simple polygon represents an active fire. In the first time step following the ignition event at  $t_0$ , fire rates of spread are calculated for each vertex of the existing polygon using equations from the FBP System and the appropriate fuel, weather, and topographic data. However, the three-dimensional locations of the polygon vertices ( $x$ ,  $y$ , and  $z$ ) are independent of the  $x$  and  $y$  coordinate system associated with the underlying fuel and topographic grids. The rate of spread ( $ROS_t$ ), flank fire spread rate ( $FROS_t$ ), and back fire spread rate ( $BROS_t$ ), as well as the duration of the time step ( $\Delta t$ ), are then used to calculate the orientation and dimensions of a theoretical elliptical “firelet” at each vertex location using the wave propagation equations of Richards (1990, 1995). The tangential envelope of the elliptical firelets at each vertex creates the new fire perimeter at  $t + \Delta t$ . Various polygon operations are carried out to check and manage intersections between the new fire perimeter and nonfuel barriers or other fires and to discretize the perimeter, including untangling loops, deleting redundant vertices, and inserting new vertices around the perimeter. Finally, potential fire behavior characteristics are calculated for the final vertex set, which can be output, viewed, and used in the next time step. This process is repeated for each time step within the burning period and can extend over multiple burning periods on successive days.

Scenario simulations and their outputs are managed and viewed using three main windows or views: the Map View displays spatial data and simulation output, the Statistics View displays the simulation statistics output, and the Component View provides functionality to manage and edit data and parameters. The scenario builder within the Component View allows users to compose and assess various “what if” scenarios. Operations performed or available in the Statistics and Map Views are further described in the section entitled “Fire Growth Simulation Outputs.”

## Model Structure

The Prometheus application is built on the Microsoft Windows platform and uses a component-based software architecture called COM. The COM modules are implemented using Microsoft's COM, a binary programming standard that allows the Prometheus object-oriented COM components (dynamic link libraries) to be reused. The specific functions of these COMs are described in detail in the *Prometheus COM Programmer's Manual* (CWFGM Project Steering Committee 2009). Four separate modules or COMs are used to store and manage fuel, topography, weather, and FWI System data; these are the FuelCom, GridCom, WeatherCom, and FWICom modules, respectively (Figure 12). More specifically, the GridCom module is used to retrieve the spatial grid data (fuel and topography). The FWI System is encapsulated in the FWICom module, and the FBP fuel types and their associated properties are encapsulated in the FuelCom module. The WeatherCom module addresses the temporal aspect of the data required to perform fire simulations. It incorporates the weather station and weather stream data. A fifth module, called FireEngine, performs and stores the fire growth calculations and fire-front propagation.

The sixth module, called PrometheusCOM, combines these five low-level interfaces into an interface with a higher level of abstraction that provides programmers with a procedural, rather than an object-oriented, programming interface (Figure 12). The PrometheusCOM is intended for use by agencies interested in developing their own user interfaces or integrating the components into other applications, such as Pandora (<http://www.firegrowthmodel.com/pandora.cfm>), Pegasus, Burn-P3 (Parisien et al. 2005, 2009; Beverly et al. 2009), and the Spatial Fire Management System (Englefield et al. 2000). These four applications were developed by the Canadian Forest Service for use by fire management agencies and fire researchers across Canada. Pandora is a Windows application that allows users to run any number of Prometheus simulations in a batch operation; it is also included as an extension in the Spatial Fire Management System. Pegasus is a new application that allows fire management staff to remotely access Prometheus via the internet. It uses simple model inputs that are sent to a centralized server for processing. Burn-P3 is a simulation model used to assess burn probability over a landscape.

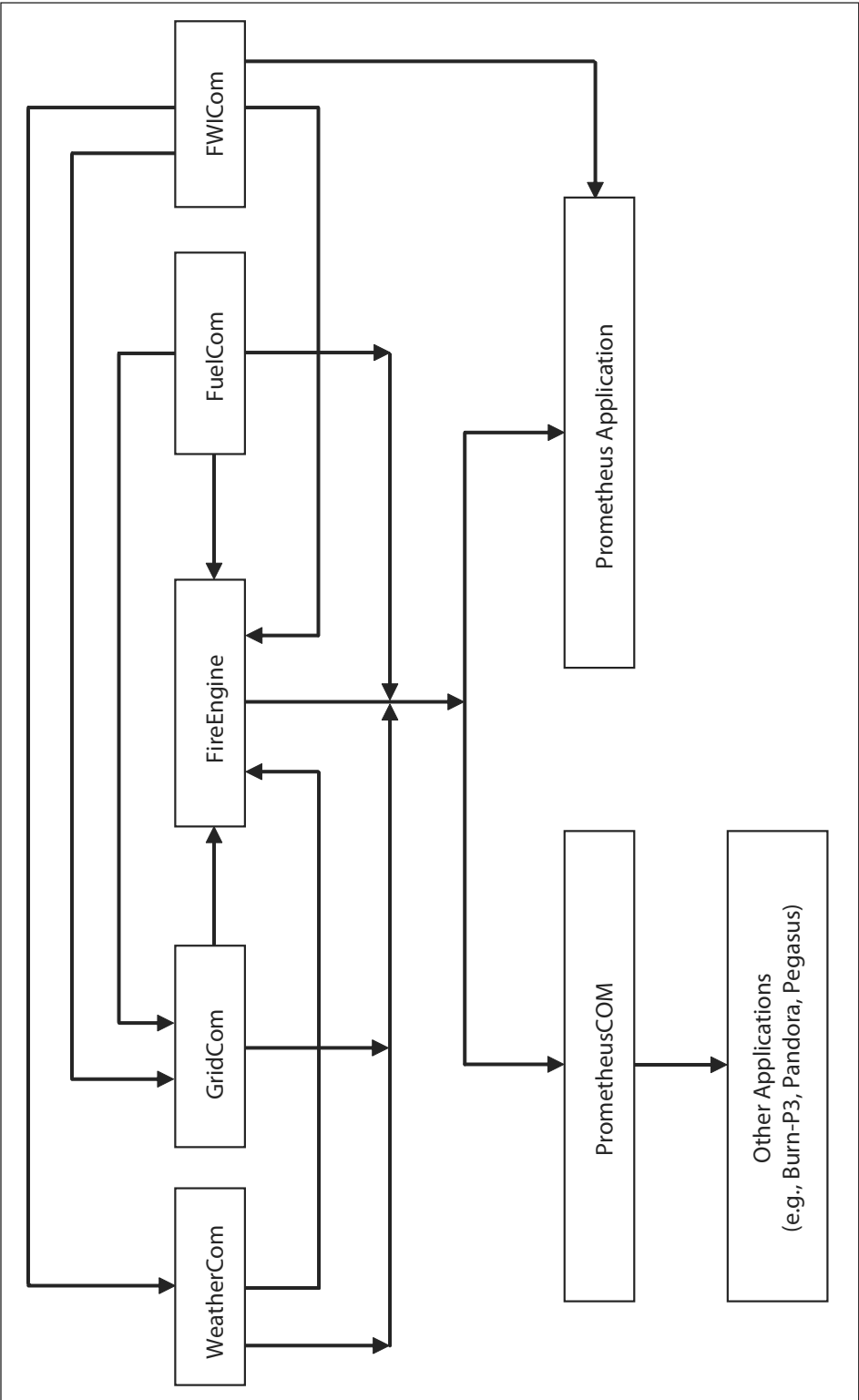


Figure 12. Prometheus Common Object Model (COM) architecture.

---

## LANDSCAPE DATA

---

Within Prometheus, fire growth is simulated with respect to a grid-based representation of the landscape. Each mandatory and optional fuel type and each optional slope, aspect, and elevation grid that is input into Prometheus must be in ESRI ASCII format, and all of these components must have the same projection and extent. Geographic features such as water courses and roads can also be represented; these are imported into Prometheus as vector files and may be provided in different projections and extents. Specific details are given in the *Prometheus Data I/O Standards Manual* (Canadian Wildland Fire Growth Simulation Model Data I/O Standards Technical Sub-Committee 2009).

### FBP Fuel-Type Grids and Lookup Tables

A fuel-type grid is a mandatory input layer, with the resolution and extent of the fuel grid defining the grain and spatial extent of the fire modeling space. Once a fuel-type grid has been input into Prometheus, it can be edited and exported for use in other applications, but its size, scale, and location cannot be changed (Figure 13). Because Prometheus uses the Canadian FBP System to calculate fire spread rates and other fire behavior characteristics, grid values must represent the 16 standard fuel types in the Canadian FBP System (Table 1). In Canada, these grids are usually derived by reclassifying forest inventory data or vegetation inventory data that have been classified from remote sensing data.

A lookup table is also required to associate each integer value in the fuel-type grid with a designated fuel type or nonfuel type. In the national FBP fuel-type lookup table (Canadian Wildland Fire Growth Simulation Model Data I/O Standards Technical Sub-Committee 2009), for example, 20 unique grid values are specified for each of the four mixedwood fuel types, corresponding to 5% increments of hardwood

and softwood composition. When Prometheus is first installed, the national default FBP fuel-type lookup table is used. Although this table cannot be changed, it can be used to create new project-specific fuel-type lookup tables. It is common practice for fire management agencies to create and customize their own application default tables.

A nonstandard fuel type designated as D-2 was created for use in Prometheus. D-2 is a leafed aspen fuel type (in contrast to the standard FBP System leafless aspen fuel type, designated as D-1) with an associated set of rules for rate of fire spread.<sup>3</sup> Fires in leafed hardwood forests are usually of very low intensity and spread very slowly, and are therefore not considered in the standard FBP System models. The Prometheus rules for fire spread in the D-2 fuel type allow for fire propagation through these stand types under some conditions; the alternative of treating leafed aspen as nonfuel under all conditions was considered unreasonably restrictive for the purposes of fire growth simulation. Various nonfuel types can also be specified, representing, for example, muskeg, alpine tundra, or other vegetation types with very limited flammability or nonvegetated areas. No fire spread will occur within nonfuel grid cells, and null grid entries are treated as nonfuels. Nonetheless, it is desirable to classify the nonfuel types to allow for dynamic fuel-type modeling. For example, in the boreal forest, treed muskeg can usually be typed as nonfuel during the spring and early summer, but when the Drought Code (*DC*, a relative measure of the moisture content of deep, compact organic layers) exceeds 300 and the grass and sedges begin to cure, these sites become flammable and should be retyped. It is easy to reclassify nonfuel types if they have already been categorized as specific nonfuel types.

---

<sup>3</sup>Because few empirical data are available on fire spread in leafed-out hardwood forests, a threshold rule, based on expert opinion and anecdotal observations, was established. When the Buildup Index (*BUI*) of the FWI System is less than 80, fire does not spread in the D-2 fuel type; however, when the *BUI* is 80 or greater, the rate of spread is 20% of the rate of spread for the D-1 fuel type (leafless aspen), a nominal spread rate suggested by the Forestry Canada Fire Danger Group (1992).



Although each scenario requires just one FBP fuel-type grid, a Prometheus project file may include multiple scenarios, each potentially having its own FBP fuel-type grid. The use of multiple grids allows for the quick comparison of scenarios representing, for example, different fuel management strategies. However, a project file can have only one lookup table. Therefore, if a project has more than one scenario, and these scenarios have different fuel-type grids, the grids must all be associated with the same lookup table (i.e., a many-to-one relationship).

### **FBP Fuel-Type Modifier Grids**

A number of FBP System fuel types have characteristics affecting fire behavior that must also be specified or that may be allowed to vary from standard values applied across a landscape; the crown base height of the C-6 (conifer plantation) fuel type (Table 2) can be varied. If spatial data are available for these modifiers, the values can be input in separate, optional grids. Fuel-type modifier grid cells must correspond to the appropriate fuel-type grid cell. If null values are encountered in the fuel-type modifier grid, then default values are used.

#### **Green-up and Grass Curing**

Green-up is the period of spring growth when leaf production occurs. In Prometheus, the green-up state is used to switch the D-1 fuel type (Leafless Aspen) to the D-2 fuel type (Leafed Aspen), the M-1 fuel type (Boreal Mixedwood—Leafless) to the M-2 fuel type (Boreal Mixedwood—Green), and the M-3 fuel type (Dead Balsam Fir/Mixedwood—Leafless) to the M-4 fuel type (Dead Balsam Fir/Mixedwood—Green). No other fuel types are affected by the green-up state. Multiple green-up grids can be imported into Prometheus, but only one such grid can be assigned to a scenario at a time.

The percent-cured parameter applies to the grass fuel types. It represents the proportion of stems that are no longer green and growing.

The percentage of this cured, or dead, material strongly influences grassland fire behavior. Multiple percent-cured grids can be imported into Prometheus, but only one such grid can be assigned to a scenario at a time.

#### **Percent Conifer and Percent Dead Fir**

The M-1 and M-2 mixedwood fuel types require specification of the percent conifer within the stand. This parameter can significantly alter the rate of spread and area burned. Often derived from the species composition data included in forest inventories, its value can be spatially captured within a separate percent-conifer grid. If no percent-conifer grid is available, then a default percent-conifer value can be specified for the entire landscape. If the fuel-type grid does not include specific mixedwood fuel types, and no percent-conifer grid is available, then fire growth simulations within a landscape characterized by high spatial variability of percent conifer should be considered unreliable. Multiple percent-conifer grids can be imported into Prometheus, but only one such grid can be assigned to a scenario at a time.

The M-3 and M-4 mixedwood fuel types require specification of the percent dead fir, analogous to the percent-conifer grids for the M-1 and M-2 fuel types. If available, these data can also be captured spatially within a separate grid. Multiple percent-dead fir grids can be imported into Prometheus, but only one such grid can be assigned to a scenario at a time.

#### **Crown Base Height**

The C-6 (conifer plantation) FBP fuel type allows for the input of variable crown base height. If available, these data can be included spatially within a separate grid. Multiple crown base height grids can be imported into Prometheus, but only one such grid can be assigned to a scenario, and applied only to the C-6 FBP fuel type.

**Table 2. Canadian Forest Fire Behavior Prediction System fuel-type parameters that can be modified for use in Prometheus**

| Fuel type            | $a_{ROS}^a$       | $b_{ROS}^a$              | $c_{ROS}^a$          | $BUI_0^b$ | $q^c$ | Max. $BE^d$ | $CBH^e$<br>(m)  | $CFL^f$<br>(kg/m <sup>2</sup> ) |
|----------------------|-------------------|--------------------------|----------------------|-----------|-------|-------------|-----------------|---------------------------------|
| C-1                  | 90                | 0.0649                   | 4.50                 | 72        | 0.90  | 1.076       | 2.0             | 0.75                            |
| C-2                  | 110               | 0.0282                   | 1.50                 | 64        | 0.70  | 1.321       | 3.0             | 0.80                            |
| C-3                  | 110               | 0.0444                   | 3.00                 | 62        | 0.75  | 1.261       | 8.0             | 1.15                            |
| C-4                  | 110               | 0.0293                   | 1.50                 | 66        | 0.80  | 1.184       | 4.0             | 1.20                            |
| C-5                  | 30                | 0.0697                   | 4.00                 | 56        | 0.80  | 1.220       | 18.0            | 1.20                            |
| C-6                  | 30                | 0.0800                   | 3.00                 | 62        | 0.80  | 1.197       | 7.0             | 1.80                            |
| C-7                  | 45                | 0.0305                   | 2.00                 | 106       | 0.85  | 1.134       | 10.0            | 0.50                            |
| D-1                  | 30                | 0.0232                   | 1.60                 | 32        | 0.90  | 1.179       | NA <sup>k</sup> | NA                              |
| M-1/M-2 <sup>g</sup> | C-2 110<br>D-1 30 | C-2 0.0282<br>D-1 0.0232 | C-2 1.50<br>D-1 1.60 | 50        | 0.80  | 1.250       | 6.0             | 0.80                            |
| M-3 <sup>h</sup>     | M-3 120<br>D-1 30 | M-3 0.0572<br>D-1 0.0232 | M-3 1.40<br>D-1 1.60 | 50        | 0.80  | 1.250       | 6.0             | 0.80                            |
| M-4 <sup>h</sup>     | M-4 100<br>D-1 30 | M-4 0.0404<br>D-1 0.0232 | M-4 1.48<br>D-1 1.60 | 50        | 0.80  | 1.250       | 6.0             | 0.80                            |
| O-1a <sup>ij</sup>   | 190               | 0.0310                   | 1.40                 | 1         | 1.00  | 1.000       | NA              | NA                              |
| O-1b <sup>ij</sup>   | 250               | 0.0350                   | 1.70                 | 1         | 1.00  | 1.000       | NA              | NA                              |
| S-1                  | 75                | 0.0297                   | 1.30                 | 38        | 0.75  | 1.460       | NA              | NA                              |
| S-2                  | 40                | 0.0438                   | 1.70                 | 63        | 0.75  | 1.256       | NA              | NA                              |
| S-3                  | 55                | 0.0829                   | 3.20                 | 31        | 0.75  | 1.590       | NA              | NA                              |

<sup>a</sup>Rate-of-spread (ROS) parameter value specific to each fuel type.  $a_{ROS}$ ,  $b_{ROS}$ , and  $c_{ROS}$  parameters for M-3 and M-4 fuel types apply when the percentage of dead fir is 100%.

<sup>b</sup> $BUI$  = Buildup Index.

<sup>c</sup> $q$  = proportion of maximum rate of spread at  $BUI$  equal to 50.

<sup>d</sup> $BE$  = Buildup Effect.

<sup>e</sup> $CBH$  = crown base height.

<sup>f</sup> $CFL$  = crown fuel load.

<sup>g</sup>Variable % conifer values apply for the M-1 and M2 fuel types.

<sup>h</sup>Variable % dead fir values apply for the M-3 and M-4 fuel types.

<sup>i</sup>Variable % grass cure values apply for O-1a and O-1b fuel types.

<sup>j</sup>Variable grass fuel load values (kg/m<sup>2</sup>) apply for the O-1a and O-1b fuel types.

<sup>k</sup>NA= not applicable.

## Landscape and Polygon Fuel-Type Patches and Layering

The FBP fuel-type grid may not accurately reflect observed fuel types. Modifying the FBP fuel-type grids is therefore an important part of model calibration. A landscape fuel patch can be created to change an existing FBP fuel type into another fuel type for the entire grid or landscape. FBP fuel types can also be changed within specified areas by delineating a polygon (patch) within the Map View or by importing a polygon fuel-type patch as a Shapefile (\*.shp) or a Generate file (\*.gen) file.

Prometheus distinguishes standard fuel types from those with modifications and provides appropriate visual cues (different icon colors) in the Component View. All modifications to the fuel types are saved in the project file.

## Slope, Aspect, and Elevation Grids

Slope, aspect, and elevation grids are optional inputs. The slope values are recorded as percentages, and the aspect values are recorded in compass degrees. The values in the elevation grid represent elevation in meters above sea level.

Elevation is used to calculate foliar moisture content (*FMC*), one of the inputs in the FBP System. Percent slope and aspect (i.e., upslope direction), when provided, are used in the calculation of net effective wind direction and wind speed. The slope, aspect, and elevation grids must be in the same projection and must have the same extent as the FBP fuel-type grid.

## Geographic Vector Data

Geographic features such as hydrography (e.g., lakes, rivers, and streams), access (e.g., roads, railway lines, trails, and utility corridors), geo-administrative boundaries (e.g., fire management areas, parks), and values at risk (e.g., communities) can be imported into Prometheus as vectors (Shapefiles or Generate files) to provide a visual reference in the Map View. These geographic data layers can also be assigned to a scenario as fuel breaks. To determine whether fuel breaks can be breached by the fire, the width of each vector data layer must be specified when these layers are imported (see section entitled "Breaching of Nonfuel Areas"). This information need not be provided in the same projection or with the same extent as the gridded data, since projection transformations are performed automatically.

---

## WEATHER AND FWI SYSTEM DATA

---

A continuous hourly time series of FWI System values is required to carry out the FBP System calculations in the FireEngine COM (Figure 12). The start and end time of the FWI stream defines the potential length of a fire simulation. The weather and FWI System stream is created in the weather and FWI COM (Figure 12).

Actual, forecasted, or calculated interpolated weather observations (temperature, relative humidity, wind speed, and precipitation) are used to calculate the codes and indices of the FWI System: Fine Fuel Moisture Code (*FFMC*), Duff Moisture Code (*DMC*), Drought Code (*DC*), Initial Spread Index (*ISI*), Buildup Index (*BUI*), and Fire Weather Index (*FWI*). The characteristics of the FWI System codes and indices, and the relationship between fuel moisture and the fuel moisture codes (*FFMC*, *DMC*, *DC*) were

described by Van Wagner (1987); the set and order of equations required to calculate the FWI System codes and indices were summarized by Van Wagner and Pickett (1985). Daily values for all of the codes and indices are calculated from daily weather observations obtained at 1200 (noon) local standard time (LST). Hourly and subhourly values of *FFMC*, *ISI*, and *FWI* are calculated from hourly and subhourly weather values, respectively. The FWI System values are used as inputs for the FBP System calculations in the FuelCOM (Figure 12).

## Weather Stations

A Prometheus project must contain at least one weather station with associated weather observations relevant to the intended fire growth simulation. Although the weather station need

not be located within the extent of the landscape, a warning will be given if it is more than 100 km from the landscape boundaries. A Prometheus project may include more than one weather station. Each weather station is described by its latitude and longitude (decimal degree format) and its elevation (meters above sea level).

These variables, along with the date, are used to calculate *FMC*, which is a seasonally varying input for the FBP System. *FMC* influences calculations related to the crown fire involvement of coniferous and mixedwood fuel types. Latitude and longitude are also used to determine the times of sunrise and sunset, which are needed for diurnal modeling of daily weather when hourly weather data are not available.

### Hourly Weather Streams

The weather stream data used in fire growth simulations consist of actual or forecasted weather and associated FWI System values with

a continuous temporal resolution of 1 h. Weather streams include a status field to indicate whether the values are actual values or values calculated from forecasted weather (Table 3). Each weather station in a Prometheus project can have multiple weather streams. If spatial weather modeling is turned off, then exactly one weather station and one of its weather streams must be assigned to each scenario. If spatial weather modeling is turned on, then multiple weather stations, and hence multiple weather streams, may be associated with a scenario, but one weather stream must be designated as the primary weather stream. Spatial weather modeling also calculates spatially explicit FWI System values (see section entitled "Spatial Interpolation").

Different methods are used to create weather streams with 1-h resolution, depending on the availability of weather data.

**Table 3. Example of an hourly weather stream exported from Prometheus, with header information**

| Date <sup>a</sup> | Hour <sup>b</sup> | Temp <sup>c</sup> | RH <sup>d</sup> | WD <sup>e</sup> | WS <sup>f</sup> | Precip <sup>g</sup> | HFFMC <sup>h</sup> | DMC <sup>i</sup> | DC <sup>j</sup> | BUI <sup>k</sup> | HISI <sup>l</sup> | HFWI <sup>m</sup> | Status <sup>n</sup> |
|-------------------|-------------------|-------------------|-----------------|-----------------|-----------------|---------------------|--------------------|------------------|-----------------|------------------|-------------------|-------------------|---------------------|
| 25/09/2001        | 0                 | 1.1               | 96              | 360             | 2               | 0                   | 96.7               | 58               | 462             | 88               | 12.09             | 33.68             | Actual              |
| 25/09/2001        | 1                 | -0.3              | 98              | 90              | 1               | 0                   | 95.0               | 58               | 462             | 88               | 9.11              | 27.83             | Actual              |
| 25/09/2001        | 2                 | -0.7              | 98              | 90              | 3               | 0                   | 93.3               | 58               | 462             | 88               | 7.95              | 25.33             | Actual              |
| 25/09/2001        | 3                 | -0.3              | 94              | 0               | 0               | 0                   | 92.2               | 58               | 462             | 88               | 5.89              | 20.50             | Actual              |
| 25/09/2001        | 4                 | 1.8               | 82              | 360             | 2               | 0                   | 91.4               | 58               | 462             | 88               | 5.77              | 20.19             | Actual              |
| 25/09/2001        | 5                 | 2.5               | 78              | 270             | 9               | 0                   | 90.5               | 58               | 462             | 88               | 7.25              | 23.76             | Actual              |
| 25/09/2001        | 6                 | 2.1               | 80              | 90              | 5               | 0                   | 89.7               | 58               | 462             | 88               | 5.31              | 19.01             | Actual              |
| 25/09/2001        | 7                 | 2.8               | 78              | 135             | 2               | 0                   | 89.2               | 58               | 462             | 88               | 4.20              | 15.96             | Actual              |
| 25/09/2001        | 8                 | 4.9               | 78              | 90              | 6               | 0                   | 88.5               | 58               | 462             | 88               | 4.68              | 17.31             | Actual              |
| 25/09/2001        | 9                 | 12.1              | 43              | 270             | 11              | 0                   | 88.6               | 58               | 462             | 88               | 6.07              | 20.92             | Actual              |

<sup>a</sup>Date = date of hourly file (dd/mm/yyyy).

<sup>b</sup>Hour = hour (0–23 format).

<sup>c</sup>Temp = temperature (°C).

<sup>d</sup>RH = relative humidity (%).

<sup>e</sup>WD = wind direction (degrees).

<sup>f</sup>WS = wind speed (km/h).

<sup>g</sup>Precip = precipitation (mm).

<sup>h</sup>HFFMC = hourly Fine Fuel Moisture Code.

<sup>i</sup>DMC = Duff Moisture Code.

<sup>j</sup>DC = Drought Code.

<sup>k</sup>BUI = Buildup Index.

<sup>l</sup>HISI = Hourly Initial Spread Index.

<sup>m</sup>HFWI = hourly Fire Weather Index.

<sup>n</sup>Status = actual or forecasted.

## Interpolating Diurnal Hourly Temperature and Wind Speed

If actual or forecasted hourly values are unavailable, the Prometheus model can use a dual sine-exponential function (Beck and Trevitt 1989), along with input maximum and minimum values, to interpolate diurnal variations in weather conditions over a 24-h period. Increased heating during the day is expressed as a truncated sine wave. Daily minimum and maximum temperatures must be input interactively via a dialog window or by importing an ASCII daily weather stream file with these values. The times at which the

minimum and maximum temperatures occur are set by applying two user-tunable parameters (Table 4): the parameter  $\alpha_T$  is the difference between the time of sunrise and the time of minimum temperature, and the parameter  $\beta_T$  is the difference between solar noon and the time of maximum temperature. The times of sunrise and sunset for any particular location are calculated internally within the Prometheus model. Nighttime cooling is modeled by means of an exponential decay function, which requires a user-tunable decay parameter ( $\gamma_T$ ). Since regionally specific values are not available for the  $\gamma_T$  parameter, a default value of  $-2.20$  is applied in Prometheus.

**Table 4. User-tunable parameters for temperature for forecasting diurnal weather conditions** (Beck and Trevitt 1989)

| Region           | Location |                |           | Parameter <sup>a</sup> |           |      |
|------------------|----------|----------------|-----------|------------------------|-----------|------|
|                  | Station  | Latitude       | Longitude | $\alpha_T$             | $\beta_T$ |      |
|                  |          | Default values |           |                        | -0.86     | 3.00 |
| British Columbia | 1110     | 57.88          | -123.61   | -0.2356                | 2.9376    |      |
|                  | 1111     | 56.03          | -121.99   | -0.8984                | 2.7739    |      |
|                  | 1314     | 53.50          | -125.77   | -1.3535                | 2.6011    |      |
|                  | 1317     | 55.13          | -126.21   | -0.8824                | 2.8301    |      |
|                  | 1502     | 54.07          | -121.83   | -1.2278                | 2.9707    |      |
|                  | 1706     | 51.90          | -124.60   | -1.0753                | 2.6498    |      |
|                  | 1731     | 52.33          | -123.39   | -0.9347                | 2.7876    |      |
|                  | 1814     | 51.52          | -119.11   | -0.7926                | 2.9628    |      |
|                  | 2035     | 50.61          | -120.83   | -0.4973                | 2.9882    |      |
|                  | 2713     | 49.78          | -116.36   | -0.3414                | 2.3543    |      |
|                  | 2805     | 56.01          | -129.09   | -1.0959                | 2.7948    |      |
|                  | 3001     | 59.34          | -125.51   | -0.5326                | 2.9447    |      |
|                  | 317      | 49.43          | -124.70   | -1.5898                | 2.6332    |      |
|                  | 905      | 59.58          | -133.66   | -2.0427                | 2.5383    |      |
| 906              | 57.85    | -130.00        | -1.7201   | 2.1466                 |           |      |
| Alberta          | C3-PO    | 49.02          | -113.60   | -0.8487                | 2.6264    |      |
|                  | P2-JA    | 56.88          | -116.55   | -0.4184                | 3.1536    |      |
| Alaska and Yukon | 319      | 66.00          | -157.56   | -2.2037                | 1.8045    |      |
|                  | 416      | 67.02          | -143.29   | -0.7896                | 2.0359    |      |
|                  | 621      | 61.64          | -156.40   | -1.4965                | 1.9343    |      |
|                  | 731      | 67.74          | -144.16   | -0.9538                | 2.2433    |      |
|                  | 936      | 62.60          | -142.00   | -0.3267                | 2.2559    |      |
| Atlantic         | NB212    | 47.04          | -66.36    | -1.0878                | 2.5439    |      |
|                  | NB301    | 46.19          | -65.43    | -0.8583                | 2.7607    |      |
|                  | NB408    | 46.71          | -66.82    | -0.6502                | 2.9872    |      |
|                  | NB408    | 47.71          | -66.82    | -0.7348                | 2.5678    |      |
|                  | NB419    | 45.57          | -67.09    | -0.6096                | 2.9651    |      |
|                  | NB513    | 47.45          | -67.63    | -0.4106                | 2.7883    |      |
| Quebec           | 111      | 45.64          | -76.01    | -0.0416                | 2.8052    |      |
|                  | 156      | 46.66          | -74.50    | -0.8182                | 2.6498    |      |
|                  | 211      | 47.10          | -78.21    | -0.1999                | 3.1846    |      |
|                  | 331      | 46.95          | -70.30    | -0.8499                | 2.6365    |      |
|                  | 432      | 48.14          | -72.63    | -0.2332                | 2.9982    |      |
|                  | 475      | 49.11          | -69.21    | -0.2598                | 2.8511    |      |
|                  | 482      | 48.71          | -66.80    | -0.5733                | 2.7888    |      |
|                  | 531      | 48.88          | -74.23    | -0.5765                | 2.6269    |      |
|                  | 562      | 50.73          | -75.05    | -0.2503                | 3.1012    |      |
|                  | 631      | 49.84          | -72.62    | -0.4623                | 3.0364    |      |
|                  | 663      | 50.65          | -69.10    | -0.1287                | 2.9442    |      |

<sup>a</sup>Parameter  $\alpha_T$  = time lag between the time of sunrise and the time of minimum temperature; parameter  $\beta_T$  = time lag between solar noon and the time of maximum temperature; parameter  $\gamma_T = -2.20$  (default value).

The interpolated diurnal trend in relative humidity is derived from the modeled changes in temperature and assumes that the absolute humidity of the air mass influencing the region remains constant during the 24-h forecast period. Relative humidity is estimated by calculating vapor pressure and saturated vapor pressure (Murray 1967).

The diurnal trend in wind speed follows that for temperature, with wind speed increasing from early morning to a maximum value in late afternoon. Daily minimum and maximum wind speed values are required as inputs to the model. The times at which the minimum and maximum wind speeds occur are also set by applying two additional user-tunable parameters: the parameter  $\alpha_{WS}$  is the difference between the time of sunrise and the time of minimum wind speed, and the parameter  $\beta_{WS}$  is the difference between solar noon and the time of maximum wind speed. Decreasing wind speeds are modeled using an exponential decay function, which requires a user-tunable decay parameter ( $\gamma_{WS}$ ).

Once a 24-h sequence of temperature, relative humidity, and wind speed has been created, these values can be manually edited in the weather stream. Wind direction is held constant during the forecast period. Although precipitation is an optional input, it is usually omitted from the forecast, since each hour is assigned a value equal to 1/24 of the input value.

Beck analyzed hourly data from 39 weather stations across Canada and Alaska (Table 4) (Beck, J.A. 2002. Table 1: Forecasting diurnal variations in meteorological parameters. PowerPoint presentation, Can. Interag. For. Fire Cent. Fire Sci. Technol. Work. Group Annu. Meet., Quebec, Quebec, 18–19 September 2003) and found that, on average, the daily minimum temperature occurs about 45 min before sunrise ( $\alpha_T = -0.77$ ), and the daily maximum temperature occurs about 3 h after solar noon ( $\beta_T = 3.00$ ). No clear trends in  $\alpha_{Tr}$ ,  $\beta_{Tr}$ , and  $\gamma_T$  were evident with latitude, and seasonal effects on these parameters were not examined; however, further analysis was recommended.

Beck did not calculate regionally specific wind speed parameters ( $\alpha_{WS}$ ,  $\beta_{WS}$ , and  $\gamma_{WS}$ ). The Prometheus model therefore uses default parameter values for wind speed ( $\alpha_{WS} = 1.00$ ,  $\beta_{WS} = 1.24$ , and  $\gamma_{WS} = -3.59$ ).

## Calculating Hourly *FFMC* and *ISI*

The moisture content of subsurface forest floor fuels, represented by *DMC* and *DC* (and therefore the *BUI*), is assumed to change little from hour to hour during a particular day, except when it rains. However, because of the fast response time of litter fuels to the cycle of daytime heating and nighttime cooling, their moisture content (represented by the *HFFMC*) can change in a way that substantially affects fire behavior. Wind speed, and therefore *ISI*, may also vary greatly during the course of a day.

Two methods are available to calculate the Hourly Fine Fuel Moisture Code (*HFFMC*). The Lawson et al. (1996) *HFFMC* method is based on analysis of diurnal trends in fine fuel moisture observed during around-the-clock sampling conducted near Prince George, BC (Muraro et al. 1969); the diurnal trend has a sine-wave form. The 24-h period beginning and ending at solar noon (spanning two calendar days) is divided into two phases: an afternoon drying and nighttime moisture recovery phase (1200–0559 LST), followed by a morning drying phase (0600–1159 LST). Expected *HFFMC* values are presented in separate tables for each phase in relation to the standard daily *FFMC* on the first day for both phases, and also in relation to relative humidity in the morning of the second day for the morning phase (Van Wagner 1972; Lawson et al. 1996).

The Van Wagner (1977) *HFFMC* method uses the same drying and wetting routines (Van Wagner and Pickett 1985; Van Wagner 1987) that are used in the standard daily *FFMC*, but at an hourly time scale and with appropriate adjustment of the log drying and wetting rates. *HFFMC* may be calculated at hourly time steps for any series of hours following an hour with a known *HFFMC* and a corresponding series of weather values. If *HFFMC* is not known, it may be initialized for any hourly series beginning at 1600 LST using the standard daily *FFMC* (initial *FFMC* and *HFFMC* values may also be derived from direct measurements of fine fuel moisture in the field at 1600 LST for *FFMC* and at any hour for *HFFMC*). The hourly drying rates were adjusted such that the *HFFMC* at 1600 LST calculated from a 24-h series over two days (1700–1600 LST) would agree with the standard daily *FFMC* for that day calculated from daily weather observations alone. Van Wagner (1977) noted that subhourly *FFMC* could be calculated

by adjusting the log drying and wetting rates for the time interval of interest.

The Lawson and Van Wagner *HFFMC* methods each have distinct advantages and disadvantages, and the choice between them for a given fire scenario can influence the final size and shape of the simulated fire. For example, the Lawson algorithm is appropriate only in the absence of rain, since it simply models the standard noon *FFMC* 24 h into the future. This restriction means that the effect of any rain event will not be incorporated into an estimate of *HFFMC* until after the next calculation of standard noon *FFMC*, at which point the Lawson algorithm calculates the *HFFMC* for the next 24 h. In contrast, the Van Wagner algorithm responds immediately to rain, lowering the *HFFMC* value accordingly. The response of these two algorithms to a 12.2-mm rain event in the afternoon (at 1500 LST) is shown in Figure 14.

The Lawson technique uses only daily *FFMC* values, and as such will create a discontinuity

in instantaneous *FFMC* values at noon LST. This is not an issue with Van Wagner *HFFMC* calculations. To address this discontinuity, Prometheus linearly interpolates Lawson *HFFMC* values from 1100 to 1200 LST. Note that this variation is not part of the Lawson technique, but is needed for realistic transitions at or around noon LST.

In the absence of rain, the overall diurnal amplitude of the *HFFMC* curve produced by the Van Wagner method is small. As a consequence, fire growth simulations for extended dry periods will exhibit nighttime growth of a fire in excess of what may actually be observed. The Lawson algorithm generates greater variation in *HFFMC* between daytime and nighttime (Figure 15), but this may not necessarily be more realistic. Actual nighttime variation may lie somewhere between the results of these two methods, and further research is required.

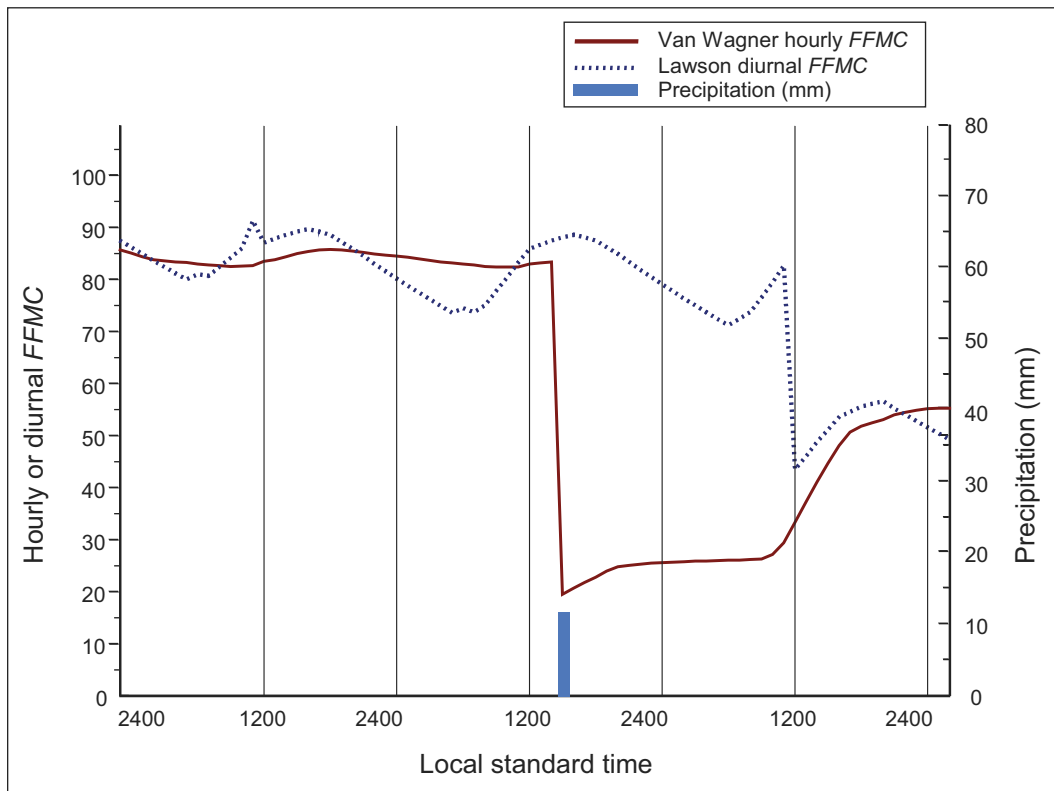


**Figure 14.** Variation in hourly Fine Fuel Moisture Code (*FFMC*) over three 24-h periods, as calculated by the Van Wagner (1977) and Lawson et al. (1996) algorithms, with rain in the afternoon of the second day. The Lawson algorithm (Lawson et al. 1996) applies total daily precipitation once a day at 1200 (noon), whereas the Van Wagner (1977) algorithm responds immediately to precipitation occurring between noon and noon on consecutive days.

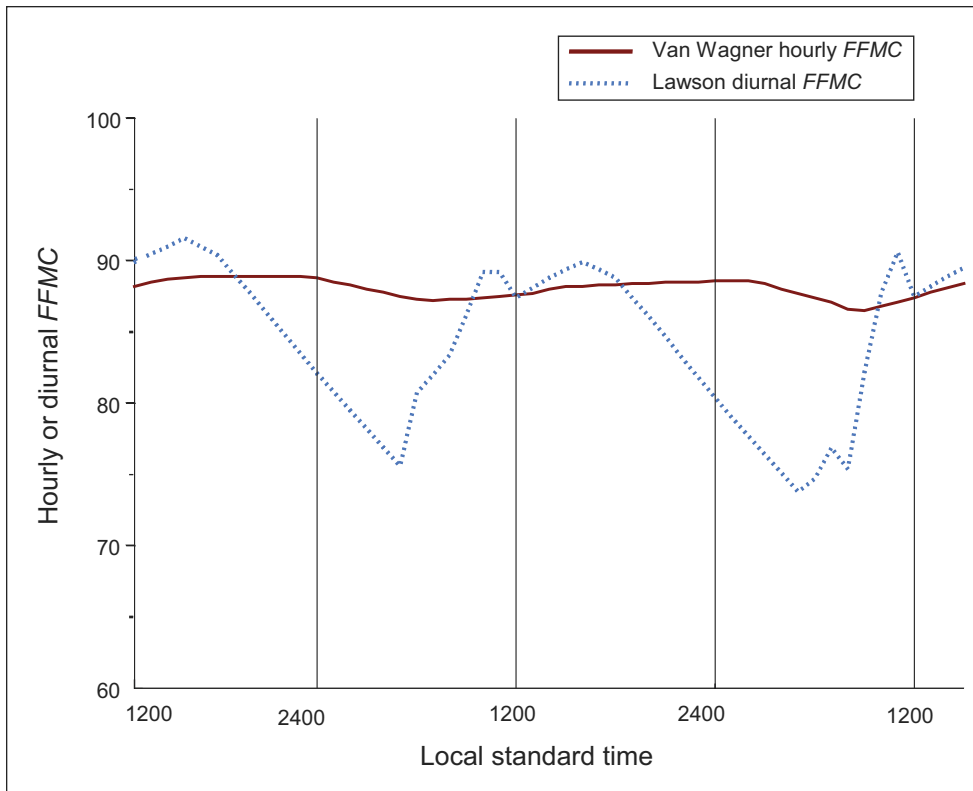


Figure 15. Variation in hourly Fine Fuel Moisture Code (FFMC) over two 24-h periods, as calculated by the Van Wagner (1977) and Lawson et al. (1996) algorithms in the absence of rain.

If the Van Wagner *HFFMC* method is used in a scenario, the burning period may be adjusted to restrict fire spread during the nighttime. Relative humidity and windspeed thresholds can also be applied to restrict fire spread to particular conditions.

The Hourly Initial Spread Index (*HISI*) is calculated from the calculated *HFFMC* and hourly wind speed. The Hourly Fire Weather Index (*HFWI*) is calculated from *HISI* and the daily *BUI*.

### Creating Weather Streams

Three different types of weather data can be used to create hourly weather streams:

- hourly weather data with FWI System values
- hourly weather data without FWI System values
- daily weather data

Daily weather data can also be input manually into Prometheus. A complete description of the specific input file formats appears in the *Prometheus Data I/O Standards Manual* (Canadian Wildland Fire Growth Simulation Model Data I/O Standards Technical Sub-Committee 2009).

The methods for creating hourly weather and FWI System streams are described for each data type in the following sections.

### Hourly Weather Data with FWI System Values

Hourly weather streams with associated FWI System values (Table 5) are used directly without further processing, provided there is a complete 24-h series for each day. If any of the weather variables are modified after import, then all of the FWI System values that depend on the edited entry are recalculated.

**Table 5. Example of an input hourly weather stream (over 3 h) with the calculated fuel moisture codes**

| Hourly <sup>a</sup> | Hour <sup>b</sup> | Temp <sup>c</sup> | RH <sup>d</sup> | Precip <sup>e</sup> | WS <sup>f</sup> | WD <sup>g</sup> | HFFMC <sup>h</sup> | DMC <sup>i</sup> | DC <sup>j</sup> |
|---------------------|-------------------|-------------------|-----------------|---------------------|-----------------|-----------------|--------------------|------------------|-----------------|
| 26/09/2001          | 0                 | 5.70              | 73              | 0.0                 | 2               | 360             | 91.0               | 60               | 488             |
| 26/09/2001          | 1                 | 6.40              | 73              | 0.0                 | 2               | 90              | 90.0               | 60               | 488             |
| 26/09/2001          | 2                 | 7.10              | 67              | 0.0                 | 3               | 90              | 90.0               | 60               | 488             |

<sup>a</sup>Hourly = date (dd/mm/yyyy); the column heading "hourly" indicates that the file type is hourly.

<sup>b</sup>Hour = hour (0–23 format).

<sup>c</sup>Temp = temperature (°C).

<sup>d</sup>RH = relative humidity (%).

<sup>e</sup>Precip = precipitation (mm).

<sup>f</sup>WS = wind speed (km/h).

<sup>g</sup>WD = wind direction (degrees).

<sup>h</sup>HFFMC = hourly Fine Fuel Moisture Code.

<sup>i</sup>DMC = Duff Moisture Code.

<sup>j</sup>DC = Drought Code.

### Hourly Weather Data without FWI System Values

Where an hourly weather stream does not include corresponding FWI System values, the *HFFMC* is calculated using either the Van Wagner algorithm (Van Wagner 1977, the default method used by Prometheus) or the Lawson algorithm (Lawson et al. 1996), as described earlier (see "Calculating the Hourly *FFMC* and *ISI*"). These methods are well defined for calculating codes forward in time. However, Prometheus can also perform calculations backward in time, using the Van Wagner algorithm for a portion of the first day in the weather stream, to attain that day's targeted *HFFMC*. Referred to as "today's *HFFMC*," this value is usually entered for 1600 LST, since the forecasted daily standard *FFMC*, calculated using noon weather observations, represents the potential fire behavior at that time.

The application of the Van Wagner *HFFMC* algorithm in Prometheus requires two inputs in addition to the standard hourly weather data:

- starting *HFFMC* value at time t for the first day of the weather stream
- previous day's precipitation (mm) from 1201 to 2359 LST

The application of the Lawson *HFFMC* algorithm in Prometheus requires two different inputs:

- daily standard (noon) *FFMC* for the previous day
- morning relative humidity for calculation period 0600–1159 LST, obtained from the weather stream

### Daily Weather Data

If hourly weather data are not available, they can be estimated from daily minimum and maximum temperature and wind speed, and minimum relative humidity (Table 6) using the procedure described in the section entitled "Interpolating Diurnal Hourly Temperature and Wind Speed." The previous day's *FFMC*, *DMC*, and *DC* and the amount of rainfall from 1201 to 2359 LST are required user inputs. The *HFFMC* value forecasted for the first day (i.e., "today's *HFFMC*") is also required. This target input is similar to that used when hourly weather data are input into Prometheus.

### Weather Grids and Patches

In Prometheus, a single weather stream represents data that applies consistently across the landscape when spatial weather modeling is turned off. The weather variables and FWI System components therefore apply across the entire landscape, irrespective of spatial or topographic variation. To model local wind phenomena, Prometheus supports ASCII wind speed and direction grids.

Wind direction and wind speed are applied to a scenario as separate grid sets. Multiple weather grid sets can be added to a scenario provided their start and end times do not overlap. Weather grids allow for the incorporation of more spatially detailed patterns of wind flow variability generated from wind simulation tools such as WindWizard (Butler et al. 2006) and WindNinja (Forthofer 2007).

**Table 6. Example of an input daily weather stream (3 days)**

| Daily <sup>a</sup> | Min_temp <sup>b</sup> | Max_temp <sup>c</sup> | RH <sup>d</sup> | Precip <sup>e</sup> | Min_ws <sup>f</sup> | Max_ws <sup>g</sup> | WD <sup>h</sup> |
|--------------------|-----------------------|-----------------------|-----------------|---------------------|---------------------|---------------------|-----------------|
| 02/05/2005         | -3.0                  | 16.0                  | 30              | 0.0                 | 0                   | 30                  | 90              |
| 03/05/2005         | 3.0                   | 12.0                  | 55              | 2.0                 | 2                   | 20                  | 180             |
| 04/05/2005         | 2.0                   | 10.0                  | 40              | 0.0                 | 2                   | 15                  | 180             |

<sup>a</sup>Daily = date (dd/mm/yyyy); the column heading "daily" indicates that the file type is daily.

<sup>b</sup>Min\_temp = minimum temperature (°C)

<sup>c</sup>Max\_temp = maximum temperature (°C).

<sup>d</sup>RH = minimum relative humidity (%).

<sup>e</sup>Precip = precipitation (mm).

<sup>f</sup>Min\_ws = minimum wind speed (km/h).

<sup>g</sup>Max\_ws = maximum wind speed (km/h).

<sup>h</sup>WD = wind direction.

A wind direction grid set can comprise one to eight grids, whereas the number of grids within a wind speed grid set is based on the wind speed ranges specified by the user. Weather grids are applied conditionally based on the observed or forecasted wind direction and wind speed values in the primary weather stream. These grids are provided at the same resolution, projection, and extent as those of the underlying FBP fuel-type grid. The weather grids are assigned user-specified start and end times, and diurnal application periods, to override the primary weather stream data.

Wind direction grids are applied to every day of a scenario for the specified start and end times. There are eight 45° predefined wind direction classes. Alternatively, a single wind direction grid can be applied for all directions. Wind speed grid sets include wind speed grids coupled with a wind direction class. For example, a wind speed grid may be available for a 30.0–39.9 km/h range, specific for the west wind direction class. This grid would be activated whenever the primary weather stream reports a wind direction between 247.5° and 292.4° and a wind speed between 30.0 and 39.9 km/h. A single wind speed grid can also be applied for all wind speeds. The primary weather stream provides wind direction and/or wind speed values for all wind direction classes and/or wind speed ranges that do not have corresponding imported grid files.

The wind speed and direction for specific areas can also be interactively modified in the Map View by creating weather patches. Alternatively, weather patches can be defined from perimeter data imported as a Shapefile (\*.shp) or a

Generate file (\*.gen). Weather patches are particularly useful for modeling the influence of localized terrain on weather. They can also be combined with weather grids. The case study in Appendix 2 includes the use of a weather patch to show that the 10-m open wind speeds recorded at the on-site weather station were not representative of the winds observed during the fire.

### Temporal Interpolation of Weather and FWI System Values

The weather stream data that are supplied for fire growth simulations have a continuous temporal resolution of 1 h. However, the spatial and temporal resolutions needed to ensure complete capture of landscape variation require more frequent sampling, so subhourly weather data must be used. Two basic methods are used to provide subhourly weather: standard and optional.

The standard approach applies piece-wise constant rules to the hourly weather stream; all weather and FWI System values therefore remain constant for the given hour. This approach, although straightforward and easy to use, may not accurately reflect weather that is in continual flux and may result in abrupt changes in weather values, and thus fire behavior, at the hourly time marker.

The optional approach applies linear interpolation to estimate the weather values at any subhourly time. These interpolated values are then used to calculate interpolated FWI System and FBP System outputs. Of note, the reported hourly wind is specified as a 10-min average,

but Prometheus uses it as a simple data point occurring at the specified time. The following weather inputs are used:

- Temperature, dew point, relative humidity, and wind speed values are linearly interpolated from adjacent hourly weather values.
- Precipitation assumes a uniform distribution of rainfall during the hour and is not scaled.
- Wind direction follows a complex set of rules that perform linear interpolation for changes in wind direction of less than 180°. A piece-wise constant approach is assumed if the hour starts or ends with no wind speed or if the wind direction changes by 180° during the hour. This piece-wise constant approach is assumed to take place at the half-hour mark.

FWI System values are then calculated from the appropriate subhourly weather values. However, the *FFMC* model's standard conversion between moisture content and code value (equation 2, Van Wagner 1987), while it accounts for single day or hourly calculations, contains a small systematic bias. This leads to an accumulated error after iterative calculations in relatively

unchanging conditions. This is a function of the constants in the equations describing what is known as the FF-scale (Van Wagner 1987). The FF-scale is a transformation to convert litter moisture content to *FFMC*. It replaced earlier *FFMC* scale equations and was adopted for the 1984 version of Van Wagner's *HFFMC* (Alexander et al. 1984).

Two new equations describing the FF-scale were therefore devised for subhourly applications (by increasing the number of significant digits for one coefficient), to minimize the conversion error:

$$MC = \frac{147.27723 \cdot (101 - HFFMC_{in})}{59.5 + HFFMC_{in}} \quad [8]$$

$$HFFMC_{out} = \frac{59.5 \cdot (250 - m)}{147.27723 + m} \quad [9]$$

where *MC* is the previous (initial) time step fine fuel moisture content, *HFFMC<sub>in</sub>* is the previous (initial) time step Hourly Fine Fuel Moisture Code, *HFFMC<sub>out</sub>* is the Hourly Fine Fuel Moisture Code at the next time step, and *m* is the new moisture content at the next time step. The remaining published Van Wagner equations and methodology are unchanged.

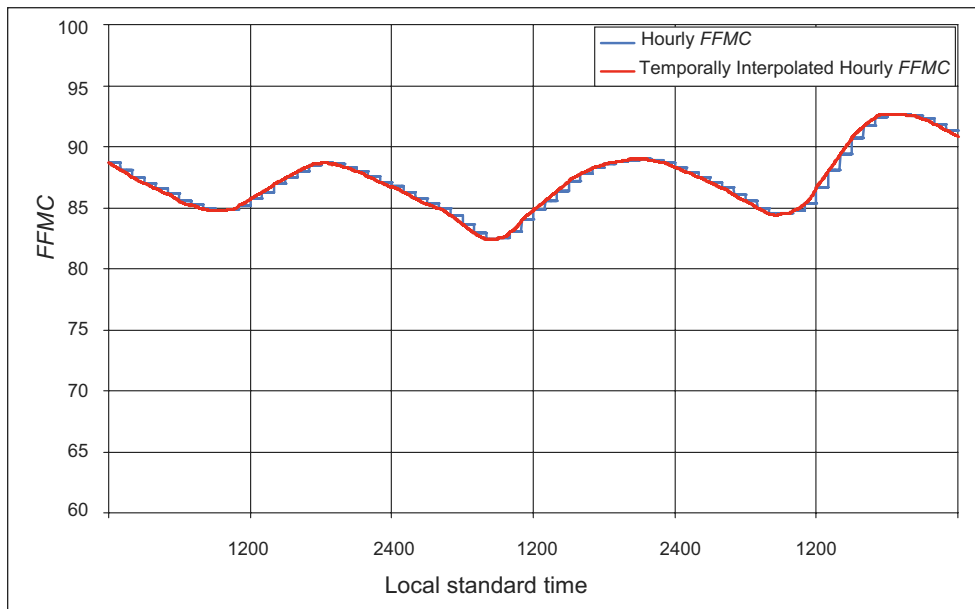


Figure 16. Effects of temporal (subhourly) interpolation on hourly Fine Fuel Moisture Code (*FFMC*) values.

However, the revised formulation, when applied to standard *HFFMC* calculations, would also result in consistent underestimation of computed *HFFMC* values. The adoption of a hybrid approach resolves the discrepancy between subhourly and hourly calculations. This method uses the original formulation to calculate *HFFMC* values and the revised formulation to calculate subhourly *FFMC* values. This approach ensures that Prometheus adheres to the existing equations and standards, while providing reasonable subhourly FWI System values (Wotton et al. 2009). Figure 16 shows the effects of temporal interpolation on *FFMC* values.

It should be noted that although weather conditions such as temperature and relative humidity may change rapidly under some circumstances (e.g., in advance of a cold front), fine fuels do not respond instantaneously. Thus, subhourly calculation of *FFMC* (*HFFMC*) may suggest a precision that is beyond the accuracy of the model.

### Spatial Interpolation

The spatial weather modeling module in Prometheus allows multiple weather stations and weather streams to be assigned to a single scenario. This module can also be applied to a single weather stream to account for variation in spatial elevation across the landscape.

Spatial interpolation allows more than one weather station, and hence weather stream, to be used to obtain spatially explicit temperature, relative humidity, and precipitation values in a scenario. When this technique is turned on, dew-point temperatures (°C) are first calculated at each weather station using equations 10 to 12 (National Oceanic and Atmospheric Administration 2008a, 2008b). The weather station temperatures (°C) and calculated dew-point temperatures (°C) are then normalized to zero meters above sea level using unsaturated and saturated lapse rates (rates of temperature change with elevation change). The lapse rate calculations require temperature, relative humidity (%), and atmospheric pressure (millibars) as inputs and are described in American Meteorological Society (2009a, 2009b). Atmospheric pressure is calculated at the elevation of the respective weather station using the approach outlined in National Aeronautics and Space Administration (2008a, 2008b).

The normalized temperatures and dew-point temperatures are spatially interpolated to all grid cells using inverse-distance weighting (exponent value of 2). The spatially interpolated temperatures and dew-point temperatures are then corrected on the basis of the elevation at each grid cell using spatially interpolated lapse rates.

Relative humidity is calculated at each cell by inverting equation 11 and using spatially interpolated inputs of vapor pressure (millibars) and saturated vapor pressure (millibars). Spatially interpolated vapor pressure is calculated for each grid cell by inverting equation 12 and inputting a spatially interpolated dew-point temperature. Likewise, spatially interpolated saturated vapor pressure is calculated for each grid cell by using equation 10 and inputting a spatially interpolated temperature.

$$VP_{sa} = 0.6112 \times 10.0^{\frac{7.5 \times T}{237.7 + T}} \quad [10]$$

$$VP = \frac{RH \times VP_{sa}}{100} \quad [11]$$

$$DP = \frac{237.7 \times \log_{10} \frac{VP}{0.6112}}{7.5 - \log_{10} \frac{VP}{0.6112}} \quad [12]$$

where  $VP_{sa}$  is the saturated vapor pressure (millibars),  $T$  is the temperature (°C),  $VP$  is the actual vapor pressure (millibars),  $RH$  is the relative humidity (%), and  $DP$  is the dew-point temperature.

Voronoi polygons are used to define areas of influence for each weather station. The precipitation recorded at each weather station is then applied uniformly to the respective areas

If spatial weather modeling is activated, then the starting codes are spatially interpolated (identified by the subscript "s"; e.g., *HFFMC<sub>s</sub>*) using inverse-distance weighting, to maintain consistency with the weather data interpolation. Changes in elevation are not accounted for when starting codes are interpolated. Instantaneous FWI System values are then calculated using the interpolated starting codes and the interpolated instantaneous weather conditions, as described previously. FWI System calculations requiring latitude as an input use the actual latitude for the specified location.

---

## FIRE GROWTH SIMULATION

---

Fire polygons and their vertices are fundamental to fire simulation in Prometheus. Fires are initiated and iteratively grown as polygons. Fire behavior (including the dimensions of theoretical firelets) is calculated for each vertex around the polygon perimeter. As new vertices are located according to the firelet dimensions, a new fire perimeter polygon is formed at each time step in a burning period. All of these processes occur within the FireEngine module.

Each vertex on a fire polygon perimeter is classified as active or inactive. An active vertex is allowed to continue to propagate in the next time step. A vertex is deactivated (becomes inactive) when it encounters a grid cell containing a nonfuel type, a fuel break, or an area that has already burned or if conditions do not allow for fire spread. Once a vertex has been flagged as inactive it cannot be reactivated, which means that Prometheus does not consider states like smoldering.

Prometheus applies an interrupt-driven propagation model. Fire polygons are displayed at intervals matching the specified display time step. However, the landscape sampling frequency (and hence internal calculations) is based on the user-defined distance resolution, its corresponding dynamic time steps, and any specific events that might interrupt the simulation (e.g., fuel break, fuel-type patch, weather patch, ignition time). The order and set of operations are described in Appendix 3.

### Scenario Settings and Parameters

Before a fire growth simulation is executed, several settings and parameters can be specified: buildup effect, terrain effect, *FMC* override, FBP System equation parameters that influence fire spread rates, fire growth at the landscape extent, the period of the day for which fire growth is to be simulated, and the spatial and temporal thresholds that influence the resolution of fire perimeters.

### Buildup Effect

The concept of fuel availability contributing to rate of spread was introduced by Van Wagner (1989). McAlpine (1995) examined several data sets and showed that a fuel consumption effect on fire spread rate occurred under low wind conditions. To incorporate this relationship, a Buildup Effect (*BE*) function is incorporated into the FBP System as a multiplier of the *ISI*. This function assumes a zero rate of spread when the *BUI* is zero. The influence of *BUI* on rate of spread increases rapidly as *BUI* increases. *BE* is 1.0 at  $BUI_0$  (average *BUI* specific to the fuel type) and levels off at a value above 1.0 (but well below 2) as *BUI* increases (Forestry Canada Fire Danger Group 1992). The Buildup Effect on spread rate can be turned on or off in Prometheus.

### Terrain Effect

A vector approach is used to blend the effects of wind speed and terrain on fire spread (McAlpine and Wakimoto 1991; Forestry Canada Fire Danger Group 1992). The effect of slope and aspect on fire spread rate and direction is converted to an "equivalent wind speed" vector, which is then added to the vector representing the observed wind speed and direction to calculate a net effective wind speed and net effective wind direction, referred to as *WSV* and *RAZ*, respectively. These operations, designated as the Terrain Effect in Prometheus, can be turned on or off depending on whether the appropriate slope and aspect landscape grids are available.

### FMC Override

The FBP System includes equations to calculate *FMC* values for any area within Canada from elevation, latitude, and longitude. If an elevation layer is not available for a particular Prometheus scenario, a default elevation should be provided. If *FMC* has been measured directly, it may be used in Prometheus through the *FMC* Override. For applications outside Canada, an *FMC* must be provided.

### FBP System Equation Parameters

The parameters used in the standard FBP fuel-type equations can be adjusted if local conditions dictate; however, users are advised to exercise caution when making such modifications. These parameters can be restored to their default values at any time. Table 2 summarizes the parameters that can be modified in the Prometheus model.

### Fire Growth at the Landscape Extent

Prometheus allows users to decide whether to stop the simulation if a vertex spreads beyond the extent of the landscape. If this option is turned off, then any vertex still within the extent of the landscape will continue to spread, which will change the subsequent shape of the fire. For example, even if the front of the fire stops at the boundary of the landscape, the flanks and back will continue to spread.

### Daily Burning Period

The burning period (the period of active fire growth) can be set before a simulation is run by defining start and end times for each day within the scenario. Optional thresholds for wind speed and relative humidity can also be specified, and fire growth will stop if these thresholds are reached. The thresholds for wind speed and relative humidity apply irrespective of the burning periods.

### Spatial and Temporal Resolution

Two types of FireEngine application settings influence the distance, or spacing, between vertices around the perimeter of a polygon and the distance between successive polygons during fire growth simulation: the scenario's spatial resolution and its temporal resolution, both of which are defined by the user.

Spatial resolution is characterized by two parameters: distance resolution and perimeter resolution. Distance resolution, referred to as  $\Delta P_{\tau}$ , specifies the maximum distance that vertices can travel before the landscape and weather are resampled and the rate and direction of fire spread recalculated. Its default value of 1 grid unit (grid cell size in meters), for example, requires the vertices to resample at a rate that is not higher than the resolution of the

landscape grids, to ensure that the heterogeneity within the landscape is captured and used in the simulation. Vertices are propagated using dynamic time steps based on the time it takes the fastest vertex to reach the specified distance resolution.

Distance resolution has a significant effect on the time required to complete a simulation and on the accuracy of the simulation's output when this setting is substantially different from the sampled resolution of the gridded data. Larger values will result in vertices skipping landscape features, whereas smaller values will increase computer processing time and may introduce "grid ghosting" effects.

Perimeter resolution, referred to as  $L_{\tau}$ , is also expressed in grid units and is the maximum allowable distance between any two adjacent vertices. When the threshold  $L_{\tau}$  is exceeded, new vertices are added to the perimeter. This influences both the smoothness of the perimeter and the ability to capture landscape variability. The effects of  $L_{\tau}$  are discussed in more detail in the section entitled "Inter-vertex Weighted Distance Threshold."

Temporal resolution is controlled by two user-defined parameters. The first is the maximum calculation time step, referred to as  $t_{\tau e}$ , which specifies the maximum duration of a time step before the landscape and weather stream must be resampled when the fire is spreading at an equilibrium rate of spread. The second temporal resolution parameter, referred to as  $t_{\tau a}$ , specifies the maximum calculation time step during acceleration. These parameters ensure that sampling occurs at reasonable increments and that variability in the weather stream is captured, especially when spread rates are slower, to avoid inappropriately underestimating fire growth during acceleration. The default values for  $t_{\tau e}$  and  $t_{\tau a}$  are 60 min and 2 min, respectively.

### Fire Initiation

Fires can be initiated in Prometheus in three ways: as very small circular polygons representing points (pseudo-points), as very thin polygons representing lines (pseudo-lines), or as any other type of polygon representing an active fire.

### Point Ignition

All lightning-caused fires and many human-caused fires originate as point ignitions. Simulation of fire spread from a point ignition is initialized by creating a 16-sided polygon (hexadecagon) approximating a circle 0.5 m in diameter and centered on an ignition point provided by the user (Figure 17a). The 16 vertices of this pseudo-point are ordered in a counterclockwise direction and become the starting points for fire propagation. The actual (single) ignition point cannot be used because the partial differential equations require neighboring vertices to correctly orient growth. Although the number of starting vertices is a user-tunable parameter, the default setting was based on an analysis of the numeric error in the curvature (caused by discretizing a circle into a polygon) relative to the number of vertices; accuracy does not improve with more than 16 vertices.

The diameter of 0.5 m for the ignition pseudo-point was chosen to represent a reasonable minimum size of a fire that may be of interest for simulation modeling. In the current version of Prometheus, this size cannot be modified. Previous versions of Prometheus associated the size of this circle with the resolution of the spatial data, but this did not consider the widths of vector fuel breaks or the association between time and the size of a theoretical fire during its acceleration phase. Intersections with vector fuel breaks are discussed in the section entitled "Vector Fuel Breaks."

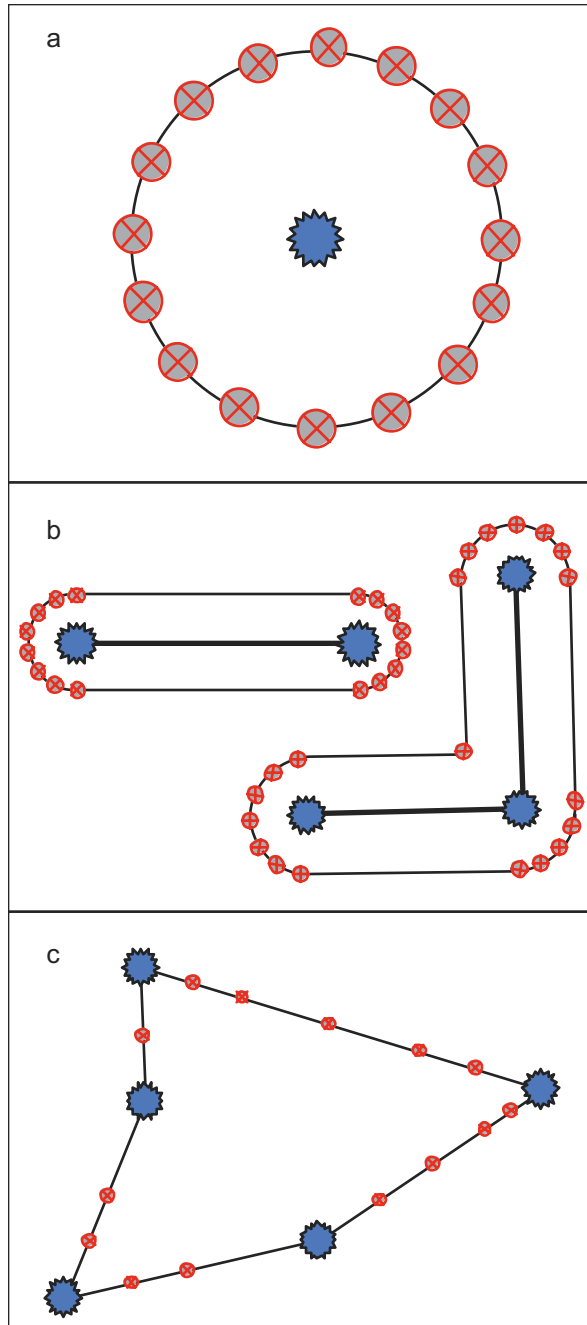


**Figure 17. Simulation of ignition in Prometheus.** a. Ignition from a pseudo-point, comprising 16 vertices (red crossed circles) around the perimeter of a circle 0.5 m in diameter (solid black line) centered on the ignition point (blue dot). b. Ignition from a pseudo-line, comprising at least 16 vertices (red crossed circles) around the perimeter of a polygon 0.5 m in width and > 0.5 m in length (thin black line) centered on an ignition line (thick black line) defined by  $n$  points ( $n \geq 2$ ) (blue dots). Eight vertices are used to define a half circle at each end of the polygon. Additional vertices are inserted only as required to accurately represent any curves along the line and to meet the specified distance between vertices ( $L_{\perp}$ ). c. Ignition from a polygon defined by  $n > 2$  polygon vertices identified by the user (blue dots) and an unlimited number of additional vertices (red crossed circles) along the ignition fire perimeter (solid black line), inserted according to the perimeter resolution.

### Line Ignition

In some fire management applications it may be of interest to simulate fire spread from an ignition line. Ignition lines may be used in some prescribed fire operations or in burn-outs conducted as part of a fire suppression action.

A line ignition is initialized by creating a polygon approximating two half circles joined by parallel lines 0.5 m apart, centered on an ignition line defined by  $n$  points (where  $n \geq 2$ ) and provided by the user (Figure 17b). This pseudo-line is represented by a default minimum of 16 vertices (as defined for point ignition), ordered in a counterclockwise direction. These vertices become the starting points for fire propagation because the two or more points defining the actual ignition line cannot be used in the partial differential equations requiring neighboring vertices.

Eight vertices are used to define a half-circle at each end of the polygon. Additional vertices are inserted only as required to accurately represent any curves along the line and to meet the specified distance between vertices ( $L_\tau$ ). The algorithm that rediscrretizes fire polygons introduces new vertices when necessary. The user-defined number of starting vertices for the ignition point is also used for the line ignition.

### Polygon Ignition

In many wildfire applications it may be of interest to simulate fire growth from an existing active fire perimeter. This process is facilitated in Prometheus through a polygon ignition.

An ignition polygon is defined by a minimum of 3 points provided by the user (Figure 17c). These points become the polygon vertices and the starting points for fire propagation. There is no maximum number of vertices for an ignition polygon.

The rotation of the vertices of the ignition polygon is first determined and corrected to a counterclockwise orientation using a technique derived from Weisstein (1999). Self-intersecting polygons are untangled to avoid confusion about the orientation of various fire fronts. Although Prometheus can theoretically grow imported polygon ignitions "inward," which would require clockwise orientation of the vertices, this feature is not currently available. Furthermore, any holes in an imported polygon ignition intended

to be grown inward will be removed. The distances between vertices may exceed  $L_\tau$ , and the algorithm that rediscrretizes fire polygons introduces new vertices when necessary.

### Fire Behavior at Vertices and Fire Statistics

The final step in initiating a fire is to calculate the fire behavior characteristics at the vertices of the ignition polygon (or the ignition pseudo-point or pseudo-line). Prometheus uses FBP System equations, FWI System values, and the fuel type, slope, and aspect of the underlying grid cell to calculate the rate of spread at each vertex on the fire perimeter for subsequent use in fire-front wave propagation equations. The development and structure of the FBP System has been described in detail elsewhere (Forestry Canada Fire Danger Group 1992; Wotton et al. 2009). Other outputs, including fire intensity and crown fraction burned, are calculated to characterize variation around the fire perimeter. Finally, the perimeter of the polygon is calculated by determining the distance between vertices and summing them. The polygonal area is calculated using the trapezoid method, whereby the polygon is divided into trapezoids and the area of all trapezoids is summed (Blakemore 1984).

### Acceleration and Use of $ROS_t$

The FBP System calculates a single equilibrium head fire rate of spread ( $ROS_e$ ) for each fuel type. However, a fire growing from a point-source ignition accelerates for a period of time until the equilibrium rate of spread is attained. For open-canopy fuel types, this elapsed time to equilibrium rate of spread is on average about 20 min (Forestry Canada Fire Danger Group 1992). Field observations suggest that longer and more variable periods are required to reach an equilibrium rate of spread in closed-canopy fuel types (Forestry Canada Fire Danger Group 1992). The elapsed time (from 20 to 75 min) depends on the amount of crown involvement. Acceleration in closed-canopy fuels is influenced by within-stand winds and by ambient winds above the stand. When the acceleration setting in Prometheus is turned on, the open-canopy and closed-canopy acceleration models (Forestry Canada Fire Danger Group 1992) are applied appropriately to each active vertex on the fire front.

Prometheus therefore uses  $ROS_t$  (head rate of spread at elapsed time  $t$ ) to correctly account for acceleration. Different ignitions may start at different times, so each fire polygon is conceivably in a different phase of its acceleration curve. If a single ignition is still accelerating, then  $t_{\tau a}$  (maximum calculation time step during acceleration) is used, rather than  $t_{\tau e}$  (maximum calculation time step during equilibrium rate of spread). The ratio between  $ROS_t$  and  $ROS_e$  determines whether an ignition is still accelerating. Equilibrium is assumed when  $ROS_t$  reaches 90% of  $ROS_e$ .

The use of  $t_{\tau a}$  ensures adequate sampling of  $ROS_t$  during this acceleration phase. This threshold is required because the FBP equation for calculating distances with consideration of acceleration (equation 72 in Forestry Canada Fire Danger Group [1992]) is not used. Using that equation would correct for changes in  $ROS_t$  during acceleration but would unnecessarily complicate the interrupt-driven time step algorithm and its logic with respect to  $L_{\tau}$ .

## Fire Perimeter Behavior and Management

In each time step following an ignition event, vertices are propagated forward at dynamic time steps. Vertices are added, removed, and adjusted to generate realistic simulations in Prometheus. The order of operations for a simulation step is as follows:

1. Calculate and adjust the new vertex locations that determine the fire perimeter for the next time step ( $\vec{P}_{j+1}$ ) based on  $\vec{P}_j$  and  $ROS$  values, using either two- or three-dimensional partial differential equations.
2. Smooth the new fire perimeter  $\vec{P}_{j+1}$ .
3. Adjust  $\vec{P}_{j+1}$  according to any landscape features that may impede advancement of the fire:
  - Deactivate vertices if grid or vector fuel breaks, other fires, or the landscape extent is encountered.
  - Breach nonfuels.
4. Rediscretize the fire perimeter:
  - Check for inter- and intra-fire intersections (which may introduce new vertices but will not change the combined shape of the fires).
  - Purge any unnecessary or redundant vertices by eliminating loops along the

fire front (without affecting the shape of the active fire front).

- Introduce any new vertices in preparation for the calculations necessary to determine  $\vec{P}_{j+2}$ .
5. Calculate new fire behavior characteristics (such as  $ROS$  and Fire Intensity  $[FI]$ ) and the polygon perimeter length and area for the final set of vertices.

The sequence of operations is detailed in Appendix 3. The logic and algorithms required to support the correct operation of the original partial differential equations can be more computationally expensive than the equations themselves, and are thus described in detail in the appendix. Original ad hoc heuristics in earlier versions of Prometheus have been replaced with well-defined algorithms that correctly handle overlapping fires and vector breaks.

## Propagation of the Fire Perimeter

The fire perimeter is propagated using the partial differential spread equations developed by Richards (1995, 1999). The discussion and equations in the following section, "Two-dimensional Transformations," are based on the following definitions:

$\Delta t$  defines the duration of the time step applied to a given simulation iteration. This temporal resolution is calculated dynamically and is expressed in seconds. It is applied uniformly to all vertices in the calculation time step.  $\Delta t$  often varies significantly between time steps.

$\vec{P}_j$  represents the set of vertices defining the fire perimeter at time iteration  $j$ . Each vertex retains a variety of statistical information, as well as state information, such as whether the vertex is active or inactive (due to no rate of spread or no fuel or because of location at an intersection with a fuel break or another fire).

$P_j^i$  defines a specific vertex on the fire perimeter at time iteration  $j$ , where  $i = 0 \dots N_j - 1$  and  $\vec{P}_j$  is divided into  $N_j$  discrete vertices,  $\vec{P}_j = \{P_j^0, \dots, P_j^{N_j-1}\}$ . The set of vertices are ordered so as to form a closed loop (polygon), so that  $P_j^0$  can be substituted for  $P_j^{N_j}$ . Vertices must be oriented counterclockwise for the fire to burn outward.

$P_{x_j}^i$ ,  $P_{y_j}^i$ , and  $P_{z_j}^i$  represent different dimensional components of  $P_j^i$ .

$\Delta P_j^i = P_{j+1}^i - P_j^i$  and is described as the change in location of a particular vertex from the current time step to the next time step.

$L_j^i = \|P_j^i - P_j^{i-1}\|$  and is described as the length of an edge defining a portion of the fire perimeter.

$ROS_{tj}^i$ ,  $FROS_{tj}^i$ ,  $BROS_{tj}^i$ , and  $RAZ_j^i$  represent the FBP outputs head fire rate of spread, flank fire rate of spread, back fire

spread rate, and net effective spread direction, respectively, for the vertex  $P_j^i$ .

### Two-dimensional Transformations

The two-dimensional differential equations described by Richards (1993) are accessed by the Prometheus COM and the Prometheus Tester Suite. Earlier versions of Prometheus (before version 5.2.2) used the two-dimensional differential equations when no digital elevation model data were present, or when the user explicitly requested these equations:

$$\Delta P_{x_j}^i = \Delta t \left( \frac{-a_e^2 \sin(\theta)[-y_s \sin \theta + x_s \cos \theta] + b_e^2 \cos(\theta)[y_s \cos \theta + x_s \sin \theta]}{\sqrt{a_e^2 [-y_s \sin \theta + x_s \cos \theta]^2 + b_e^2 [y_s \cos \theta + x_s \sin \theta]^2}} + c_e \sin \theta \right) \quad [13]$$

$$\Delta P_{y_j}^i = \Delta t \left( \frac{-a_e^2 \cos(\theta)[-y_s \sin \theta + x_s \cos \theta] - b_e^2 \sin(\theta)[y_s \cos \theta + x_s \sin \theta]}{\sqrt{a_e^2 [-y_s \sin \theta + x_s \cos \theta]^2 + b_e^2 [y_s \cos \theta + x_s \sin \theta]^2}} + c_e \cos \theta \right) \quad [14]$$

where

$$a_e = \frac{ROS_{tj}^i + BROS_{tj}^i}{2} \quad [15]$$

$$b_e = FROS_{tj}^i \quad [16]$$

$$c_e = \frac{ROS_{tj}^i - BROS_{tj}^i}{2} \quad [17]$$

$$\theta = RAZ_j^i \quad [18]$$

$$x_s = \frac{P_{x_j}^{i+1} - P_{x_j}^{i-1}}{2 \Delta s} \quad [19]$$

$$y_s = \frac{P_{y_j}^{i+1} - P_{y_j}^{i-1}}{2 \Delta s} \quad [20]$$

$$\Delta s = \frac{2\pi}{N_j} \quad [21]$$

$N_j =$  number of vertices at time step  $j$

The values  $a_e$ ,  $b_e$ , and  $c_e$  define the dimensions of the theoretical ROS ellipse at  $P_j^i$  (ignition point), as shown in Figures 1 and 18. The angle  $\theta$  orients the ellipse and represents the direction for maximum potential fire spread.

The values  $x_s$  and  $y_s$  determine the direction at which the growth vector (within the theoretical ellipse) will extend from  $P_j^i$ . They are the central difference approximations to  $dx/ds$  and  $dy/ds$ . Figure 18 illustrates how the  $x_s$  and  $y_s$  variables in the two-dimensional partial differential equations interact.

The values  $\Delta P_{x_j}^i$ ,  $\Delta P_{y_j}^i$ , and  $P_j^i$  together determine the location of  $P_{j+1}^i$ . The theoretical ellipse defined at  $P_j^i$ , and its orientation, is assumed to be the same at the neighboring vertices. Vectors tangential to and including the ellipses are conceptually extended to the point of intersection.  $P_{j+1}^i$  is placed on the ellipse along the vector from  $P_j^i$  through the point of intersection. This technique assumes no slope and also assumes that  $RAZ(\theta)$  is locally constant (i.e., duplicated at the two neighboring vertices). The assumption that neighboring vertices have the same ellipse shape and orientation has proven reasonable for fire growth simulation.

The  $a_e$ ,  $b_e$ , and  $c_e$  parameters are used to define the dimensions of an ROS ellipse. In previous versions of Prometheus, the ellipse represented distances traveled. The current approach allows  $\Delta t$  to be calculated (rather than requiring that it be provided), on the basis of the maximum ROS and the  $L_{\tau}$ ,  $t_{\tau e}$ , and  $t_{\tau a}$  tuning parameters.

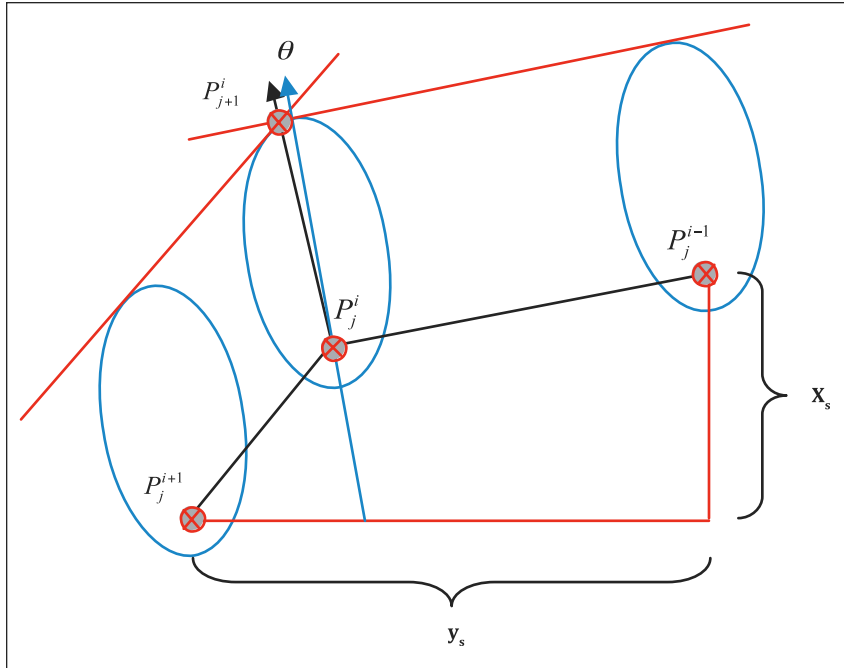


**Figure 18.** Formation of a new fire perimeter (red line) using the tangential envelope of the theoretical firelets (blue ellipses) projected from vertices (red crossed circles) along the existing fire perimeter (solid black line).  $P_j^i$  = specific vertex on the fire perimeter,  $j$  = time step,  $x_s$  and  $y_s$  = Euclidean distances from the ignition points,  $\theta$  = spread direction vector.

### Transformations for Sloping Terrain

The two-dimensional equations described above are appropriate for flat terrain. However, in three dimensions, the theoretical ellipses must be oriented onto the surface, which may have a slope. The three-dimensional equations resolve this issue by providing a geometric framework for the growing ellipses on the surface plane at each vertex. These equations are applied in Prometheus version 5.3 for both two- and three-dimensional surfaces. Richards (1999) described the basis of the three-dimensional equations in detail. The three-dimensional surface defined by Richards is expressed as a continuous equation,  $z = F(x, y)$ . Data about elevation (as well as slope and slope azimuth) are sampled across the landscape at the grid-cell resolution and are stored in a digital elevation map. The data set for this model is treated as a piece-wise constant, where elevations, slope, and slope azimuth are not interpolated between sample locations.

The three-dimensional partial differential equations are calculated in a multistep process. The equations for calculating  $a_e$ ,  $b_e$ , and  $c_e$  are consistent with those used for the two-dimensional partial differential equations.

$\vec{N}_j^i$  is defined as the unit length vector, which is normal to the surface at  $P_j^i$ . Whereas Richards (1999) calculated this vector on the basis of partial derivatives of the surface equation [ $z = F(x, y)$ ], Prometheus simply uses the information about slope, aspect and azimuth provided (or calculated) by the rasterized elevation grid. Although  $P_{j+1}^i$  will in all likelihood reside in a different cell on the digital map, which may contain different digital elevation model data, only the surface at  $P_j^i$  is examined.

$\vec{\theta}_j^i$  is similar to  $\theta$ , used in the two-dimensional equations, in that it is defined as the effective wind direction at  $P_j^i$ ; however, it is expressed as a vector of unit length in three dimensions and follows the landscape terrain.  $\theta_{x_j}^i$  and  $\theta_{y_j}^i$  are calculated from  $RAZ_j^i$ , and, for consistency,  $\theta_z^i$  is calculated from the data provided about slope, aspect, and azimuth (this angle is used to orient the theoretical ellipse at  $P_j^i$ ).

$\vec{r}_j^i$  is the unit tangent vector to the curve  $P_j$  at the vertex  $P_j^i$ ; it points in the direction along which  $\theta$  increases. In two dimensions,  $\vec{r}_j^i$  would be  $(x_s, y_s)$ , where  $x_s$  and  $y_s$  are calculated as in equations 19 and 20. As for  $\vec{\theta}_j^i$ ,  $r_{x_j}^i$  and  $r_{y_j}^i$

are calculated in a consistent manner (with the calculation for  $r_{y_j}^i$  being similar to that for  $r_{x_j}^i$ , as shown in equation 22), and  $r_{z_j}^i$  is calculated from  $r_{x_j}^i$ ,  $r_{y_j}^i$ , slope, aspect, and azimuth.

$$r_{x_j}^i = \frac{L_j^{i+1}(P_{x_j}^{i+1} - P_{x_j}^i) - L_j^i(P_{x_j}^{i-1} - P_{x_j}^i)}{\|L_j^{i+1}(P_{x_j}^{i+1} - P_{x_j}^i) - L_j^i(P_{x_j}^{i-1} - P_{x_j}^i)\|} \quad [22]$$

Given these vectors, the following can be defined:

$$\vec{n}_j^i = \vec{r}_j^i \times \vec{N}_j^i \quad [23]$$

$$\cos \varphi = \vec{n}_j^i \cdot \vec{\theta}_j^i \quad [24]$$

$$\sin \varphi = (\vec{N}_j^i \times \vec{\theta}_j^i) \cdot \vec{n}_j^i \quad [25]$$

Finally, the vertex is moved as follows:

$$\Delta P_{x_j}^i = \Delta t \left( \left[ \frac{a_e^2 \cos \varphi}{\sqrt{a_e^2 \cos^2 \varphi + b_e^2 \sin^2 \varphi}} + c \right] \theta_{x_j}^i + \left[ \frac{b_e^2 \sin \varphi}{\sqrt{a_e^2 \cos^2 \varphi + b_e^2 \sin^2 \varphi}} \right] (N_{y_j}^i \theta_{z_j}^i - N_{z_j}^i \theta_{y_j}^i) \right) \quad [26]$$

$$\Delta P_{y_j}^i = \Delta t \left( \left[ \frac{a_e^2 \cos \varphi}{\sqrt{a_e^2 \cos^2 \varphi + b_e^2 \sin^2 \varphi}} + c \right] \theta_{y_j}^i + \left[ \frac{b_e^2 \sin \varphi}{\sqrt{a_e^2 \cos^2 \varphi + b_e^2 \sin^2 \varphi}} \right] (N_{z_j}^i \theta_{x_j}^i - N_{x_j}^i \theta_{z_j}^i) \right) \quad [27]$$

$\Delta P_{z_j}^i$  is not calculated; if it is needed, it is derived from the data layer for the digital elevation model in Prometheus.

further investigation allows quantification of the effect of changes in the smoothing value, users should exercise caution in applying this function.

### Smoothing the Perimeter

An active fire front may contain hundreds of active vertices, in which case the perimeter may not be smooth. To provide a more visually appealing (smoother) perimeter output, a smoothing algorithm was introduced into Prometheus. Given a smoothing factor,  $\omega$ ,

$$P_{j+1}^i = P_j^i + \omega \frac{(\Delta P_j^{i-1} + \Delta P_j^{i+1})}{2} + \Delta P_j^i (1 - \omega) \quad [28]$$

This operation is performed on all active vertices. Smoothing is disabled when the default value of  $\omega = 0.0$  is used. A value of  $\omega = 0.4$  appears to generate a suitable balance between the desired subjective qualities of the display and computational accuracy when the default value for  $L_\tau$  is used.

Although this smoothing algorithm affects the absolute mathematical accuracy of the fire growth model, it does negate some of the limitations of representing the natural landscape as discrete cells.  $L_\tau$  and  $\Delta t$  have a direct effect on the performance of this smoothing equation, so these values must be chosen with care. Until

### Perimeter Adjustment for Fuel Breaks and Landscape Boundaries

Vertices propagated during Prometheus fire growth simulations may encounter three situations that require evaluation:

- the landscape boundary;
- gridded fuel breaks (nonfuel cells in the fuel-type grid, e.g., lakes, plowed fields); and
- vector fuel breaks (e.g., rivers, roads).

When a vertex of a fire reaches the landscape boundary, the simulation is conditionally stopped and the user is warned, but only if this scenario parameter is turned on. Alternatively, if this feature is turned off, the path along which a vertex advances, from  $P_j^i$  to  $P_{j+1}^i$ , is clipped at the plot boundaries, and  $P_{j+1}^i$  is marked as inactive, but the fire continues to grow.

When a vertex of a fire encounters a fuel break, either the vertex is marked as inactive (which stops the fire) and the perimeter is adjusted, or the vertex is allowed to breach the fuel break and continue to advance in the next simulation step.

### *Gridded Fuel Breaks*

Barriers to fire spread are collectively typed as nonfuel in the FBP fuel-type grids used in the Prometheus model. These barriers could represent, for example, bodies of water, nonflammable vegetation, or areas for which no data are available. In Prometheus, grid breaks occur around nonfuel cells, as well as at the limits of the landscape extent.

Prometheus performs a ray-tracing operation from  $P_j^i$  to  $P_{j+1}^i$  to detect all cell boundaries. If a nonfuel or no-data cell is encountered, then the location for  $P_{j+1}^i$  is changed to that cell boundary to prevent the fire from advancing into that cell. No new fire vertices are introduced during these operations, so a fire may appear to include portions of the nonfuel or null data cells. This condition is within the accuracy of the model and is therefore deemed acceptable.

Landscape features may change from cell to cell. These changes are not tracked, and updated *ROS* and *RAZ* values are not recomputed during the ray-tracing operation, so as to avoid grid cell "ghosting" side effects. Any such recomputation scheme would implicitly and incorrectly introduce assumptions regarding where changes in fuel type occur.

### *Vector Fuel Breaks*

Geographic features that might obstruct the progress of a fire, such as rivers and roads, may be imported and used as vector fuel breaks in

Prometheus scenarios. Detecting and integrating these features to more accurately update the fire shape involves a complicated, multistep process that results in an approximate solution.

The first step of the process detects and corrects vertex paths that intersect with fuel breaks. The vector  $\Delta P_j^i$  is truncated at the first point of intersection with any vector fuel break. Figure 19a shows the theoretical growth of the fire perimeter, and Figure 19b shows how the paths of travel for vertices intersecting the break are truncated at the point of contact with the break.

Next, the area for each vector fuel break, represented as a polygon, is subtracted from the area of the fire, also represented as a polygon, by applying a polygon difference operation, as defined by Vatti (1992) (Figure 19c). Although Vatti (1992) defined what a polygon difference operation is, the Prometheus implementation is unique and is consistent with the untangling operation, described later.

Vertices that were relocated during the initial intersection operation, or introduced during the polygon difference operation, are set as inactive.

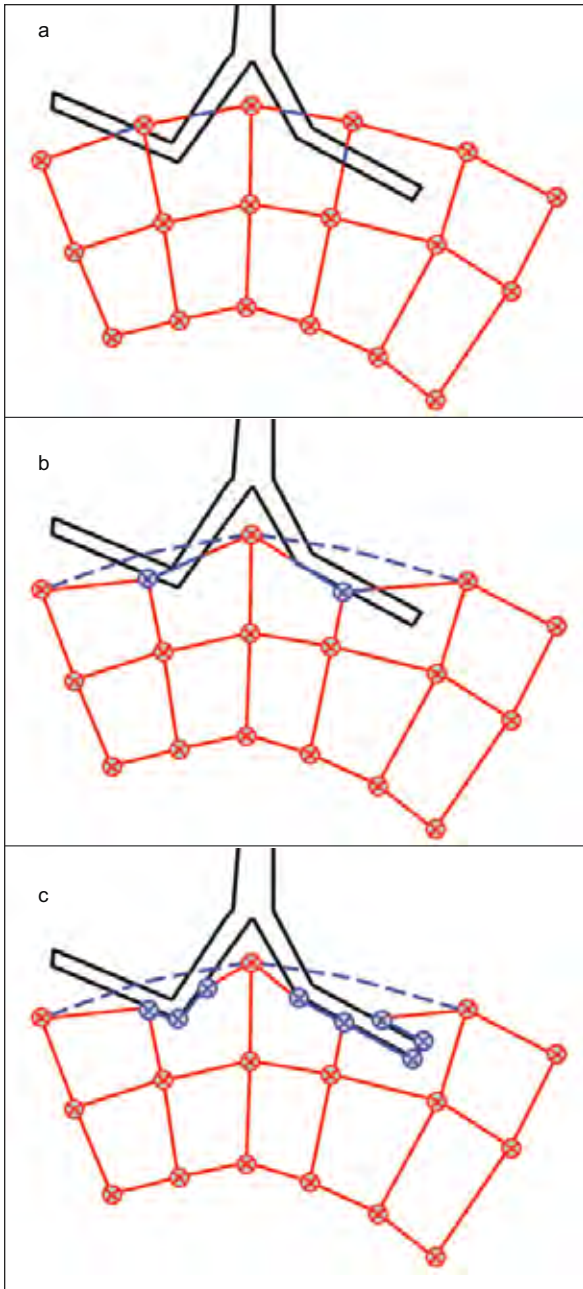


**Figure 19. Integration of a fire perimeter (red lines) defined by  $n$  vertices (red crossed circles) and a fuel break (black lines) in Prometheus.** a. Portions of the fire perimeter intersecting the fuel break (blue sections) become inactive and are removed because they occur in nonfuel areas. b. The fire either cannot breach or breaching has been turned off in Prometheus. Vertices belonging to the perimeter projected to cross the fuel break (dashed blue line) are pulled back to the edge of the fuel break (blue crossed circles). c. The remaining nonfuel areas are removed from the fire area. Additional vertices are inserted along the fuel break interface but become inactive (blue crossed circles). The active fire perimeter continues to grow around the fuel break, while the portions along the fuel break (blue lines) remain inactive.

### Breaching of Nonfuel Areas

Breaching of nonfuel areas occurs when a natural barrier (e.g., lake, river) or an anthropogenic barrier (e.g., road, plowed field) fails to stop the advancing fire front. Although ember transport resulting in new spot fires downwind of the head fire is the primary cause, breaching can also occur by direct flame contact, thermal radiation, or fire whirls (Countryman 1971; Wilson 1988). Barriers to fire spread are usually typed as nonfuel in the FBP System fuel-type grid, but can also be imported as vector data. During the import routine, the vector data must be assigned a width attribute.

In September 2004, eight fire research and fire operations experts participated in a one-day workshop to discuss the current state of knowledge with respect to incorporating spotting and breaching into the Prometheus model (Alexander et al. 2004). They supported the following two recommendations:

- Incorporate a simple rule of thumb (Byram 1959) for breaching a barrier to fire spread (i.e., the width of the barrier must be 1.5 times the expected flame length to prevent breaching). Fogarty and Alexander (1999) reported a reasonable agreement between Byram's (1959) rule of thumb and the 90% probability of a grass fire breaching a firebreak where trees were absent within 20 m of the firebreak, based on Wilson's (1988) model for intensities greater than 1000 kW/m.
- Incorporate Albini's models for maximum spotting distance (Albini 1979, 1981, 1983; Chase 1981, 1984; Morris 1987) as an auxiliary calculator or as a tabulated output to give users the option of adding spot fires across a firebreak as new ignition points.

The workshop participants also concluded that additional research is required to better understand and model the conditions that are present when a barrier is likely to be breached.

The breaching rule of thumb used in Prometheus is based on the relationship between fire intensity ( $FI$ , kW/m) and flame length ( $L_{Fl}$ , m) developed

by Byram (1959) for surface fires (Alexander 1982):

$$L_F = 0.0775 \times FI^{0.46} \quad [29]$$

The minimum barrier width ( $MBW$ , m) is calculated by the following formula:

$$MBW = 1.5 \times L_F \quad [30]$$

It is assumed that equation 29 is also valid for intermittent or passive crown fires. For fully developed active or continuous crown fires, the flame height, assumed to be equivalent to flame length, is approximated as 2.5 times the stand height (Alexander 2006). Default heights are used for the FBP System fuel types (Alexander 2004).

As noted in the previous section "FBP Fuel-Type Grids and Lookup Tables", it is recommended that the nonfuel areas be classified. In the boreal forest, treed muskeg areas normally are effective fuel breaks, but when DC exceeds some critical threshold value, these areas will burn. Classifying different nonfuel types, such as treed muskeg, allows for dynamic fuel-type modeling.

The grid resolution is an important factor in determining whether nonfuel areas in the FBP

System fuel-type grid will be breached. In Alberta, grid resolutions of 25 m and 100 m are generally used for operational simulations. A fire with an intensity of 10 000 kW/m will breach a single 25-m nonfuel cell but not a 100-m nonfuel cell. Prometheus accounts for the occurrence of multiple barriers along the path of a propagated vertex, and ray tracing is used to search for barriers. Multiple barriers may be breached, depending on the width of the intercepted barriers and the time remaining in the time step.

Prometheus accommodates breaching of vector fuel breaks, since the widths of these features are provided. The *Prometheus Data I/O Standards Manual* (Canadian Wildland Fire Growth Simulation Model Data I/O Standards Technical Sub-Committee 2009) describes the optional use of a vector attribute file. When breaching a vector break, the travel length of  $\Delta P_j^i$  through the vector break is calculated, with consideration of the width of the break, as well as the angle at which the growth vector contacts the break. This travel length across the break is used to determine if breaching will be successful. For example, a head fire making contact normal to the vector break will breach more easily than a head fire making contact at an angle that results in a longer travel path (see Figure 20).

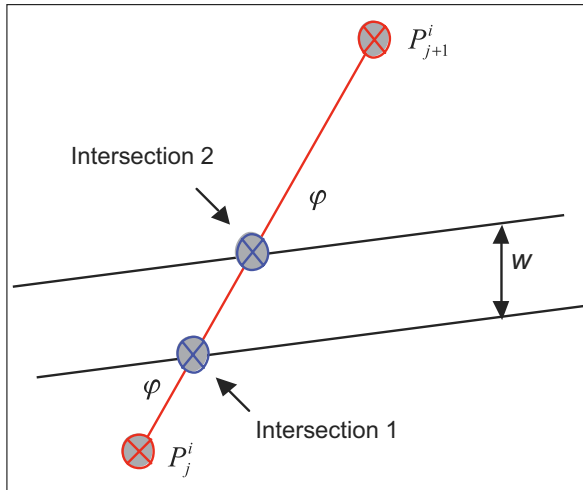


**Figure 20. Breaching a vector fuel break.** The travel length through the vector fuel break is calculated, with consideration for the width of the fuel break ( $w$ ), as well as the angle at which the growth vector contacts the fuel break ( $\varphi$ ). This travel length inside the fuel break is used to determine if breaching is successful. Red crossed circles represent vertices along the fire perimeter, ( $P_j^i, P_{j+1}^i$ ) and blue crossed circles are vertices at the intersection of the vector fuel break.

In rare instances, a point  $P_{j+1}^i$  is calculated to land inside a vector break. In this situation,  $\Delta P_j^i$  is modified (increased in length) to allow  $P_{j+1}^i$  to land just beyond the vector break. If breaching is unsuccessful, then  $\Delta P_j^i$  will be shortened and the vertices repositioned back to the edge of the vector break. If breaching is successful, then  $P_{j+1}^i$  is left at that modified location (Figure 21). The introduction of this minor error to  $\Delta P_j^i$  is deemed acceptable to allow breaching to occur in this situation.

Figure 21 illustrates how two vertices breach the front, the path of another vertex is extended to complete a successful break, and a fourth vertex fails to breach the vector break. This figure also illustrates how the nonfuel area defined by the vector break is excluded from the fire.

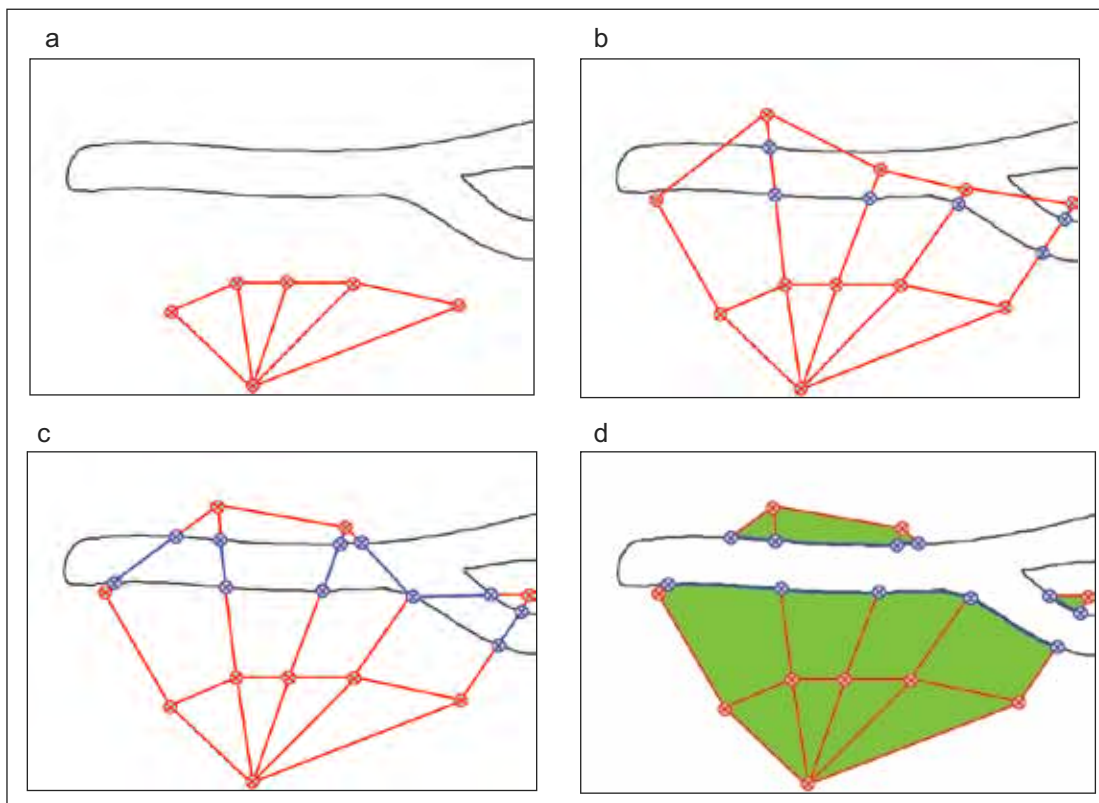


**Figure 21. Progression of steps during the breaching of a fuel break.** a. A fire perimeter (red line) defined by  $n$  vertices (red crossed circles) is approaching a fuel break (black line). b. Inactive vertices (blue crossed circles) are introduced along vertex paths intersecting the fuel break at the fuel break boundary. c. The length of the vertex paths that cross the fuel break (blue lines) are determined. If the crossing distance is greater than the threshold distance, the vertices on the far side of the fuel break are allowed to propagate in the next time step. d. The final fire area (green) after breaching.

### Polygon Untangling and Rationalization

Although the Marker method used in Prometheus to propagate fire perimeters produces representative fire shapes, it often creates complex formations along fire fronts (Figure 22). These situations occur when two fire fronts contact each other, or when varying terrain causes the fire front to intersect itself. The latter effect occurs because the partial differential equations are concerned only with a vertex's immediate neighbors and the underlying data, and because of artifacts introduced by the discretization of continuous temporal and spatial data.

Richards and Bryce (1995) defined an approach for using a turning (or winding) number algorithm to detect the interior of a fire polygon. This algorithm works with self-intersecting (i.e., complex) polygons, but fails when portions of the polygon become tangled (i.e., intersect while changing orientation). These situations will generally not occur when homogeneous spread directions (*RAZ*) are used, as is the case with a steady wind on a uniform slope. However,

in complex terrain, the influences of wind and slope on spread rate will interact (as described in the section entitled "Terrain Effect"), resulting in a heterogeneous *RAZ* input data set, which will in turn cause the fire to self-intersect often, creating loops and tangles along the fire front. A number of algorithms for simplifying the polygons were examined in an effort to deal with this problem, but they were neither reliable nor plausible for fire growth simulation. Thus a new "untangling" algorithm was developed to detect and correct these features by reorienting specific portions of the fire perimeter (polygon) (Bose et al. 2009). This algorithm will also detect interior portions of the fire that should continue to exist (and burn inward), while removing errant or unnecessary interior edges, creating  $n$  simple (nonintersecting) polygons from one complex polygon. Once simple polygons have been generated, the original Richards and Bryce (1995) algorithm is used to determine interior (burned) regions of the fire. Removing unnecessary interior edges results in more accurate perimeter and area statistics.

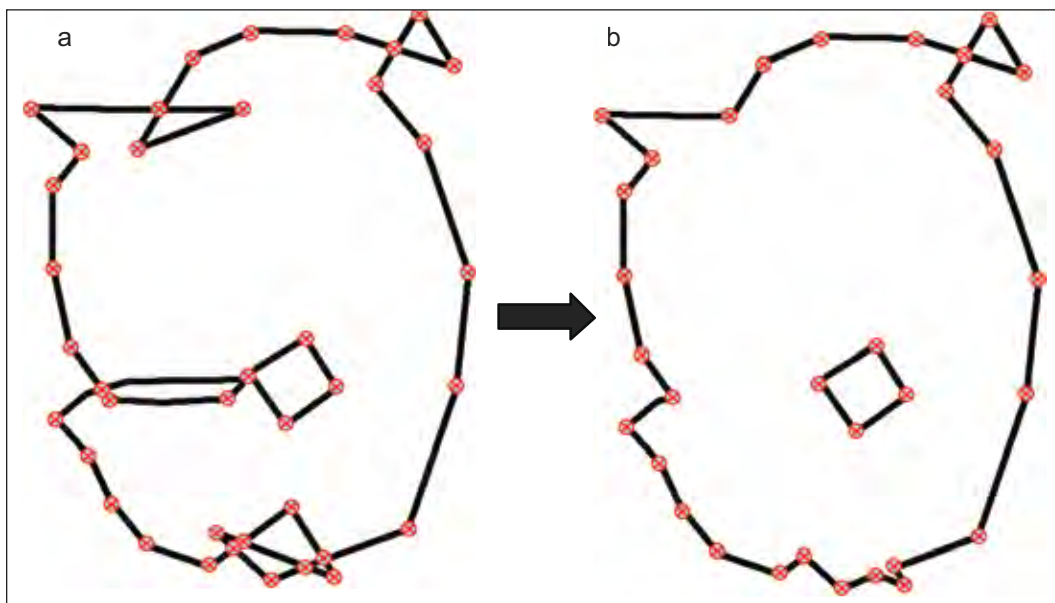


**Figure 22. Untangling of a fire perimeter.** a. Portions of the fire perimeter (black line) defined by the vertices (red crossed circles) that cross itself are identified, and vertices belonging to the tangles become inactive. b. A new fire perimeter is formed from the remaining active vertices, including any unburned interior areas.

The untangling algorithm is based on the two-color theorem for planar curves. The algorithm assumes that at least one edge entering an intersection has a known orientation, whereby one side of the edge lies outside the polygon and the other side lies inside the polygon. On the basis of this first edge, the other three edges associated with the intersection can be examined and conditionally reoriented. Once all edges have been reoriented, they are recombined into a set of simple polygons. All exterior polygons and interior polygons with no edges having corrected orientations are retained. Interior polygons with edges that no longer have their original orientation are discarded. The starting edge must be known to be exterior to all polygons. This algorithm retains counterclockwise outer polygon orientations, which are needed for the partial differential equations, and automatically retains interior polygons, which are completely oriented clockwise so that they may burn inward. Figure 22 shows a fire perimeter before and after untangling.

Changes in the logic used to traverse the polygon and reorient its edges allow the untangling operation to perform all traditional polygon set operations: union, difference, intersection, and exclusive-or, as defined by Vatti (1992) and by Greiner and Hormann (1998).

Many unusual situations, such as coincident edges and intersections where many edges participate, complicate the implementation of this algorithm. Further details on the implementation, performance, and caveats of this approach to simplifying a complex polygon are described in Bose et al. (2009).

### Polygon Intersections and Unions

In Prometheus, multiple fires can be simulated at the same time. In this situation, the fires may ultimately contact each other. When independent fire polygons overlap, the vertices defining shared edges are marked as inactive (fire spread is halted). However, because  $\Delta t$  (the duration of the time step) is discrete, contacting fires may overlap before propagation can be halted. If two fires originating from the same (multipoint) ignition overlap, they are joined using a polygon union operation, and shared edges are removed. However, if multiple fires originating from different ignitions contact each

other and overlap, they are not merged but are retained as individual polygons for the purposes of calculating the fire perimeter and area (see Figure 23). In these situations, the larger fire assumes “ownership” of the overlapping area. However, careful selection of  $\Delta P_t$  (the distance resolution) will limit the extent of overlap during any given time step. The polygon set difference algorithm, used to deal with vector breaks, is used to adjust the overlapping polygons.

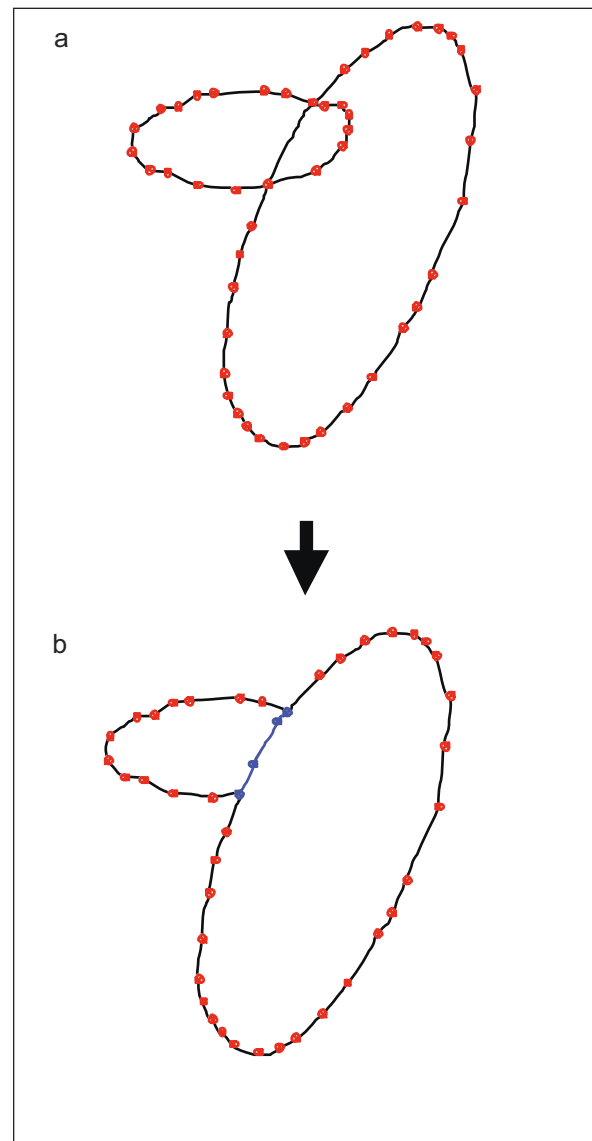


**Figure 23. Intersection of two fires associated with different ignitions.** a. The two fires intersect. b. The intersecting area and perimeter are assigned to the larger of the two fires. The vertices defining the intersecting portions of the perimeter are set to inactive (blue circles).

## Rediscretization of the Fire Perimeter

### Adding Vertices

As the initial ignition vertices begin to grow, new vertices must be added along the perimeter of the fire to avoid missing landscape features. Similarly, as the fire front folds back upon itself, other vertices can be removed. These procedures are referred to as rediscretization of the fire perimeter (Richards and Bryce 1995).

In Prometheus,  $L_\tau$  (the largest distance between any two adjacent vertices) can be fine-tuned to generate the desired accuracy, resolution, and computational speed, as well as the desired appearance of the final fire perimeter.

New vertices are added only along the active portions of the fire front, at a midpoint between existing neighboring vertices, and only when conditions are appropriate. There is no effort to create a smooth line through existing vertices, because doing so would inappropriately extrapolate information from existing vertices and potentially create unexpected errors, as well as duplicating behavior already modeled by the partial differential equations. The partial differential equations effectively smooth the fire front in subsequent time steps.

The vertex insertion technique is executed iteratively to introduce a maximum of five new vertices between any two existing vertices. This limitation is imposed to prevent the introduction of an unreasonably large number of vertices at any given time step, regardless of the active fire shape (which would otherwise happen at extremely sharp turns along the fire front). However, there is no upper limit to the number of vertices that constitute the entire fire perimeter.

### Inter-vertex Weighted Distance Threshold

As the curvature of the fire increases (for example, around a specific feature), it is advantageous to increase the number of vertices to more accurately describe the shape. The following equations outline how  $L_\tau$  is adjusted on the basis of local curvature of the fire front.

$\beta_j^i$  is the interior angle of the fire front, expressed in radians, at vertex  $P_j^i$ .

$$\beta_j^i = \angle P_j^{i-1} P_j^i P_j^{i+1} \quad [31]$$

$$\text{If } (\beta_j^i \leq \pi), \text{ then } \beta_j^{i'} = \beta_j^i, \text{ else } \beta_j^{i'} = 2\pi - \beta_j^i \quad [32]$$

Given Figure 24,

$$\text{if } \left( \frac{L_j^i}{L_\tau} > \sin \frac{\beta_j^{i'}}{2} \right), \text{ then insert vertex } \left( \frac{P_{x_j}^i + P_{x_j}^{i-1}}{2}, \frac{P_{y_j}^i + P_{y_j}^{i-1}}{2} \right) \text{ between } P_j^{i-1}, P_j^i \quad [33]$$

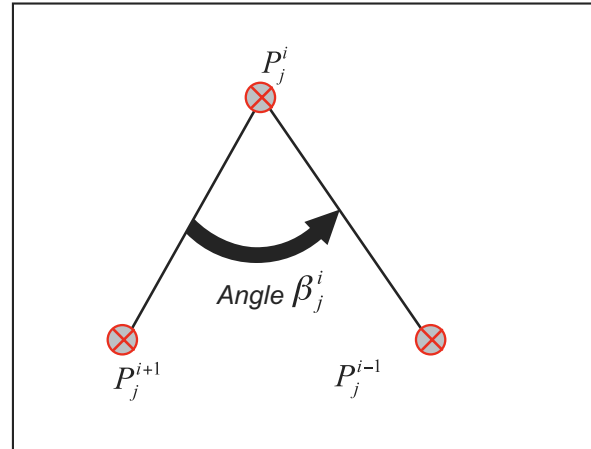


Figure 24. Interior angle  $\beta_j^i$  of the fire front at vertex  $P_j^i$ , defined by three vertices (red crossed circles), where  $i$  is the  $x, y$  location of vertex  $i$  and  $j$  is the time step.

Similarly,

if  $\left(\frac{L_j^{i+1}}{L_\tau} > \sin \frac{\beta_j^i}{2}\right)$ , then insert vertex

$$\left(\frac{P_{x_j}^{i+1} + P_{x_j}^i}{2}, \frac{P_{y_j}^{i+1} + P_{y_j}^i}{2}\right) \text{ between } P_j^i, P_j^{i+1} \quad [34]$$

Equation 34 is applied to consider both convex and concave angles. Along a straight surface of the fire front (where  $\beta_j^i = \pi$ ), the maximum distance between vertices is  $L_\tau$ . As the angle  $\beta_j^i$  becomes sharper, the maximum allowable distance between neighboring vertices decreases; this decrease is nonlinear, to avoid undesirable fire behavior (Figure 25). For example, if  $\beta_j^i = \pi/2$  (90°), then the maximum distance allowed is actually 70.7% of  $L_\tau$ . If  $\beta_j^i = \pi/4$  (45°), then the maximum distance allowed is actually 38% of  $L_\tau$ , and so on. This technique forces the existence of more vertices in areas of the fire perimeter that exhibit high angularity.

The distance threshold is also used to avoid placing vertices too close to one another.

Specifically,

if  $L_j^i < \frac{L_\tau}{1000}$ , then prevent any vertex

insertion along  $\overline{P_j^{i-1}P_j^i}$  [35]

Similarly,

if  $L_j^{i+1} < \frac{L_\tau}{1000}$ , then prevent any vertex

insertion along  $\overline{P_j^iP_j^{i+1}}$  [36]

The value for  $L_\tau$  will directly affect the outputs of the Prometheus model, so the user must choose an appropriate value (or must avoid modifying the default values). For example, an inappropriately small value for  $L_\tau$  will cause “ghosting” effects from the underlying grid features to appear along the fire perimeter in an undesirable and unrealistic manner. Conversely, if  $L_\tau$  is too large, there is a risk that the simulation will miss features in the landscape grid.

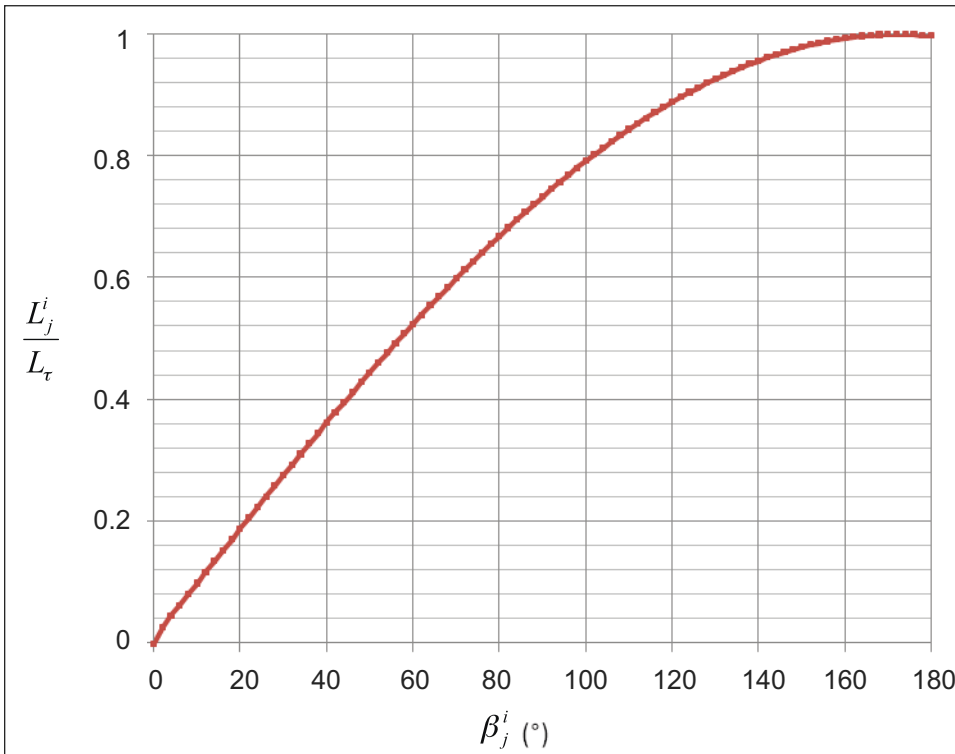


Figure 25. Relationship between the maximum allowable distance between  $L_j^i/L_\tau$  neighboring vertices and the threshold angle  $\beta_j^i$ .

## Vertex Fire Behavior and Fire Polygon Statistics

The last operations in a simulation step calculate fire behavior characteristics for the final set of active polygon vertices and also calculate the final polygon perimeter and area, as described previously in the section entitled "Fire Initiation." Vector fuel break areas are always excluded from burned fire areas. This ensures that the fire area and shape statistics are correct and consistent. In addition, the active fire perimeter statistic remains correct, but the total fire

perimeter statistic will include both sides of the contacted vector fuel break. Users have the option of exporting only the active portions of the fire perimeter or the entire fire perimeter. As well, interior fire perimeters may be retained or removed during the export routine. The fire characteristics determined at the end of each simulation step can be viewed as tables or maps, as described in the following section, "Fire Growth Simulation Outputs."

---

## FIRE GROWTH SIMULATION OUTPUTS

---

The primary outputs from Prometheus are, for each time step in a simulation, the  $x$  and  $y$  coordinates for each vertex, the order of the vertices, the primary FBP System output values, and the perimeter length and area of the polygon defined by the vertices. These and other data can be examined in the Prometheus Statistics and Map Views, or they can be exported in data files. An area-based representation of fire behavior (in grid cells) over the course of a simulation can also be estimated from the fire characteristics calculated for all of the perimeter vertices using point-raster interpolation techniques.

### Statistics View

The Prometheus model displays statistical output in a tabular form for each scenario. The Statistics View is updated after each display time step during execution of the fire simulation. The Statistics View may present any of the following types of data: temperature, dew point, relative humidity, wind direction, wind speed, precipitation, *HFFMC*, *HISI*, *HFWI*, *tFFMC* (instantaneous *FFMC* with consideration for temporal interpolation), *tISI* (instantaneous *ISI* with consideration for temporal interpolation), *tFWI* (instantaneous *FWI* with consideration for

temporal interpolation), *FFMC*, *DMC*, *DC*, *BUI*, time step area, total area, area growth rate, active perimeter, active perimeter growth rate, perimeter, perimeter growth rate, fire intensity percentage classes, rate-of-spread percentage classes, number of active vertices, total number of vertices, cumulative number of vertices, and number of fire fronts. For each time step, the maximum values for *ROS*, *FI*, crown fraction burned, crown fuel consumption, surface fuel consumption, and total fuel consumption can also be displayed, then printed or exported as a text file.

### Map View

During and after a simulation, polygon vertices and/or perimeters can be displayed in the Map View (Figure 26) and overlaid onto various grid layers (e.g., FBP fuel type, fuel polygon patches, elevation, slope, slope azimuth, weather patches) and geographic features (e.g., rivers and lakes). Single or multiple two-dimensional Map Views can be opened and saved as graphic files (\*.bmp). Vertex tracking (whereby every calculation time step is displayed) is possible if the display time step is set to 0.

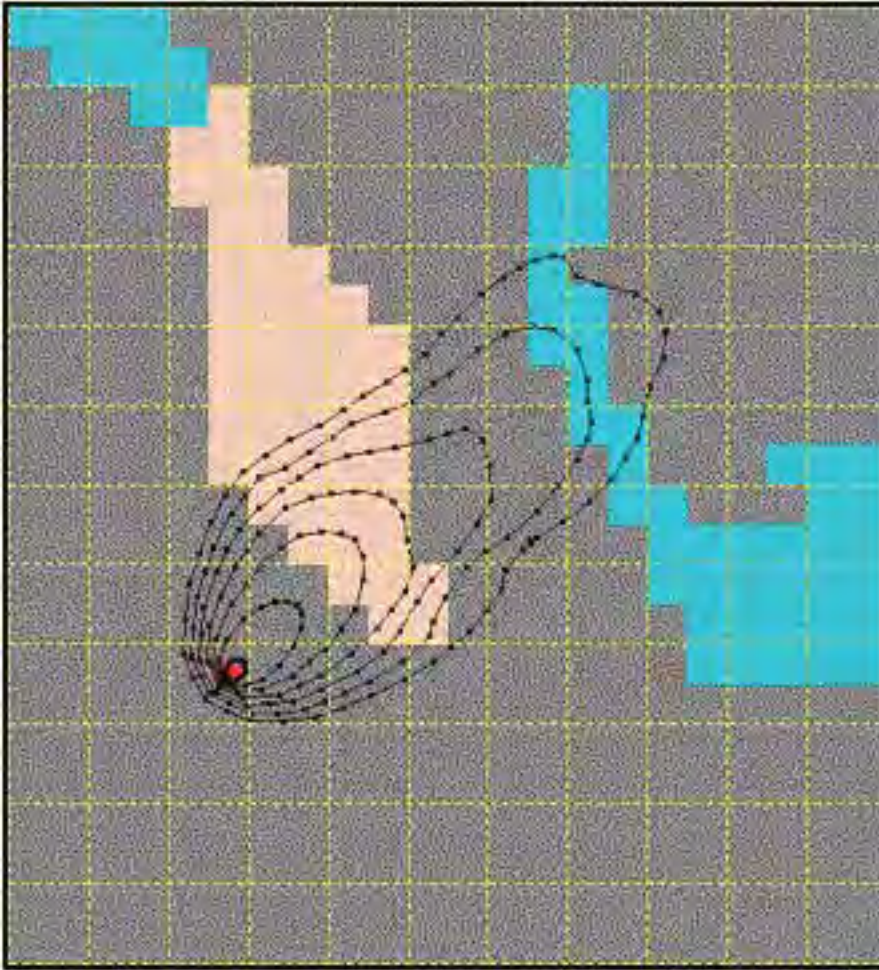


**Figure 26.** Thirty-five-minute simulation output in the Prometheus Map View using a distance resolution of one grid cell (25 m) and a display interval of 5 min. The colors represent different fuel types (gray is C-2, beige is O-1a, and blue is C-1). The red circle represents the ignition point, and the black dots represent the individual vertices along the fire perimeters.

A trace query tool for Map Views is available to display outputs of the FireEngine Calculator (i.e., the simulation) and the FBP Calculator. The query tool displays the x and y coordinates, latitude and longitude, FBP fuel type, and various optional outputs selected by the user (Table 7).

The outputs of the FireEngine Calculator are the specific simulated outputs associated with the already-burned vertex closest to the cursor location. These outputs are provided for

any queried location within the fire. The FBP Calculator estimates the fire behavior potential for any queried cell within the grid. This output, which is independent of the FireEngine simulation output, assumes weather conditions and ignition at the simulation's current time and queried location. The FBP Calculator can be used to assess fire behavior potential for the entire landscape, including areas outside of the currently simulated fire.

**Table 7. Fire Behavior Prediction (FBP) Calculator<sup>a</sup> and FireEngine Calculator<sup>b</sup> outputs**

| FBP Calculator                                     | FireEngine Calculator                      |
|----------------------------------------------------|--------------------------------------------|
| Head fire intensity ( <i>HFI</i> )                 | Fire intensity ( <i>FI</i> )               |
| Flank fire intensity ( <i>FFI</i> )                | NA <sup>c</sup>                            |
| Back fire intensity ( <i>BFI</i> )                 | NA                                         |
| Equilibrium head fire spread rate ( <i>HROS</i> )  | Rate of spread ( <i>ROS</i> ) <sup>d</sup> |
| Equilibrium flank fire spread rate ( <i>FROS</i> ) | NA                                         |
| Equilibrium back fire spread rate ( <i>BROS</i> )  | NA                                         |
| Surface fire rate of spread ( <i>RSS</i> )         | NA                                         |
| NA                                                 | Surface fuel consumption ( <i>SFC</i> )    |
| NA                                                 | Crown fuel consumption ( <i>CFC</i> )      |
| NA                                                 | Total fuel consumption ( <i>TFC</i> )      |
| NA                                                 | Crown fraction burned ( <i>CFB</i> )       |
| NA                                                 | Spread direction                           |
| NA                                                 | Fire type                                  |
| Time                                               | Time                                       |

<sup>a</sup>The FBP System outputs assume a point ignition in every grid cell.

<sup>b</sup>The FireEngine outputs represent the predicted fire behavior associated with the nearest vertex.

<sup>c</sup>NA = not applicable.

<sup>d</sup>Either  $ROS_e$  (equilibrium) or  $ROS_t$  (after elapsed time  $t$ ).

### Vector Output

Fire perimeters can be exported in Generate (\*.gen) or Shapefile (\*.shp) (vector) formats for use in a geographic information system. Further information about these file formats is available in the *Prometheus Data I/O Standards Manual* (Canadian Wildland Fire Growth Simulation Model Data I/O Standards Technical Subcommittee 2009). Although individual vertex attributes cannot be exported in the Prometheus application, the PrometheusCOM provides this functionality.

### Raster Output

Primary FBP System outputs (rate of spread; surface, crown and total fuel consumption; and fire intensity) and burn status (0 = not burned, 1 = burned) can be derived for each grid cell underlying the simulated burned area for use in fire effects applications, postfire recovery planning, and landscape fire analysis (Parisien et al. 2005). In addition, weather (temperature, dew-point temperature, relative humidity, wind direction, wind speed, precipitation) and FWI System values (*FFMC*, *ISI*, *FWI*) can also be derived for each grid cell. These statistics are useful for examining spatial weather outputs. The projection, extent, and resolution of the

resultant fire behavior grids are equivalent to those of the original raster fuel-type grid used to create the project file (\*.fgm) and can be exported from Prometheus in ASCII format.

This procedure requires mapping the primary FBP system values calculated for the polygon vertices (point locations) during the fire growth simulation back onto the landscape grid. The challenge is that the fire vertex locations seldom match the centroids of grid cells. Thus, the values for each grid cell must be interpolated. A primary concern with any interpolation technique is determining which vertices and grid cells should be considered. The vertex-to-raster interpolation in Prometheus includes all active fire vertices for every display and hidden (calculated but not displayed) time step and all grid cells whose centroids fall within the final fire perimeter.

Three techniques can be used for the vertex-to-raster interpolation of primary FBP System values: nearest vertex to center of grid cell, inverse distance weighting, and Voronoi area weighting. Voronoi-Delaunay models are particularly useful because they identify the natural neighbors of any point that should be used for the interpolation.

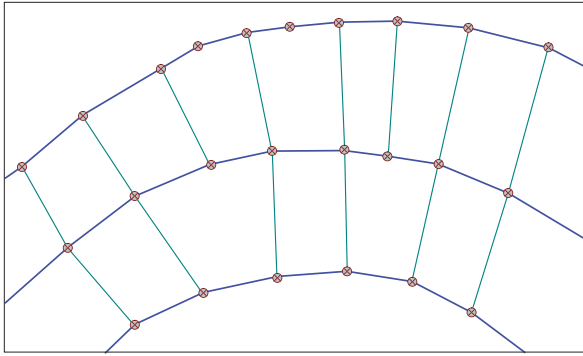


**Figure 27. Propagation of a fire perimeter over three time steps.** Blue lines track the fire front and green lines indicate the paths of the vertices. Red crossed circles represent vertices along the fire front.

Figure 27, representing a portion of a fire during three time steps, illustrates these interpolation techniques.

#### *Nearest Vertex to Center of Grid Cell*

This mode is the quickest method available for export to a raster grid and is consistent with the Map View trace query operation. However, multiple fire perimeters may be present within a specific grid cell. Regardless of this possible outcome, the statistics for the vertex that is closest to the center of the raster grid cell are exported.

#### *Inverse Distance Weighting*

Inverse distance weighting adds the centroid of a raster cell to the Voronoi diagram. For example, in Figure 28a, the candidate grid cell is overlaid on the fire perimeters, with all natural neighbor lines shown.

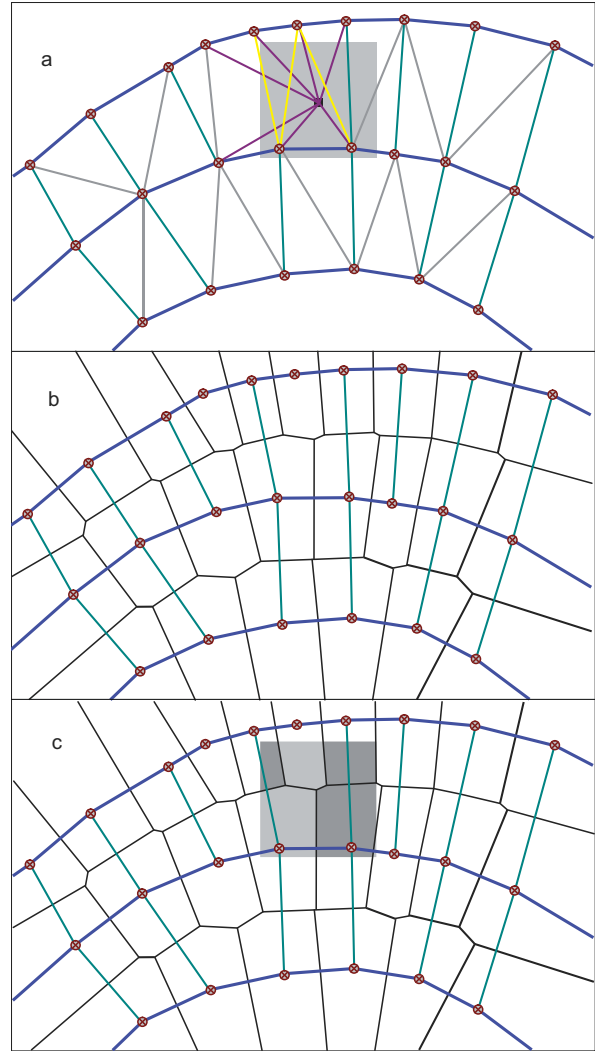


**Figure 28. Interpolation of fire characteristics associated with the vertices (red crossed circles) along the fire perimeters (blue lines) to a grid cell.** a. Nearest-vertex and inverse distance weighting interpolation methods. Vertices along any fire perimeter that are natural neighbors of the centroid (black square) within the grid cell (gray area) and the distance between the natural neighbors and vertices (purple lines) are identified. In the nearest-vertex method, the fire characteristics associated with the closest neighboring vertex to the centroid are assigned to the grid cell. In the inverse distance weighting method, fire characteristics for the cell are determined as the product of the weighted average of the distance between a natural neighbor vertex and the cell centroid (purple lines) and the fire value for the particular fire characteristic at the respective vertices. b and c. Voronoi interpolation method. b. Voronoi polygons (black lines) are determined showing the area of influence for each vertex. Fire characteristics are assigned to the Voronoi polygons associated with each vertex. c. The candidate grid cell (gray square) is intersected with the Voronoi polygons and the intersecting areas are determined. The fire characteristics for the grid cell are determined as the product of the weighted average of the proportion of each intersecting area and the grid cell size and the value of the fire characteristics for the respective Voronoi polygon.

Once the centroid's natural neighbors have been identified, the following equation is applied.

$$S = \frac{\sum_{i=1}^n \left( \frac{S_i}{D_i^2} \right)}{\sum_{i=1}^n \left( \frac{1}{D_i^2} \right)} \quad [37]$$

where  $S$  is the interpolated value,  $n$  is the number of natural neighbors,  $S_i$  is the statistic value at a given natural neighbor vertex, and  $D_i$  is the distance from the centroid to a given natural neighbor vertex.

In the current version of Prometheus, this technique is limited to an inverse distance-squared equation. Although inactive vertices are used in defining Voronoi regions, they are not included in the equation, to avoid inappropriate bias of the interpolated value.

#### *Voronoi Area Weighting*

In a Voronoi diagram, every location within the region of a vertex is closer to that vertex than

to any other vertex. This property identifies the area of influence of a given vertex (Figure 28b, black lines).

The area for a given cell is compared with each Voronoi region with which it intersects to generate weighting (Figure 28c). The vertices used in this technique are not necessarily the same as those used for interpolation by inverse distance weighting.

The following equation is used for the Voronoi area weighting technique:

$$S = \frac{\sum_{i=1}^n (S_i \cdot AREA(V_i \cap V_c))}{\sum_{i=1}^n (AREA(V_i \cap V_c))} \quad [38]$$

where  $S$  is the interpolated value,  $n$  is the number of natural neighbors,  $S_i$  is the statistic value at a given natural neighbor vertex,  $V_i$  is the Voronoi region for a given vertex, and  $V_c$  is the Voronoi region (a square) for the grid cell of interest.

---

## MODEL VALIDATION, LIMITATIONS, AND CALIBRATION

---

### Validation

The basis of the Prometheus fire growth simulation model is the FBP System, which has been adopted by fire management agencies across Canada. Wotton et al. (2009) reported validation of the FBP System (i.e., predictions versus observations) and also considered some of the assumptions made during its development. The accuracy of Prometheus is limited to the accuracy of the FBP System.

Prometheus generates the same output for every scenario using a particular combination of input data, parameters, and settings. This deterministic output is considered to correctly represent the primary outputs of the FBP System (e.g., spread rate, fuel consumption, and fire intensity). However, when testing Prometheus against the secondary outputs of the FBP System (e.g., spread distance, fire area, and perimeter) the user is restricted to simple ellipses, because no other model is available that produces comparable spatial output for heterogeneous conditions with the FBP System.

#### Prometheus Tester Suite

Further validation was conducted through independent comparisons. Area statistics output from Prometheus (version 5.2.2) was compared with output from a stand-alone FBP calculator program (generated from FBP source code). Two general data sets were developed to generate perfect circles and ellipses using a constant, homogeneous fire environment. Area statistics outputs were generated for each data set using 20-, 60-, 100-, 140-, 180-, 220-, and 260-min periods. Tests were conducted with smoothing ( $\omega$  set to 0.05, 0.10, 0.15, 0.20, 0.25, 0.30, 0.35, 0.40, 0.45, and 0.50) and without smoothing ( $\omega = 0.0$ ). Extended calculation time steps (12, 24, 36, and 48 h) were also tested. Preliminary evaluation of the results of validation testing indicated that the propagation methods used in Prometheus are working correctly. Without smoothing, the difference in the mean area burned between the Prometheus output and the theoretical ellipse was 1.7% (standard deviation = 3.1), based on a 25-m grid, 32 starting vertices for the ignition point (with circle diameter 0.5 m), elapsed time of 60 min, and a

perimeter resolution of 1 grid unit. (In version 5.3, the default number of starting vertices for the ignition point was changed from 32 to 16.) The difference can be explained, in part, by the use of different starting ignition points: the theoretical FBP System ellipse uses a single point, whereas the Prometheus application represents ignition as a small circle of vertices. Despite these findings, further analysis is required to justify the recommended default settings. For example, tests conducted assumed homogeneous conditions that do not necessarily validate settings used in a simulation involving heterogeneous data inputs.

Although the output generated by Prometheus is mathematically correct, it will not precisely match reality in time and space. Regardless of the propagation model chosen, the FWI and FBP system models are only approximations of reality, and the variability and uncertainty of both the fire process and the fire environment cannot be modeled exactly. The creation of data layers simplifies the real world. One suggested approach to reduce error is to increase the temporal and spatial resolution of the input data. This approach might appear to increase the output accuracy of the model, but if it is carried too far, it may exceed the accuracy used in the development of the FBP rate-of-spread equations and hence offer a false sense of accuracy. Also, despite the increase in accuracy of the model outputs with increased resolution of the input data, stochastic processes such as spotting and gusting winds cannot be modeled deterministically.

Even though software implementations can be tested to verify accuracy and correctness, models cannot be proven correct in an absolute sense. Watts (1987) suggested that model validation is therefore a process of invalidation. As the difficulty of invalidating the outputs of the model increases, confidence in and acceptance of those outputs also increase. Acceptance of the model outputs should result in a corresponding level of decision support. Therefore, model validation can be considered a process of decision support validation, answering the question "Did the model provide support for a particular fire management decision?" Unfortunately, this type of validation is rarely considered.

## Case Studies

The Prometheus Project Steering Committee recognized the importance of and need for establishing an accessible library of Prometheus case studies. Learning through examination of case studies is a common training tool. It provides an environment conducive to understanding the strengths and weaknesses of predicting fire growth with a simulation model. Case studies are effective in identifying data gaps, as well as the limitations of the model for a particular simulation. Changing the model inputs and comparing the projected fire growth with actual fire growth helps to assess the relative importance and accuracy of the variables and parameters influencing fire behavior. The ability to use multiple Map Views also facilitates this assessment.

A primary source for case studies is the 32-hour Prometheus course, which gives students the skills and familiarity with the Prometheus model they need to apply the model in supporting various fire management activities. Course certification requires completion of a case study. An example of a case study that utilizes the Prometheus fire growth simulation model is presented in Appendix 2.

## Limitations and Assumptions

Fire growth simulation models do not always produce outputs consistent with observed fire growth, and the differences in area and shape may be significant. Three main sources of error account for these differences: model error, user error, and data error (McHugh 2006). It is often difficult to identify which source of error is the most important for a particular fire simulation.

### Model Error

Model error may arise from both the underlying fire growth model (e.g., the Canadian FBP System or the USDA BEHAVE System) and the propagation algorithm. Error associated with the model includes simplification of processes (such as acceleration and fire shape) that may be inappropriate in some circumstances and lack of representation of processes that may be important in certain situations (e.g., interactions between fires and between fires and the upper atmosphere, long-range spotting), but which are less well understood or difficult to represent.

As discussed in the section entitled "Acceleration and Use of  $ROS_t$ ," the acceleration period does not vary significantly with fuel type, nor does the length-to-breadth ratio vary with time. The impact of changes in acceleration period and length-to-breadth ratio, though considered insignificant, is not yet fully understood.

With no wind, and on level terrain, a fire will develop a circular shape. With a prevailing wind or sloped terrain, the shape of a fire becomes an ellipse (Luke and McArthur 1978). The ellipse is convenient for mathematical modeling, but, as discussed in the section entitled "Fire Growth Simulation under Homogeneous Conditions," other shapes have also been described. The double ellipse was programmed into the Prometheus model for evaluation purposes. Preliminary analysis of the outputs of modeling with this shape suggests that the differences in area burned are noticeable but not significant. The ellipse model assumes that all portions of the ellipse, including the perimeter, are actively burning. Prometheus makes no attempt to predict if portions of the perimeter are inactive or smoldering. Similarly, Prometheus does not directly model suppression.

Prometheus can simulate multiple fires but not their interactions. For example, the in-drafts from a large, high-intensity fire can influence the behavior (e.g., rate of spread or spread direction) of an adjacent fire that is smaller and less intense. Smoke may travel from one fire to another, causing a reduction in temperature and an increase in relative humidity. These types of interactions, which are difficult to model, are not addressed in the FBP System and hence are not included in Prometheus. Prometheus is also unable to simulate fire whirls, fire tornados, and other extreme fire and atmosphere-coupled disturbances. Although the conditions are known when these phenomena occur, operational predictions of occurrence and behavior are not possible at this time (Alexander 2005). Prometheus does not model long-range spotting, although it does model breaching. Short-range spotting is implicitly accounted for in existing FBP equations.

Cui and Perera (2008) quantified the errors associated with the propagation algorithm by comparing three simulation models that all used the Canadian FBP System (Prometheus,

BFOLDS, and Wildfire). Their results indicated that the propagation algorithm may account for significant errors. To improve the application of fire growth simulation models for operational use, Cui and Perera (2008) suggested further investigation to better understand the sources of simulation errors and their interactions. The effect of spatial resolution is also influenced by vertex sampling intensity (i.e., time step or temporal resolution and perimeter resolution). Cui and Perera (2008) noted that the fire sizes and shapes generated by Prometheus were influenced by the spatial resolution of the input landscape grids. They suggested that this sensitivity is due to the use of static discrete time steps to advance the fire front, but they did not assess the effect of variable discrete time steps. In Prometheus version 5.x, the time step methodology was modified to incorporate the use of dynamic time steps (see the section entitled "Spatial and Temporal Resolution").

### User Error

User error encompasses the use of incorrect data, settings, or parameters. Model outputs may also be interpreted incorrectly. Garland (1988) described a hypothetical court case in which a resource professional is charged with seven offenses related to the use of models for natural resource decision-making, most of which were user errors. A common user error identified by Garland (1988) is the failure to identify the model's assumptions and limitations. For example, Prometheus assumes that the entire perimeter is either actively burning or not; it ignores other states such as smoldering. Although portions of the perimeter may be inactive, extinguishment of specific fuel types has not been incorporated into the model. Failing to recognize the limitations of models and applying them outside the range of the data used to build them is another user error. For example, the use of Prometheus with nonstandard fuel types will likely result in inaccurate simulations, and it will certainly result in outputs that cannot be validated. In the Prometheus model, users may change the default input parameters (e.g., crown base height, crown fuel load); however, there are few or no empirical data to support such changes. Models that are not based on scientific evidence and that have not been validated or tested for quality assurance should not be used.

Doing so can be considered both a model error and a user error. In addition, users should not assume that all model outputs are correct.

Using models inappropriately for decision-making is another type of user error. Although a fire simulation model provides guidance, it is by no means the only tool or information available to assist fire managers in making decisions. For example, the allocation of suppression resources should consider suppression capability, values at risk, and fire risk potential (i.e., new ignitions), as well as anticipated fire growth. Fire growth simulation models can be used to help make decisions about the type, number, and placement of suppression resources, but the inability of such models to account for on-site conditions that will influence operational activities (e.g., ease of travel, crew productivity, stream-crossing locations, locations of escape routes) limits their use for this purpose.

Finally, temporal or spatial scaling of outputs from the Prometheus model to make decisions about larger and more complex landscapes, or decisions about landscapes in other ecoregions, is another user error.

### Data Error

The ability of Prometheus to provide reasonably accurate perimeter forecasts to support fire operations depends on the accuracy of the forecasted weather, in particular, wind speed and direction. For this reason, multiple scenarios, with a range of wind speeds, are usually modeled to avoid data errors in this area.

A common data error is the inadequate representation of variability in the fuel complex by the FBP fuel-type grid. For example, the stands within grid cells may not be continuous, homogeneous, or uniform in structure and density.

In addition, it is well recognized that the 16 standard FBP fuel types do not represent some of the major fuel types found in Canada, including shrubs and several tall closed-canopy forest types (e.g., Engelmann spruce, *Picea engelmannii* Parry ex Englem.; white spruce, *Picea glauca* (Moench) Voss; subalpine fir, *Abies lasiocarpa* (Hook.) Nutt.; western hemlock, *Tsuga heterophylla* (Raf.) Sarg.), or fuel conditions after insect outbreaks in many forest types (at present, only

balsam fir [*Abies balsamea* (L.) Mill.]) killed by spruce budworm [*Choristoneura fumiferana* (Clemens)] is represented in the FBP system). In this situation, the “best-fit” approach used to select a fuel type may introduce significant data error.

It is reasonable to assume that the accuracy of a simulation increases as the spatial and temporal accuracy of the input data increases. However, exceedingly fine spatial and temporal resolution does not necessarily provide added value or accuracy, and coarse spatial and temporal resolution can simplify the landscape variability to the point of introducing unacceptable errors. Using a spatial resolution that is greater than the sampled data will cause some features to be skipped and will place unreasonably high importance on specific features that are not skipped. This practice should be avoided unless conditions are known to be relatively homogeneous.

Prometheus can use any spatial resolution. In Alberta, FBP fuel-type grids have been created by reclassifying the 1:20 000 Alberta Vegetation Inventory (Tymstra and Ellehoj 1994), which has a minimum polygon size of 2 ha. This scale equates to a grid resolution of about 140 m, whereas grid resolutions of 25 m and 100 m are typically used for fire growth simulations in this province. The effect of different grid resolutions was tested on the simulated fire growth of the 2001 Chisholm fire in Alberta. Grids with resolution of 5 m, 100 m, and 1 000 m were all resampled from the 25-m grid. Although a more rigorous study is required for definitive conclusions, the preliminary analysis suggested

that grid resolution can influence simulation results. Specifically, the 5-m and 100-m grids provided reasonable outputs, but the 1 000-m grid did not.

Tables 8, 9, and 10 summarize the differences in area and perimeter calculations for three wildfires when the perimeter resolution ( $L_{\tau}$ , the spacing between vertices along the fire perimeter) and the distance resolution ( $\Delta P_{\tau}$ , the maximum distance a vertex can travel before the landscape is resampled) were modified in synchrony from 1 to 5 (i.e., 1 = width of 1 grid cell, 5 = width of 5 grid cells). These tunable parameters specify the sampling frequency of the underlying landscape grids. The lower the settings for distance and perimeter resolution, the higher the sampling intensity. Simulations for two wildfires (the 2001 Dogrib fire and the 2006 Willmore fire) showed a decreasing trend for area burned as the distance and perimeter resolution increased. In contrast, as the distance and perimeter resolution settings increased for simulation of the Myers Lake fire (which burned in a more heterogeneous landscape with many small lakes), the area burned increased slightly. This result suggests that the sampling of fuel types in a heterogeneous environment, over time and through space, is an important though frequently overlooked consideration. Directly affecting these results is the original sampling of data and any sampling or resampling applied to create the landscape grids used in Prometheus. A more comprehensive analysis is required to assess the impact of sampling and of changing the settings for distance and perimeter resolution on area burned.

**Table 8. Area and perimeter calculations for the 2001 Dogrib fire<sup>a</sup>**

| Distance resolution <sup>b</sup><br>– perimeter resolution <sup>c</sup> | Area<br>(ha) | Change<br>in area<br>(%) | Active<br>perimeter<br>(km) <sup>d</sup> | Change<br>in active<br>perimeter (%) | Perimeter<br>(km) | Change<br>in perimeter<br>(%) |
|-------------------------------------------------------------------------|--------------|--------------------------|------------------------------------------|--------------------------------------|-------------------|-------------------------------|
| 1–1                                                                     | 146.07       |                          | 5.73                                     |                                      | 5.73              |                               |
| 2–2                                                                     | 141.39       | –3.20                    | 5.49                                     | –4.19                                | 5.49              | –4.19                         |
| 3–3                                                                     | 142.12       | –2.70                    | 5.48                                     | –4.36                                | 5.48              | –4.36                         |
| 4–4                                                                     | 134.30       | –8.06                    | 5.34                                     | –6.81                                | 5.34              | –6.81                         |
| 5–5                                                                     | 130.19       | –10.87                   | 5.50                                     | –4.01                                | 5.50              | –4.01                         |

<sup>a</sup>Scenario parameter settings include use of a 25-m grid, no smoothing, and variable settings for the distance resolution and perimeter resolution. The simulation is for 3 h (1300–1600 local daylight time).

<sup>b</sup>Maximum distance a vertex can travel before resampling the landscape.

<sup>c</sup>Maximum distance between vertices along the fire perimeter.

<sup>d</sup>Active perimeter represents portions of the perimeter where the vertices are still active and contributing to spread.

**Table 9. Area and perimeter calculations for the 2004 Myers Lake fire<sup>a</sup>**

| Distance resolution <sup>b</sup><br>– perimeter resolution <sup>c</sup> | Area<br>(ha) | Change<br>in area<br>(%) | Active<br>perimeter<br>(km) <sup>d</sup> | Change<br>in active<br>perimeter (%) | Perimeter<br>(km) | Change in<br>perimeter<br>(%) |
|-------------------------------------------------------------------------|--------------|--------------------------|------------------------------------------|--------------------------------------|-------------------|-------------------------------|
| 1–1                                                                     | 2852.55      |                          | 24.74                                    |                                      | 41.45             |                               |
| 2–2                                                                     | 3145.64      | 10.27                    | 27.17                                    | 9.82                                 | 44.56             | 7.50                          |
| 3–3                                                                     | 3536.53      | 23.98                    | 25.83                                    | 4.41                                 | 48.27             | 16.45                         |
| 4–4                                                                     | 3653.40      | 28.07                    | 25.76                                    | 4.12                                 | 46.94             | 13.24                         |
| 5–5                                                                     | 3897.04      | 36.62                    | 31.43                                    | 27.04                                | 54.28             | 30.95                         |

<sup>a</sup>Scenario parameter settings include use of a 100-m grid, no smoothing, and variable settings for the distance resolution and perimeter resolution. The simulation is for 24 h (1420–1420 local daylight time).

<sup>b</sup>Maximum distance a vertex can travel before resampling the landscape.

<sup>c</sup>Maximum distance between vertices along the fire perimeter.

<sup>d</sup>Active perimeter represents portions of the perimeter where the vertices are still active and contributing to spread.

**Table 10. Area and perimeter calculations for the 2006 Willmore fire<sup>a</sup>**

| Distance resolution <sup>b</sup><br>– perimeter resolution <sup>c</sup> | Area<br>(ha) | Change<br>in area<br>(%) | Active<br>perimeter<br>(km) <sup>d</sup> | Change<br>in active<br>perimeter (%) | Perimeter<br>(km) | Change in<br>perimeter<br>(%) |
|-------------------------------------------------------------------------|--------------|--------------------------|------------------------------------------|--------------------------------------|-------------------|-------------------------------|
| 1–1                                                                     | 3567.89      |                          | 29.29                                    |                                      | 59.63             |                               |
| 2–2                                                                     | 3382.11      | –5.21                    | 31.48                                    | 7.48                                 | 55.93             | –6.20                         |
| 3–3                                                                     | 3217.11      | –9.83                    | 32.52                                    | 11.03                                | 51.26             | –14.04                        |
| 4–4                                                                     | 3074.68      | –13.82                   | 30.26                                    | 3.31                                 | 45.04             | –24.47                        |
| 5–5                                                                     | 3228.48      | –9.51                    | 31.30                                    | 6.86                                 | 46.65             | –21.77                        |

<sup>a</sup>Scenario parameter settings include use of a 100-m grid, no smoothing, and variable settings for the distance resolution and perimeter resolution. The simulation is for 6 h (1330–1930 local daylight time).

<sup>b</sup>Maximum distance a vertex can travel before resampling the landscape.

<sup>c</sup>Maximum distance between vertices along the fire perimeter.

<sup>d</sup>Active perimeter represents portions of the perimeter where the vertices are still active and contributing to spread.

## Calibration

Model calibration is the process of adjusting input data, parameters, and settings to ensure that predicted behavior matches observed fire behavior as closely as possible. Analysts using the FBP System may make adjustments to FBP fuel-type parameters in certain situations, and these adjustments will be carried over into Prometheus. If required, a landscape or polygon patch can be used to change fuel types. New fuel types can also be created by copying a fuel type and then modifying its parameters. Empirical data are as yet insufficient to support making changes to parameters, so users must apply trial and error and expert opinion in making such changes. The following supported FBP tuning parameters are exceptions to this rule:

- changing the percent cured and fuel load for the grass fuel types (O-1a and O-1b);
- changing the crown base height for the C-6 fuel type;
- changing the softwood and hardwood composition for the mixedwood fuel types; and
- changing the green-up status for the D-1/D-2, M-1/M-2, and M-3/M-4 FBP fuel types.

It may also be necessary to calibrate weather input. If the forecasted weather is based on observations from a weather station that is not representative of the fire area, it may be necessary to edit the hourly weather stream. A weather patch can also be used to locally modify

or replace wind speed and wind direction (e.g., to represent winds in a valley). The diurnal algorithm used in Prometheus does not model frontal passages, gusting, or extended burning periods (e.g., nighttime burning). The weather stream must therefore be edited manually to incorporate such features.

As well as calibrating fuel and weather, the user can also calibrate scenario parameters. The effects of changing these tunable parameters are not very well understood, and they represent an interesting area for further

research. Nevertheless, users can change these parameters on the basis of trial and error and expert opinion. The following tunable parameters can be changed by the user:

- maximum calculation time steps ( $t_{\tau e}$  and  $t_{\tau a}$ )
- perimeter resolution ( $L_{\tau}$ )
- distance resolution ( $\Delta P_{\tau}$ )
- smoothing parameter ( $\omega$ )

---

## CONCLUSIONS

---

Prometheus is a spatially explicit, deterministic fire growth simulation model. Although further validation is required to compare predicted and observed wildfire metrics, the vector approach for propagation of fire using the FBP system provides realistic outputs that are now being used by fire management agencies for decision support. The Prometheus model is used across Canada to provide operational and strategic assessments of potential fire behavior, as well as long-term projections and decision support for the management of large fires. It is also being used to simulate the growth of wildfires that escape initial attack, which is useful for assessing strategies used to analyze escaped fires.

Prometheus has also proven effective in assessing communities' fire risk and in the design of FireSmart<sup>4</sup> community plans. Interestingly, a recent user survey revealed that, to date, most uses of Prometheus have been for education, training, planning, budget and policy analysis, and assessment of climate change impacts.

The strength of the Prometheus model lies in its flexibility, which allows users to change the fire environment inputs and to integrate the model with other applications such as Pandora, Burn-P3, Pegasus, and the Spatial Fire Management System. However, further investigation is required to quantify and document the effect on area burned and perimeter outputs of changes in and interactions between tunable parameters and grid resolutions.

Fire growth simulation is a relatively immature field of fire research, and there are many opportunities for improvement. Recent efforts to engage the mathematics and statistics communities in evaluating new methods of propagating fire in these models, including the use of level set methods and the incorporation of stochasticity, will further advance the ability to effectively and efficiently provide decision support through fire growth simulations.

---

<sup>4</sup>FireSmart is an integrated initiative to reduce the threat of wildfire to people, property, and other values at risk (see <http://www.partnersinprotection.ab.ca>).

---

## ACKNOWLEDGMENTS

---

We thank Mark Finney, Thomas Hillen, Rob McAlpine, and Marty Alexander for constructive comments and suggestions that greatly improved this report. In particular, Marty Alexander provided input to and review of the section on breaching of fire breaks. The project also relied on invaluable contributions from the mathematics and statistics research community, especially Chris Bose, Anne Bourlioux, John Braun, Thomas Hillen, and the members of the 10th Problem Solving Workshop of the Pacific Institute for the Mathematical Sciences.

We are grateful to Alberta Sustainable Resource Development for its leadership in initiating this project (through the Foothills Model Forest) and for its continued support. The Prometheus Project Steering Committee provided strategic direction to guide the development of the Prometheus fire growth simulation model. Fire management agencies across Canada supported and funded this vision.

We thank Tracy Price and Neal McLoughlin for providing technical assistance to compile the data and produce graphic elements of this report. Robert Macdonald (formerly with RamSoft Systems Ltd.) and Dennis Yuan (formerly with CGI) contributed to the design and development of earlier versions of the Prometheus model.

---

## LITERATURE CITED

---

- Abell, C.A. 1940. Rates of Initial Spread of Free-Burning Fires on the National Forests of California. USFS California Forest and Range Experiment Station Research Note No. 24. 26 p.
- Albini, F.A. 1979. Spot fire distance from burning trees — a predictive model. US Dep. Agric., For. Serv., Intermt. For. Range Exp. Stn., Ogden, UT. Gen. Tech. Rep. INT-56. 73 p.
- Albini, F.A. 1981. Spot fire distance from isolated sources — extensions of a predictive model. US Dep. Agric., For. Serv., Intermt. For. Range Exp. Stn., Ogden, UT. Res. Note INT-309. 9 p.
- Albini, F.A. 1983. Transport of firebrands by line thermals. *Combust. Sci. Technol.* 32:277–288.
- Alexander, M.E. 1982. Calculating and interpreting forest fire intensities. *Can. J. Bot.* 60:349–357.
- Alexander, M.E. 2004. Nominal diameter-at-breast height and tree height values for Canadian Forest Fire Behavior Prediction (FBP) System Fuel Types for use in Albini's maximum spotting distance model. FERIC Wildland Fire Operations Research Group, Hinton, AB.
- Alexander, M.E. 2005. Limitations on accuracy of wildland fire behavior predictions [on-line]. FERIC, Pointe-Claire, QC. Accessed 18 October 2007. <<http://fire.feric.ca/other/LimitationsAccuracyofWildlandFireBehaviorPredictions.htm>>.
- Alexander, M.E. 2006. Models for predicting crown fire behavior — a review. Pages 173–225 in V Short course on fire behavior, 25–26 November 2006, Figueira da Foz, Portugal. Association for the Development of Industrial Aerodynamics, Forest Fire Research Centre, Coimbra, Portugal.
- Alexander, M.E.; Lee, B.S.; Lee, C.Y. 1984. Hourly calculation of the fine fuel moisture code, initial spread index and fire weather index with the Texas Instruments model 59 hand-held calculator. *Can. For. Serv., North. For. Cent., Edmonton, Alta. Study NOR 5-19, File Rep. No. 7.* 17 p.
- Alexander, M.E.; Tymstra, C.; Frederick, K.W. 2004. Incorporating breaching and spotting considerations into PROMETHEUS — the Canadian wildland fire growth model. Chisholm/Dogrib Fire Research Initiative Quicknote 6. Foothills Model Forest, Hinton, AB. 2 p. Also available at <[http://www.fmf.ab.ca/CDFR/CDFR\\_Qn6.pdf](http://www.fmf.ab.ca/CDFR/CDFR_Qn6.pdf)>.
- American Meteorological Society. 2009a. Mixing ratio. Glossary of meteorology. <<http://msglossary.allenpress.com/glossary/search?id=mixing-ratio1>>. Accessed November 5, 2009. 1 p.
- American Meteorological Society. 2009b. Moist-adiabatic lapse rate. Glossary of meteorology. <<http://msglossary.allenpress.com/glossary/search?id=moist-adiabatic-lapse-rate1>>. Accessed November 5, 2009. 1 p.
- Anderson, D.H.; Catchpole, E.A.; de Mestre, N.J.; Parkes, T. 1982. Modelling the spread of grass fires. *J. Aust. Math. Soc. (Ser. B)* 23:451–466.
- Anderson, H.E. 1982. Aids to determining fuel models for estimating fire behavior. US Dep. Agric., For. Serv., Intermt. For. Range Exp. Stn., Ogden, UT. Gen. Tech. Rep. INT-122. 22 p.
- Anderson, H.E. 1983. Predicting wind-driven wildland fire size and shape. US Dep. Agric., For. Serv., Intermt. For. Range Exp. Stn., Ogden, UT. Res. Pap. INT-305. 26 p.
- Anderson, D.W. 2000a. Exploring possibilities in nature using LANDMINE. Pages 18–19 in B.C. Hawkes and M.D. Flannigan, eds. Landscape fire modeling—challenges and opportunities. Proc. Landsc. Fire Model. Workshop, Victoria, British Columbia, 15–16 November 1999. *Can. For. Serv., North. For. Cent., Edmonton, AB. Inf. Rep. NOR-X-371.*
- Anderson, D.W. 2000b. Landscape-level fire activity on foothills and mountain landscapes of Alberta. *Alta. Foothills Disturb. Ecol. Res. Ser. Rep. 2.* Bandaloop Landscape-Ecosystem Services, Belcarra, BC. 44 p.
- Baines, P.G. 1990. Physical mechanisms for the propagation of surface fires. *Math. Comput. Model.* 13(12):83–94.
- Beck, J.A.; Trevitt, A.C.F. 1989. Forecasting diurnal variations in meteorological parameters for predicting fire behavior. *Can. J. For. Res.* 19(6):791–797.
- Beer, T. 1990. The Australian national bushfire model project. *Math. Comput. Model.* 13(12):49–56.
- Beer, T.; Enting, I.G. 1990. Fire spread and percolation modelling. *Mathl. Comput. Modelling.* 13(11):77–96.
- Beverly, J.L.; Herd, E.P.K.; Conner, J.C.R. 2009. Modeling fire susceptibility in west central Alberta, Canada. *For. Ecol. Manag.* 258:1465–1478.
- Blakemore, M. 1984. Generalization and error in spatial databases. *Cartographica* 21:131–139.
- Bose, C.; Bryce, R.; Dueck, G. 2009. Untangling the Prometheus nightmare. Pages 74–80 in R.S. Anderssen, R.D. Braddock, and L.T.H. Newham, Eds. Proc. 18th IMACS World Congress MODSIM09 and International Congress on Modelling and Simulation, Cairns, Australia, 13–17 July 2009. Modelling and Simulation Society of Australia and New Zealand Inc. and International Association for Mathematics and Computers in Simulation.
- Boychuk, D.; Braun, J.; Kulperger, R.J.; Krougly, Z.L.; Stanford, D.A. 2009. A stochastic forest fire growth model. *Environ. Ecol. Stat.* 16(2):133–151.
- Burgan, R.E.; Rothermel, R.C. 1984. BEHAVE: fire behavior prediction and fuel modeling system. US Dep. Agric. For. Serv. Gen. Tech. Rep. INT-167. 126 p.

- Butler, B.W.; Finney, M.; Bradshaw, L.; Forthofer, J.; McHugh, C.; Stratton, R.; Jimenez, D. 2006. WindWizard: a new tool for fire management decision support. Pages 787–796 in P.L. Andrews and B.W. Butler, Compilers. Fuels management — how to measure success. Conf. Proc., Portland, Oregon, 28–30 March 2006. US Dep. Agric., For. Serv., Rocky Mt. Res. Stn., Fort Collins, CO. RMRS-P-41. 10 p.
- Byram, G.M. 1959. Combustion of forest fuels. Pages 61–89 in K.P. Davis, Ed. Forest fire: control and use. McGraw-Hill, New York.
- Caballero, D. 2006. Taxicab geometry: some problems and solutions for square grid-based fire spread simulation. In D.X. Viegas, Ed. Proc. 5th Int. Conf. For. Fire Res., Figueira, Portugal, 27–30 November 2006. CD-ROM.
- Canadian Wildland Fire Growth Simulation Model Data I/O Standards Technical Sub-Committee. 2009. Prometheus data I/O standards manual. 12 p.
- Catchpole, E.A.; de Mestre, N.J.; Gill, A.M. 1982. Intensity of fire at its perimeter. Aust. For. Res. 12:47–54.
- Chase, C.H. 1981. Spot fire distance equations for pocket calculators. US Dep. Agric., For. Serv., Intermt. For. Range Exp. Stn., Ogden, UT. Res. Note INT-310. 21 p.
- Chase, C.H. 1984. Spotting distances from wind-driven surface fires – extensions of equations for pocket calculators. US Dep. Agric., For. Serv., Intermt. For. Range Exp. Stn., Ogden, UT. Res. Note INT-346.
- Clark, T.L.; Coen, J.L.; Latham, D. 2004. Description of a coupled atmosphere–fire model. Int. J. Wildland Fire 13:49–63.
- Clark, T.L.; Jenkins, M.A.; Coen, J.L.; Packham, J. 1996. A coupled atmospheric–fire model: convective Froude number and dynamic fingering. Int. J. Wildland Fire 6:177–190.
- Coen, J.L. 2005. Simulation of the Big Elk fire using coupled atmosphere–fire modeling. Int. J. Wildland Fire 14:49–59.
- Coleman, J.; Sullivan, A. 1996. A real-time computer application for the prediction of fire spread across the Australian landscape. Simulation 67(4):230–240.
- Cotterell, A.F. 1986. A dictionary of world mythology. Oxford Univ. Press, Oxford, UK. 314 p.
- Countryman, C.M. 1971. Fire whirls: why, when and where. US Dep. Agric., For. Serv., Pac. Southwest For. Range Exp. Stn., Berkeley, CA. 14 p.
- Cui, W.; Perera, A.H. 2008. A study of simulation errors caused by algorithms of forest fire growth models. Ont. For. Res. Instit., Sault Ste. Marie, ON, For. Res. Rep. No. 167. 17 p.
- Cumming, S. 2000. Multiscale models of fire in boreal forests. Pages 23–24 in B.C. Hawkes and M.D. Flannigan, eds. Landscape fire modeling—challenges and opportunities. Proc. Landsc. Fire Model. Workshop, Victoria, British Columbia, 15–16 November 1999. Can. For. Serv., North. For. Cent., Edmonton, AB. Inf. Rep. NOR-X-371.
- Curry, J.R. 1936. Fire behavior studies on the Shasta Experimental Forest. USDA Forest Service, Fire Control Notes 1:2–30.
- Curry, R.J.; Fons, W.L. 1938. Rate of spread of surface fires in the ponderosa pine type of California. J. Agric. Res. 54(4):239–268.
- CWFGM Project Steering Committee. 2009. Prometheus COM programmer's manual. 111 p.
- Dijkstra, E.W. 1959. A note on two problems in connexion with graphs. Numer. Math. 1:269–271.
- Englefield, P.; Lee, B.S.; Suddaby, R.M. 2000. Spatial Fire Management System. Paper 489 in Proc. 20th ESRI Int. User Conf. Environmental Systems Research Institute, Redlands, CA. <<http://gis.esri.com/library/userconf/proc00/professional/papers/PAP489/p489.htm>>.
- Fall, A.; Fall, J. 1996. SELES: a spatially explicit landscape event simulator. In Proc. 3rd Int. Conf. Workshop Integr. Geogr. Inf. Syst. Environ. Model., Santa Fe, New Mexico, 21–26 January 1996. National Center for Geographic Information and Analysis, City. CD-ROM.
- Feunekes, U. 1991. Error analysis in fire simulation models. M.Sc.F. thesis, Univ. New Brunswick, Fredericton, NB. 75 p.
- Feunekes, U. 1995. FireNB fire spread simulation. FireNB user's guide. REMSFOT Inc., Fredericton, NB. 14 p.
- Finney, M.A. 2002. Fire growth using minimum travel time methods. Can. J. For. Res. 32:1420–1424.
- Finney, M.A. 2004. FARSITE: fire area simulator — model development and evaluation. Rev. ed. US Dep. Agric., For. Serv. Res. Pap. RMRS-RP-4. 48 p.
- Fogarty, L.G.; Alexander, M.E. 1999. A field guide for predicting grassland fire potential: derivation and use. Nat. Resour. Can., Can. For. Serv., Ottawa, Ont., For. Res., Rotorua, New Zealand, and Natl. Rural Fire Authority, Wellington. New Zealand. Fire Technol. Transfer Note 20. 10 p.
- Fons, W.T. 1946. Analysis of fire spread in light forest fuels. J. Agric. Res. 72(3):93–121.
- Forestry Canada Fire Danger Group. 1992. Development and structure of the Canadian Forest Fire Behavior Prediction System. For. Can., Sci. Sustain. Dev. Dir., Ottawa, ON. Inf. Rep. ST-X-3. 63 p.
- Forthofer, J.M. 2007. Modeling wind in complex terrain for use in fire spread prediction, M.Sc. Thesis, Colorado State University, Fort Collins, CO. 123 p.
- Frandsen, W.H.; Andrews, P.L. 1979. Fire behavior in nonuniform fuels. US Dep. Agric., For. Serv., Intermt. For. Range Exp. Stn., Ogden, UT. Res. Pap. INT-232. 34 p.
- French, I.A. 1992. Visualization techniques for the computer simulation of bushfires in two dimensions. M.Sc. thesis, Univ. New South Wales, Australia. 140 p.
- Garland, J.L. 1988. My chance: a modeler's day in court. J. For. 84(4): inside back cover.

- Gisborne, H.T. 1927. Meteorological factors in the Quartz Creek forest fire. *Monthly Weather Review*. 55: 56–60.
- Green, D.G. 1983. Shapes of simulated fires in discrete fuels. *Ecol. Model.* 20:21–32.
- Green, D.G.; Gill, A.M.; Noble, I.R. 1983. Fire shapes and the adequacy of fire-spread models. *Ecol. Model.* 20:33–45.
- Green, D.G.; Tridgell, A. 1990. Interactive simulation of bushfires in heterogeneous fuels. *Math. Comput. Model.* 13(12):57–66.
- Greiner, G.; Hormann, K. 1998. Efficient clipping of arbitrary polygons. *ACM TOG*. 17(2):71–83.
- Hirsch, K.G. 1996. Canadian Forest Fire Behavior Prediction (FBP) System: user's guide. *Nat. Resour. Can., Can. For. Serv., Northwest Reg., North. For. Cent., Edmonton, Alberta. Spec. Rep. 7.* 121 p.
- Huygens, C. 1962. *Treatise on light* (S.P. Thompson, translator). Dover Publ., New York. (Original work published 1912.) 128 p.
- Hyman, J.M. 1984. Numerical methods for tracking interfaces. *Physica* 12D:396–407.
- Johnston, P.; Milne, G.; Kelso, J. 2006. A heat transfer simulation model for wildfire spread. *In* D.X. Viegas, Ed. *Proc. 5th Int. Conf. For. Fire Res., Figueira, Portugal, 27–30 November 2006.* CD-ROM. 15 p.
- Kay, J. 1927. Forest fire research. *Forestry Chronicle*. 4(4): 30–37.
- Keane, R.E.; Cary, G.J.; Davies, I.D.; Flannigan, M.D.; Gradner, R.H.; Lavorel, S.; Lenihan, J.M.; Li, C.; Rupp, T.S. 2004. A classification of landscape fire succession models: spatial simulations of fire and vegetation dynamics. *Ecol. Model.* 179:3–27.
- Knight, I.; Coleman, J. 1993. A fire perimeter expansion algorithm based on Huygens' wavelet propagation. *Int. J. Wildland Fire* 3(2):73–84.
- Kourtz, P. 1977. An application of Landsat digital technology to forest fire fuel type mapping. Pages 1111–1115 *in* P.L. Andrews and B.W. Butler, Compilers. *Proc. 11th Int. Symp. Remote Sens. Environ., Ann Arbor, Michigan. Environmental Research Institute of Michigan.*
- Kourtz, P.; Nozaki, S.; O'Regan, W.G. 1977. Forest fires in the computer — a model to predict the perimeter location of a forest fire. *Fish. Environ. Can., Ottawa, ON. Inf. Rep. FF-X-65.*
- Kourtz, P.H.; O'Regan, W.G. 1971. A model for a small forest fire ... to simulate burned and burning areas for use in a detection model. *For. Sci.* 17(2):163–169.
- Lawson, B.D.; Armitage, O.B. 2008. Weather guide for the Canadian Forest Fire Danger Rating System. *Nat. Resour. Can., Can. For. Serv., North. For. Cent., Edmonton, AB.* 73 p.
- Lawson, B.D.; Armitage, O.B.; Hoskins, W.D. 1996. Diurnal variation in the Fine Fuel Moisture Code: tables and computer source code. *Can. – B.C. Partnership Agreement on For. Resour. Dev.: FRDA II, Can. For. Serv., B.C. Minist. For., Victoria, BC.* FRDA Rep. 245. 20 p.
- Linn, R.R. 1997. Transport model for prediction of wildfire behaviour. Los Alamos National Laboratory, Scientific Rep. LA13334-T, Los Alamos, NM. 195 p.
- Linn, R.R.; Cunningham, P. 2005. Numerical simulations of grass fires using a coupled atmosphere-fire model: Basic fire behaviour and dependence on wind speed. *J. Geophys. Res.* 110, doi:10.1029/2004JD005597.
- Luke, R.H.; McArthur, A.G. 1978. Bushfires in Australia. *Commonw. Sci. Ind. Res. Org., Div. For. Res., For. Timber Bur., Canberra, Australia.* 359 p.
- Mackay, G.; Jan, N. 1984. Forest fires as a critical phenomena. *J. Phys.* 19:281–287.
- McAlpine, R.S. 1989. Temporal variations in elliptical forest fire shapes. *Can. J. For. Res.* 19:1496–1500.
- McAlpine, R.S. 1995. Testing the effect of fuel consumption on fire spread rate. *Int. J. Wildland Fire* 5(3):143–152.
- McAlpine, R.S.; Wakimoto, R.H. 1991. The acceleration of fire from point source to equilibrium spread. *For. Sci.* 37(5):1314–1337.
- McArthur, A.G. 1966. Weather and grassland fire behaviour. *Commonw. Aust. For. Timber Bur. Leaflet.* 100. 23 p.
- McHugh, C.W. 2006. Considerations in the use of models available for fuel treatment analysis. Pages 81–105 *in* P.L. Andrews and B.W. Butler, Compilers. *Fuels management — how to measure success: Conf. Proc., Portland, Oregon, 28–30 March 2006.* US Dep. Agric., For. Serv. Rocky Mt. Res. Stn., Fort Collins, CO. RMRS-P-41.
- Mell, W.E.; Manzello, S.L.; Maranghides, A. 2006. Numerical modeling of fire spread through trees and shrubs. Pages 1–12 *in* D.X. Viegas Ed. *Proceedings Fifth International Conference on Forest Fire Research, November 27–30, 2006, Coimbra, Portugal.*
- Messier, C.M.; Fortin, M.-J.; Schmiegelow, F.K.A.; Doyon, F.; Cumming, S.G.; Kimmins, J.P.; Welham, C.; Nelson, J. 2003. Modelling tools to assess the sustainability of forest management scenarios. Pages 531–580 *in* P.J. Burton, C. Messier, D.W. Smith, and W.L. Adamowicz, Eds. *Towards sustainable management of the boreal forest.* NRC Res. Press, Ottawa, ON.
- Morris, G.A. 1987. A simple method for computing spotting distances from wind-driven surface fires. *US Dep. Agric., For. Serv., Intermt. Res. Stn., Ogden, UT. Res. Note INT-374.*

- Muraro, S.J.; Russell, N.R.; Lawson, B.D. 1969. Development of diurnal adjustments table for Fine Fuel Moisture Code. Can. For. Serv., Pac. For. Res. Cent., Victoria, BC. Inf. Rep. BC-X-35.
- Murray, F.W. 1967. On the computation of saturation vapour pressure. *J. Appl. Meteorol.* 6:203–204.
- National Oceanic and Atmospheric Administration. 2008a. Vapor Pressure. NOAA Tech. Rep. <http://www.srh.noaa.gov/elp/wxcalc/formulas/vaporPressure.pdf>. Viewed January 30, 2009. 1 p.
- National Oceanic and Atmospheric Administration. 2008b. Wet-bulb temperature and dewpoint temperature from air temperature and relative humidity. NOAA Tech. Rep. <http://www.srh.noaa.gov/elp/wxcalc/formulas/wetBulbTdFromRh.pdf>. Viewed January 30, 2009. 2 p.
- Olsen, C.F. 1941. An analysis of the Honey Fire. *Fire Control Notes*. 5:161–178. [reprint: *Fire Management Today*. 63(3): 29–41].
- Opperman, T.; Gould, G.; Finney, M.; Tymstra, T. 2006. Applying fire spread simulators in new Zealand and Australia: Results from an international seminar. Pages 201–212 *in Proc. 1st Int. Conf. Math. Model., St. Louis, Missouri*. USDA For. Serv. RMRS-P-41.
- O'Regan, W.G.; Kourtz, P.; Nozaki, S. 1976. Bias in the contagion analog to fire spread. *For. Sci.* 2(1):61–68.
- O'Regan, W.G.; Nozaki, S.; Kourtz, P. 1973. A method for using directional rates of spread to predict forest fire configurations. Western States Section/The Combustion Institute. WSS/CI Paper 73–17 (unpaginated).
- Parisien, M.A.; Kafka, V.G.; Hirsch, K.G.; Todd, J.B.; Lavoie, S.G.; Maczek, P.D. 2005. Mapping wildfire susceptibility with the BURN-P3 simulation model. *Nat. Resour. Can., Can. For. Serv., North. For. Cent., Edmonton, AB. Inf. Rep. NOR-X-405*. 36 p.
- Parisien, M.-A.; Miller, C.; Ager, A.A.; Finney, M.A. 2009. Use of artificial landscapes to isolate controls on burn probability. *Landsc. Ecol.* Published online Sept. 4, 2009. DOI 10.1007/s10980-009-9398-9. 15 p.
- Peet, G.B. 1967. The shape of mild fires in Jarrash forest. *Aust. For.* 31(2):121–127.
- Perera, A.H.; Yemshanov, D.; Schnekenburger, F.; Weaver, K.; Baldwin, D.J.B.; Boychuk, D. 2002. Boreal Forest Landscape Dynamics Simulator (BFOLDS): a grid-based spatially stochastic model for predicting crown fire regime and forest cover transition. *Ont. For. Res. Inst., Sault Ste. Marie, ON. For. Res. Rep.* 152. 60 p.
- Prometheus Project Steering Committee. 1999. Development and application of a wildland fire growth model. Proposal to Foothills Model Forest. 28 p.
- Richards, G.D. 1990. An elliptical growth model of forest fire fronts and its numerical solution. *Int. J. Numer. Math. Eng.* 30:1133–1149.
- Richards, G.D. 1993. The properties of elliptical fire growth for time dependent fuel and meteorological conditions. *Combust. Sci. Technol.* 92:145–171.
- Richards, G.D. 1995. A general mathematical framework for modeling two-dimensional wildland fire spread. *Int. J. Wildland Fire.* 5(2):63–72.
- Richards, G.D. 1999. The mathematical modelling and computer simulation of wildland fire perimeter growth over a 3-dimensional surface. *Int. J. Wildland Fire.* 9(3):213–221.
- Richards, G.D.; Bryce, R.W. 1995. A general mathematical framework for modelling two-dimensional wildland fire spread. *Int. J. Wildland Fire.* 5(2):73–79.
- Roberts, S. 1989. A line element algorithm for curve flow problems in the plane. *Aust. Natl. Univ., Cent. Math. Anal., Canberra, Australia*. CMA-R58-89.
- Rogeanu, M.P.; Woodard, P.M.; Feunekes, U. 1998. Landscape disturbance modelling. Pages 461–466 *in Proc. 13th Conf. Fire For. Meteorol., Lorne, Australia, 27–31 October 1996*. Int. Assoc. Wildland Fire.
- Rothermel, R.C. 1972. A mathematical model for predicting fire spread in wildland fires. *US Dep. Agric., For. Serv., Intermt. For. Range Exp. Stn., Ogden, UT. Res. Pap.* INT-115. 52 p.
- Rothermel, R.C.; Anderson, H.E. 1966. Fire spread characteristics determined in the laboratory. *US Dep. Agric., For. Serv., Intermt. For. Range Exp. Stn., Ogden, UT. Res. Pap.* INT-30. 34 p.
- Sanderlin, J.C.; Sunderson, J.M. 1975. A simulation for wildland fire management planning support (FIREMAN). Vol. 2. Prototype models for FIREMAN (Part II): Campaign fire evaluation. Mission Research Corp. Contract 21-343, Spec. 222. 249 p.
- Sanderlin, J.C.; Van Gelder, R.J. 1977. A simulation of fire behaviour and suppression effectiveness for operation support in wildland fire management. Pages 619–630 *in Proc. 1st Int. Conf. Math. Model., St. Louis, MO*.
- Scott, J.H.; Burgan, R.E. 2005. Standard fire behavior fuel models: a comprehensive set for use with Rothermel's surface fire spread model. *US Dep. Agric., For. Serv., Rocky Mtn. Res. Stn., Fort Collins, CO. Gen. Tech. Rep.* RMRS-GTR-153. 72 p.
- Shimrat, M. 1962. Position of point relative to polygon. Algorithm 112 *in Collected algorithms from ACM 1*. *Comm. ACM.* 5(8):434.
- Stewart, F.R. 1971. A mechanistic fire spread model. *Combust. Sci. Technol.* 4:177–186.
- Suffling, R.; Grant, A.; Feick, R. 2008. Modeling prescribed burns to serve as regional firebreaks to allow wildfire activity in protected areas. *For. Ecol. and Manage.* 256(11):1815–1824.
- Todd, B. 1999. User documentation for the Wildland Fire Growth Model and the Wildfire\_Display Program. *Can. For. Serv., North For. Cent., Edmonton, AB.* 37 p. Draft rep.

- Tolhurst, K.G.; Chong, D.M.; Strandgard, M.N. 2006. Wildfire risk management model for strategic management. *For. Ecol. Manag.* 234(Suppl. 1):S211.
- Tymstra, C.; Ellehoj, E.A. 1994. Fire behaviour prediction and fuel type mapping using the Alberta Vegetation Inventory. Pages 887-893 *in* Proc. GIS'94 Symp., Vancouver, British Columbia, February 1994.
- Tymstra, C.; Flannigan, M.; Armitage, O.B.; Logan, K. 2007. The impact of climate change on area burned in Alberta's boreal forest. *Int. J. Wildland Fire* 16:153-160.
- Tymstra, C.; Mayer, B.; MacGregor, B. 2005. The 2002 House River wildfire, Alberta, Canada. *Fire Manag. Today* 64(4):16-18.
- Van Wagner, C.E. 1963. On working fire behavior data into forest fire control planning. *Annu. Inspect. Conf. Lower Ottawa For. Prot. Assoc., Hull, QC*, 18 April 1963.
- Van Wagner, C.E. 1966. Three controlled fires in jackpine slash. *Can. Dep. For., Ottawa, ON. Publ.* 1146. 22 p.
- Van Wagner, C.E. 1969. A simple fire growth model. *For. Chron.* 45:103-104.
- Van Wagner, C.E. 1972. A table of diurnal variation in the fine fuel moisture code. *Can. For. Serv., Petawawa For. Exp. Stn., Chalk River, ON. Inf. Rep.* PS-X-38.
- Van Wagner, C.E. 1973. Rough prediction of fire spread rates by fuel type. *Can. For. Serv., Petawawa For. Exp. Stn., Chalk River, ON. Inf. Rep.* PS-X-42.
- Van Wagner, C.E. 1977. A method of computing fine fuel moisture content throughout the diurnal cycle. *Fish. Environ. Can., Can. For. Serv., Petawawa For. Exp. Stn., Chalk River, ON. Inf. Rep.* PS-X-69. 15 p.
- Van Wagner, C.E. 1987. Development and structure of the Canadian Forest Fire Weather Index System. *Can. For. Serv., Ottawa, ON. For. Tech. Rep.* 35. 37 p.
- Van Wagner, C.E. 1989. Prediction of crown fire behavior in conifer stands. Pages 207-212 *in* Proceedings of Tenth Conference of Fire and Forest Meteorology, 17-21 April 1989, Ottawa, ON. Forestry Canada, Ottawa, ON.
- Van Wagner, C.E.; T.T. Pickett. 1985. Equations and FORTRAN program for the Canadian Forest Fire Weather Index System. *Can. For. Serv., For. Tech. Rep.* 33. 18p.
- Vatti, B.R. 1992. A generic solution to polygon clipping. *CACM.* 35(7):56-63.
- Watts, J.M., Jr. 1987. Validating fire models [editorial]. *Fire Technol.* 23:93-94.
- Weisstein, E.W. 1999. Regular polygon. In: *MathWorld* — A Wolfram web resource. Wolfram Research, Champaign, IL. <<http://mathworld.wolfram.com/RegularPolygon.html>>.
- Wilson, A.A.G. 1988. Width of firebreak that is necessary to stop grass fires: some field experiments. *Can. J. For. Res.* 18:682-687.
- Wotton, B.M.; Alexander, M.E.; Taylor, S.W. 2009. Updates and revisions to the 1992 Canadian Forest Fire Behavior Prediction System. *Nat. Resour. Can., Can. For. Serv., Great Lakes For. Cent., Sault Ste. Marie, ON. Inf. Rep.* GL-X-10. 45 p.







|                             |                                                                                                                                       |
|-----------------------------|---------------------------------------------------------------------------------------------------------------------------------------|
| $\alpha_T$                  | Parameter for the diurnal temperature curve that defines the time lag between the time of sunrise and the time of minimum temperature |
| $\alpha_{WS}$               | Parameter for the diurnal temperature curve and defines the time lag between the time of sunrise, and the time of minimum wind speed  |
| $\beta_j^i$                 | Interior angle of the fire front at vertex $P_j^i$ expressed in radians, at vertex $P_j^i$                                            |
| $\beta_T$                   | Parameter for the diurnal temperature curve that defines the time lag between solar noon and the time of maximum temperature          |
| $\beta_{WS}$                | Parameter for the diurnal temperature curve and defines the time lag between solar noon, and the time of maximum wind speed.          |
| $\Delta P_j^i$              | Change in location of a vertex from time step $i$ to time step $i+1$                                                                  |
| $\Delta P_\tau$             | Distance resolution, the maximum distance that vertices can travel before the landscape and weather are resampled                     |
| $\Delta t$                  | Time step duration                                                                                                                    |
| $\gamma_T$                  | Parameter for the diurnal temperature curve that is a decay function for nighttime cooling                                            |
| $\gamma_{WS}$               | Parameter for the diurnal temperature curve and is a decay function for wind speed during the night time                              |
| $\theta$                    | Counterclockwise angle from the positive $x$ axis to the spread direction vector                                                      |
| $\bar{\theta}_j^i$          | Effective wind direction at $P_j^i$                                                                                                   |
| $\varphi$                   | Cartesian angle from the wind direction vector to the vector from the burning cell to an adjacent cell                                |
| $\phi$                      | Angle from the positive $x$ axis to the vector from the center of the ellipse to a point on the subtending circle                     |
| $\omega$                    | Smoothing factor                                                                                                                      |
| $a_e$                       | Forward spread distance from center of ellipse                                                                                        |
| $b_e$                       | Flank spread distance                                                                                                                 |
| $c_e$                       | Forward spread distance from ignition point to center of ellipse                                                                      |
| $a_{ROS}, b_{ROS}, c_{ROS}$ | Rate-of-spread parameters for each FBP fuel type                                                                                      |
| $BE$                        | Buildup Effect                                                                                                                        |
| $BFI$                       | Back fire intensity                                                                                                                   |
| $BROS$                      | Equilibrium back fire spread rate                                                                                                     |
| $BROS_t$                    | Back fire rate of spread after elapsed time $t$                                                                                       |
| $BRSS$                      | Surface fire rate of spread of the back fire in fuel type C-6                                                                         |
| $BUI$                       | Buildup Index                                                                                                                         |
| $BUI_0$                     | Mean $BUI$ for a particular fuel type                                                                                                 |
| $CBH$                       | Height to live crown base (also known as crown base height)                                                                           |
| $CFB$                       | Crown fraction burned                                                                                                                 |
| $CFC$                       | Crown fuel consumption                                                                                                                |
| $CFL$                       | Crown fuel load                                                                                                                       |
| $DBt$                       | Back fire spread distance at elapsed time $t$                                                                                         |
| $DC$                        | Drought Code                                                                                                                          |

|                                   |                                                                                        |
|-----------------------------------|----------------------------------------------------------------------------------------|
| $DFt$                             | Flank fire spread distance at elapsed time $t$                                         |
| $DHt$                             | Head fire spread distance at elapsed time $t$                                          |
| $D_i$                             | Distance from the centroid to a given natural neighbor vertex                          |
| $DMC$                             | Duff Moisture Code                                                                     |
| $DP_s$                            | Spatially interpolated dew point temperature                                           |
| $E$                               | Eccentricity                                                                           |
| $FFI$                             | Flank fire intensity                                                                   |
| $FFMC$                            | Fine Fuel Moisture Code (daily)                                                        |
| $FI$                              | Fire intensity                                                                         |
| $FMC$                             | Foliar Moisture Content                                                                |
| $FROS$                            | Equilibrium flank fire rate of spread                                                  |
| $FROS_t$                          | Flank fire rate of spread after elapsed time $t$                                       |
| $FRSS$                            | Surface rate of spread of the flank fire in fuel type C-6                              |
| $FWI$                             | Fire Weather Index                                                                     |
| $HFI$                             | Head fire intensity                                                                    |
| $HFFMC$                           | Hourly Fine Fuel Moisture Code                                                         |
| $HFFMC_{in}$                      | Previous (initial) Hourly Fine Fuel Moisture Code to calculate the moisture content    |
| $HFFMC_{out}$                     | New Hourly Fine Fuel Moisture Code at the next time step                               |
| $HFWI$                            | Hourly Fire Weather Index                                                              |
| $HISI$                            | Hourly Initial Spread Index                                                            |
| $HROS$                            | Equilibrium head rate of spread                                                        |
| $ISI$                             | Initial Spread Index                                                                   |
| LST                               | Local standard time                                                                    |
| $L_F$                             | Flame length                                                                           |
| $L_j^i$                           | Length of one segment (edge) of the fire perimeter                                     |
| $L_\tau$                          | Perimeter resolution, the maximum allowable distance between any two adjacent vertices |
| $m$                               | New moisture content at the next time step                                             |
| $MBW$                             | Minimum barrier width, for breaching                                                   |
| $MC$                              | Previous (initial) moisture content                                                    |
| $\vec{N}_j^i$                     | Unit length vector                                                                     |
| $PC$                              | Percent conifer                                                                        |
| $PDF$                             | Percent dead fir                                                                       |
| $P_j^i$                           | Vertex $i$ in $\vec{P}_j$                                                              |
| $\vec{P}_j$                       | Ordered set of vertices defining the fire perimeter at time iteration $j$              |
| $P_{x_j}^i, P_{y_j}^i, P_{z_j}^i$ | Dimensional components of $P_j^i$                                                      |

|               |                                                                                                                       |
|---------------|-----------------------------------------------------------------------------------------------------------------------|
| $q$           | Proportion of maximum rate of spread at $BUI$ equal to 50                                                             |
| $\vec{r}_j^i$ | Unit tangent vector to the curve $P_j$ at the vertex $P_j^i$                                                          |
| $RAZ$         | Net effective spread direction                                                                                        |
| $RH$          | Relative humidity                                                                                                     |
| $RH_s$        | Relative humidity calculated from spatially interpolated inputs                                                       |
| $ROS$         | Rate of spread (either $ROS_e$ or $ROS_t$ )                                                                           |
| $ROS_0$       | Rate of spread with no wind                                                                                           |
| $ROS_e$       | Equilibrium head fire rate of spread                                                                                  |
| $ROS_t$       | Head fire rate of spread after elapsed time $t$                                                                       |
| $RSS$         | Surface fire rate of spread                                                                                           |
| $S_i$         | Statistic value at a given natural neighbor vertex                                                                    |
| SFC           | Surface fuel consumption                                                                                              |
| $t_0$         | Start time for simulation or ignition                                                                                 |
| $t_d$         | Display time step $d$                                                                                                 |
| $tFFMC$       | Instantaneous FFMC with consideration for temporal interpolation; does not necessarily consider spatial interpolation |
| $tFWI$        | Instantaneous FWI with consideration for temporal interpolation; does not necessarily consider spatial interpolation  |
| $t_j$         | Simulated time step $j$                                                                                               |
| $tISI$        | Instantaneous ISI with consideration for temporal interpolation; does not necessarily consider spatial interpolation  |
| $t_n$         | End time for simulation                                                                                               |
| $t_{\tau a}$  | Maximum calculation time step during acceleration                                                                     |
| $t_{\tau e}$  | Maximum calculation time step during equilibrium rate of spread                                                       |
| $T$           | Temperature                                                                                                           |
| $T_s$         | Spatially interpolated temperature                                                                                    |
| $TFC$         | Total fuel consumption                                                                                                |
| $V_c$         | Voronoi region (a square) for the grid cell of interest                                                               |
| $V_i$         | Voronoi region for a given vertex                                                                                     |
| $VP$          | Vapor pressure (millibars)                                                                                            |
| $VP_{sa}$     | Saturated vapor pressure (millibars)                                                                                  |
| $w$           | Width of a fuel break                                                                                                 |
| $WD$          | Wind direction                                                                                                        |
| $WS$          | Wind speed                                                                                                            |
| $WSV$         | Net effective wind speed, based on the influence of both wind and slope                                               |



---

## APPENDIX 2

---

### PROMETHEUS CASE STUDY: SHARPSAND PRESCRIBED BURN (2007)



## Introduction

On 13 May 2007, the Canadian Forest Service (CFS) and the Ontario Ministry of Natural Resources (OMNR) conducted a 0.9-ha prescribed burn. The fire, known as SAU 13, escaped control and grew to over 1 500 ha within 24 h. Significant rainfall halted the spread of the fire late on 14 May 2007, and suppression efforts by OMNR brought the fire under control in about 3 days.

This case study briefly describes the fire environment and observed fire behavior, and then demonstrates how the Prometheus fire growth simulation model can be used to retrospectively explain some of the behavior characteristics of this fire.

## Location

The burn plot (lat. 46.78°; long. 83.33°) was selected from a large cluster of experimental burn plots established initially in the 1970s near Sharpsand Creek, approximately 80 km northeast of Sault Ste. Marie in OMNR's Northeast Region. The burn plot of concern to this case study is known as plot 1 (subdivided into two subplots, 1a and 1b).

## Fire Chronology

The northerly subplot (1b) was ignited 13 May 2007 at approximately 1243 local standard time (LST). Ignition of the entire perimeter of the

plot with hand-held drip torches continued for about 5 min, and by 10 min after ignition began, the entire plot was on fire. The initial surface fire almost immediately moved into the crowns as torching began within 30 s of completion of the final upwind (south) ignition line along the baseline fuel break between subplots 1a and 1b. As the fire spread rapidly downwind across the plot, active crowning commenced, and a convection column formed, drawing in the other perimeter ignition lines.

The convection column generated many firebrands, which were carried across the fuel breaks. These firebrands ignited many spot fires in adjacent fuels outside the plot. Spot fires in the previously partially burned (1991) plot 2, adjacent to subplot 1b, quickly coalesced into a torching fire under the influence of the convection column over subplot 1b, and the fire began its run toward Sharpsand Creek. Within a half hour of ignition being completed, the fire was about 20 ha in size, and by 3 h it had reached about 200 ha, with crowning and spotting. After 4 h, the fire covered about 500 ha, and by 0630 LST the following morning, it had reached its final size of 1 555 ha (Figure A2.1).

Suppression efforts during the afternoon of 13 May were concentrated on the west flank of the fire.

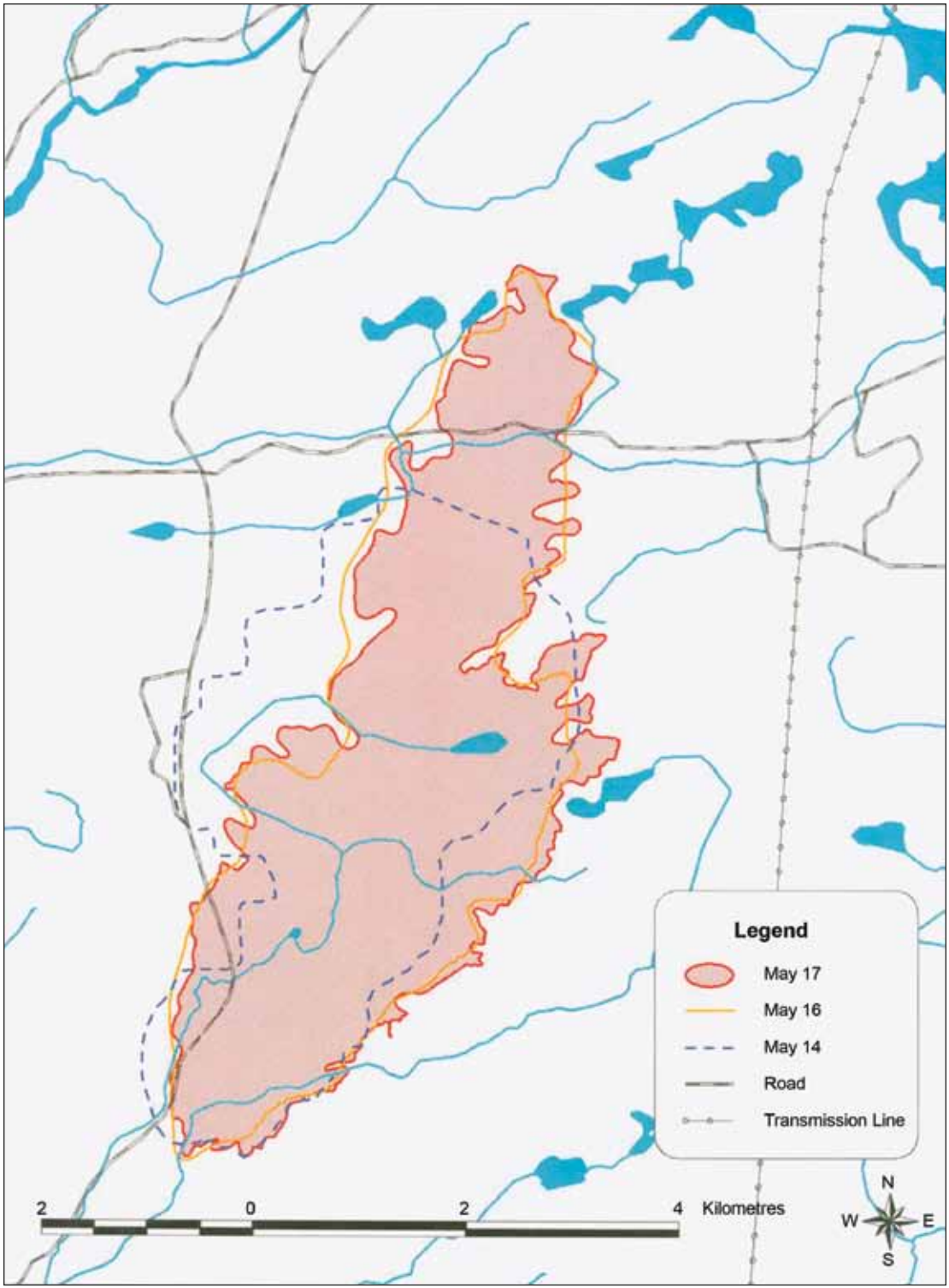


Figure A2.1. Sharsand Fire progression map.

## Fire Environment

### Fuel

The Sharpsand Creek jack pine (*Pinus banksiana*) stand originated naturally following the 1948 Chapleau-Mississauga fire and earlier wildfires (Stocks 1987). The forest floor cover consisted of feather mosses such as *Pleurozium schreberi* and *Hylocomium splendens*, with scattered understory shrubs such as low bush blueberry (*Vaccinium angustifolium*), Labrador tea (*Ledum groenlandicum*), and hazel (*Hamamelis virginiana*). The stand was 60 years old, fully stocked, and 20 m in height, with a scattered black spruce (*Picea mariana*), balsam fir (*Abies balsamea*), and white birch (*Betula papyrifera*) understory. Herbaceous growth was minimal. Ladder fuels from the understory to crown fuels were minimal. The organic layer was uncompacted and relatively shallow, consisting of feather moss, a needle layer, and a minimal loading of dead down woody material.

The Canadian Forest Fire Behavior Prediction (FBP) System fuel types present within and around the SAU 13 fire perimeter are shown in Figure A2.2.

## Topography

The plots were located on level ground on a glacial outwash plain adjacent to Sharpsand Creek, where soils are stony humoferric podzols of glacio-fluvial origin (Stocks 1987). Plot 1 is flat, except for a gentle to moderate 10%–30% north-facing slope north of the plot. According to OMNR (2007), the soil consisted of sand and gravel about 1 m deep.

The topography immediately north of plot 1b was also generally flat at an elevation of about 360 m above sea level. The topography of the northern half of the SAU 13 fire consisted of a series of hills ranging between 350 m and 530 m in height (Figure A2.3).

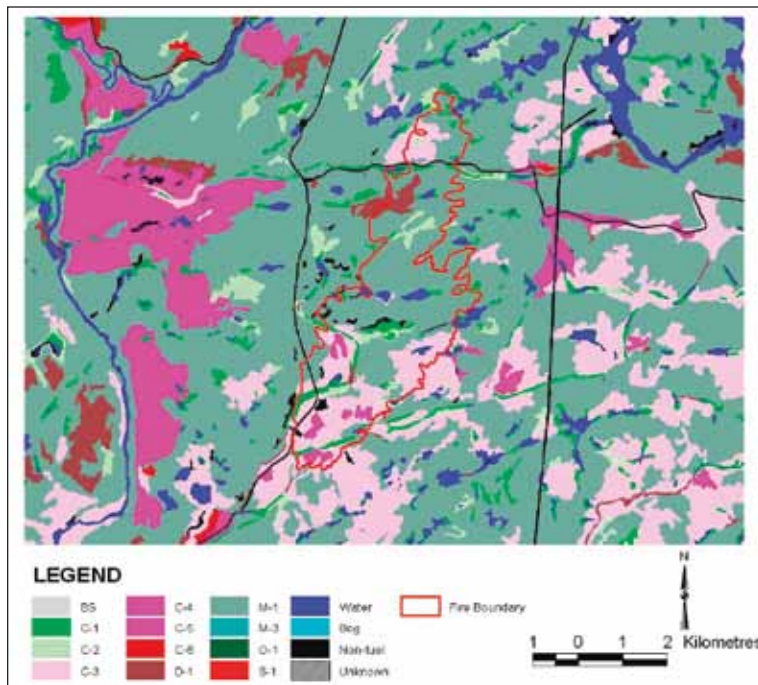


**Figure A2.2.** Canadian Forest Fire Behavior Prediction System fuel types in and around the SAU 13 fire. Adapted from Lawson and Armitage (2008), with permission of Canadian Forest Service, Northern Forestry Centre.

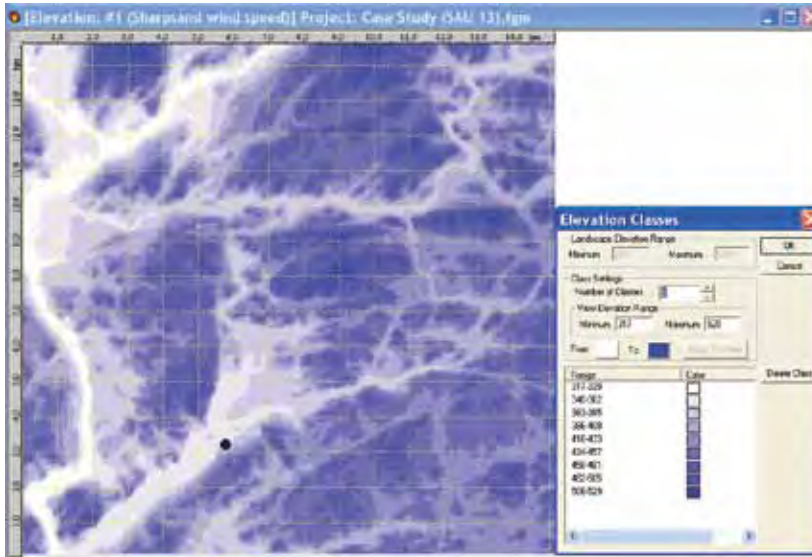


Figure A2.3. Range of elevation (meters above sea level) within and around the SAU 13 fire.

## Fire Weather

An on-site weather station (Sharpsand) was established adjacent to the 2007 experimental burn plot 1B, in a portion of plot 2 that had been partially burned in 1991. The clearing size for the weather station did not meet the standard for fire weather stations recommended for Canadian Forest Fire Danger Rating System applications (Lawson and Armitage 2008). As a result, the wind speeds measured at this station were not a true representation of 10-m open wind speeds, which are required to calculate components of the Fire Weather Index (FWI)

System and the FBP System. For this reason, the higher forecasted winds for the Sharpsand area were deemed more appropriate for modeling fire growth using Prometheus and predicting fire behavior using the FBP System.

The daily fire weather observations and fire danger conditions for 12–15 May are summarized in Table A2.1. The hourly weather observations for the afternoon of 13 May are included within the Prometheus Statistics View (as illustrated in the section “Prometheus Fire Growth Simulations for the SAU 13 Fire”).

Table A2.1. Fire weather observations and fire danger conditions at 1200 local standard time, 12–15 May 2007

| Date   | Temp.<br>(°C) | RH<br>(%) | Wind      |                 | Precip.<br>(mm) | Fire Weather Index System components |     |     |      |     |      |
|--------|---------------|-----------|-----------|-----------------|-----------------|--------------------------------------|-----|-----|------|-----|------|
|        |               |           | Direction | Speed<br>(km/h) |                 | FFMC                                 | DMC | DC  | ISI  | BUI | FWI  |
| May 12 | 12.6          | 25        | 267       | 7.5             | 0.0             | 91.8                                 | 71  | 121 | 8.1  | 70  | 22.8 |
| May 13 | 18.7          | 21        | 182°      | 9.5             | 0.0             | 92.7                                 | 75  | 127 | 10.1 | 74  | 27.3 |
| May 14 | 11.0          | 79        | 189°      | 7.9             | 0.2             | 86.1                                 | 75  | 131 | 3.6  | 75  | 13.0 |
| May 15 | 9.9           | 91        | 336°      | 6.8             | 10.7            | 28.5                                 | 39  | 115 | 0.0  | 42  | 0.0  |

RH = relative humidity, FFMC = Fine Fuel Moisture Code, DMC = Duff Moisture Code, DC = Drought Code, ISI = Initial Spread Index, BUI = Buildup Index, FWI = Fire Weather Index.

## Fire Behavior

Pre-green-up conditions and low foliar moisture content (91%) on 13 May affected the fire behavior within subplot 1b and contributed to the observed fire behavior once the fire escaped from the plot. Both intermittent and continuous crown fires, as well as spotting, were present throughout the fire run on the afternoon of 13 May.

The fire progression map (Figure A2.1) shows the southern portion of the 6.5-km fire run over 5 h, which reached within 500 m south of Black Creek Road when sketch-mapped at 1745 LST (see red dashed line). Fire spread through the evening carried the fire an additional 2.5 km to its final size (1 555 ha), as mapped at 0630 LST on 14 May. The estimated fire perimeter was 35 km. The escaped fire run from plot 1b to the sketched fire perimeter at 1745 LST (south of Black Creek Road) represents an average free-running rate of spread (ROS) of 21.8 m/min (6 550 m/5.0 h).

### Prometheus Fire Growth Simulations for the SAU 13 Fire

The SAU 13 fire consisted of one continuous fire run on the afternoon and evening of 13 May 2007. The following three Prometheus fire growth simulations attempt to model growth of the fire from the time of escape (1254 LST) to 1745 LST, when an estimated fire perimeter was recorded by the fire boss (see dashed red line on the fire progression map [Figure A2.1]). The approximate length of this fire run was

6.5 km. The approximate total length of the SAU 13 fire was 9 km (see bold red line on the fire progression map [Figure A2.1]).

For the following three scenarios, temporal interpolation was turned on and spatial interpolation was turned off. The advanced scenario options used in these simulations are shown in Figure A2.4.

#### Fire Growth Simulation Scenario 1

- Simulation used unadjusted wind speeds from the Sharpsand weather station.
- The result of this simulation was a fire with an approximate spread distance of 2 km and an area burned of 232 ha.

#### Fire Growth Simulation Scenario 2

- Simulation used wind speeds forecasted by OMNR for the afternoon of 13 May 2007.
- The result of this simulation was a fire with an approximate spread distance of 4.5 km and an area burned of 758 ha.

#### Fire Growth Simulation Scenario 3

- Simulation used wind speeds forecasted by OMNR for 13 May 2007 and a weather patch (1.5× forecasted wind speed from 1330 LST to 1530 LST).
- The result of this simulation was a fire with an approximate spread distance of 6.5 km and an area burned of 1140 ha (Figures A2.5 and A2.6).



Figure A2.4 Advanced scenario options used in three simulations of the SAU 13 fire.

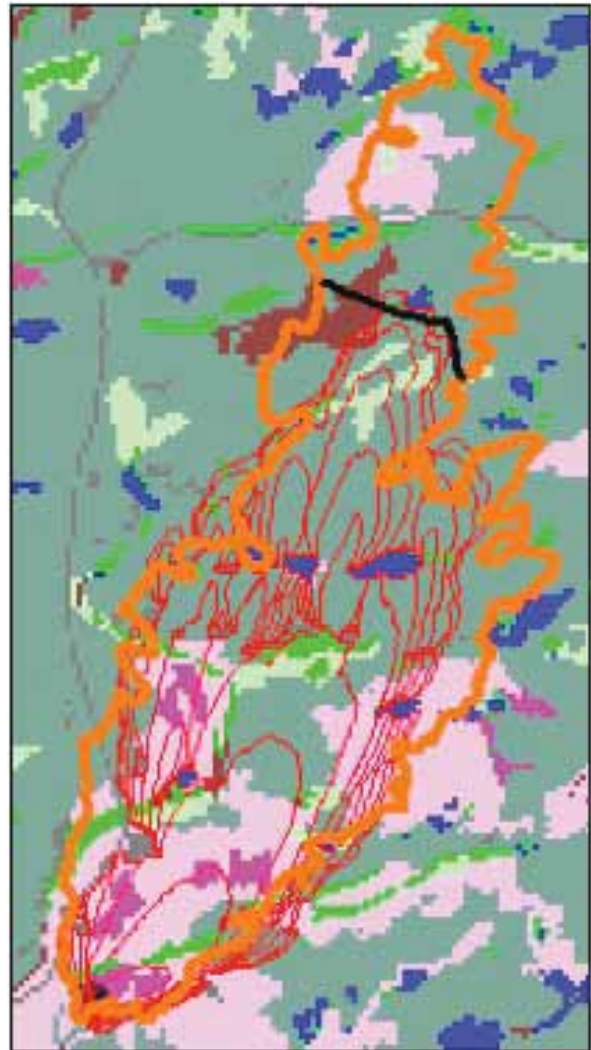


Figure A2.5. Fuel-type Map View for fire growth simulation scenario 3, showing estimated forward spread distance at 1745 local standard time (LST) (black line), final fire perimeter (orange line), and Prometheus 30-min fire progression perimeters to 1745 LST (red lines).

| Time Step | Date and Time         | Eloped Time | Temp (°C) | RH (%) | WD (°) | WS (km/h) | Precip (m) | HFFMC | HISI | HFWI | FFMC | DMC  | DC    | BUI  | Time Step Area (ha) | Total Area (ha) | Active Perimeter (km) | Perimeter (km) |
|-----------|-----------------------|-------------|-----------|--------|--------|-----------|------------|-------|------|------|------|------|-------|------|---------------------|-----------------|-----------------------|----------------|
| 1         | May 12, 2007 12:00:00 | 00:00:00    | 18.7      | 21.0   | 192    | 19.0      | 0.0        | 90.5  | 12.0 | 30.9 | 92.7 | 75.1 | 126.4 | 74.7 | 0.00                | 0.00            | 0.00                  | 0.00           |
| 2         | May 13, 2007 12:30:00 | 00:30:00    | 20.0      | 20.5   | 219    | 23.0      | 0.0        | 90.5  | 12.0 | 30.9 | 92.7 | 75.1 | 126.4 | 74.7 | 0.00                | 0.00            | 0.00                  | 0.00           |
| 3         | May 13, 2007 13:00:00 | 01:00:00    | 21.3      | 20.0   | 255    | 27.0      | 0.0        | 91.1  | 19.6 | 42.6 | 92.7 | 75.1 | 126.4 | 74.7 | 0.03                | 0.03            | 0.06                  | 0.06           |
| 4         | May 13, 2007 13:30:00 | 01:30:00    | 20.4      | 20.0   | 231    | 24.5      | 0.0        | 91.1  | 19.6 | 42.6 | 92.7 | 75.1 | 126.4 | 74.7 | 14.20               | 14.23           | 1.62                  | 1.62           |
| 5         | May 13, 2007 14:00:00 | 02:00:00    | 19.6      | 20.0   | 207    | 22.0      | 0.0        | 91.8  | 16.8 | 38.6 | 92.7 | 75.1 | 126.4 | 74.7 | 64.53               | 78.75           | 3.92                  | 4.01           |
| 6         | May 13, 2007 14:30:00 | 02:30:00    | 19.1      | 21.5   | 205    | 21.9      | 0.0        | 91.8  | 16.8 | 38.6 | 92.7 | 75.1 | 126.4 | 74.7 | 139.31              | 218.06          | 7.18                  | 8.03           |
| 7         | May 13, 2007 15:00:00 | 03:00:00    | 18.6      | 23.0   | 204    | 21.0      | 0.0        | 92.3  | 17.1 | 39.1 | 92.7 | 75.1 | 126.4 | 74.7 | 166.71              | 384.77          | 8.29                  | 11.12          |
| 8         | May 13, 2007 15:30:00 | 03:30:00    | 18.1      | 22.5   | 196    | 23.5      | 0.0        | 92.3  | 17.1 | 39.1 | 92.7 | 75.1 | 126.4 | 74.7 | 134.28              | 519.05          | 12.84                 | 18.16          |
| 9         | May 13, 2007 16:00:00 | 04:00:00    | 17.5      | 22.0   | 187    | 26.0      | 0.0        | 92.8  | 23.7 | 48.1 | 92.7 | 75.1 | 126.4 | 74.7 | 122.29              | 651.35          | 14.41                 | 22.33          |
| 10        | May 13, 2007 16:30:00 | 04:30:00    | 17.8      | 22.5   | 193    | 19.0      | 0.0        | 92.8  | 23.7 | 48.1 | 92.7 | 75.1 | 126.4 | 74.7 | 164.33              | 815.68          | 18.82                 | 29.16          |
| 11        | May 13, 2007 17:00:00 | 05:00:00    | 18.1      | 23.0   | 198    | 12.0      | 0.0        | 92.2  | 10.8 | 28.7 | 92.7 | 75.1 | 126.4 | 74.7 | 147.10              | 962.78          | 18.83                 | 32.06          |
| 12        | May 13, 2007 17:30:00 | 05:30:00    | 17.0      | 25.5   | 209    | 14.5      | 0.0        | 92.2  | 10.8 | 28.7 | 92.7 | 75.1 | 126.4 | 74.7 | 133.76              | 1096.54         | 18.99                 | 34.91          |
| 13        | May 13, 2007 17:45:00 | 05:45:00    | 16.4      | 26.8   | 214    | 15.8      | 0.0        | 92.2  | 10.8 | 28.7 | 92.7 | 75.1 | 126.4 | 74.7 | 65.36               | 1161.90         | 17.72                 | 34.99          |

Figure A2.6. Prometheus Statistics View for fire growth simulation scenario 3.

## Discussion

One potential use of the Prometheus Fire Growth Simulation Model is to verify the recorded weather conditions during the course of the fire. For example, Prometheus was used in a technical fire behavior review (Ember Research Services Ltd. 2008) to help verify that the 10-m open wind speeds recorded at the Sharpsand weather station were not representative of the winds observed during the SAU 13 fire on the afternoon of 13 May 2007. The physical location of the Sharpsand weather station in relation to the edge of the adjacent stand and surrounding vegetation did not conform to published standards (Lawson and Armitage 2008), which would have resulted in recorded wind speeds that were lower than they should have been.

The result of fire growth scenario 1, using the wind speeds recorded at the Sharpsand weather station, confirms the underestimation of 10-m open winds speeds at this weather station. With the recorded wind speeds, the fire was predicted to travel only 2 km between the time of escape (1254 LST) and 1745 LST on the same afternoon. This distance is considerably less than the observed spread distance of 6.5 km during this period.

Fire growth scenario 2 used the winds from the wildfire/prescribed burn forecast issued by OMNR on the morning of 13 May 2007. With these forecasted wind values, Prometheus predicted a spread distance of 4.5 km between 1254 LST and 1745 LST. This spread distance is still 2 km short of the observed spread distance during this period.

One potential explanation for this shorter spread distance is the fact that forecasted winds do not take into account any potential increase in wind speed at ground level due to the interaction between the fire column and the higher wind speeds in the upper atmosphere. To account for the potential increase in wind speeds at ground level due to this fire-atmosphere interaction, a weather patch was applied in fire growth scenario 3 for the period between 1330 and 1530 LST (the time of peak fire behavior). This weather patch increased the forecasted wind speed by 50%. Using the forecasted wind speeds and the weather patch resulted in a predicted spread distance of 6.5 km (Figures A2.5 and A2.6).

## Conclusions

With the Prometheus Fire Growth Simulation Model, it was possible to verify that the recorded wind speeds from the Sharpsand weather station were not representative of the 10-m open wind speeds observed during the fire on the afternoon of 13 May 2007.

Using the forecasted wind speeds instead of the wind speeds recorded by the on-site weather station resulted in a better estimate of the fire spread distance; however, the forecasted winds were also too low to account for the observed fire behavior and the spread distances observed up to 1745 LST on 13 May 2007.

Using a weather patch to estimate the influence of increased wind speeds at ground level due to the interaction between the fire column and the upper atmosphere resulted in a very accurate estimate of spread distance and fire shape from the time of the fire's escape (1254 LST) until 1745 LST, when the first estimated fire perimeter was recorded by the fire boss.

## Literature Cited

- Ember Research Services Ltd. 2008. 2007 Sharpsand prescribed burn – (SAU 13). A technical review of fire behavior factors contributing to the escape. Report submitted to Tim Lynham, Gt. Lakes For. Cent., Can. For. Serv., and Rob McAlpine, For. Fire Manag. Sect., Ont. Minist. Nat. Resour.
- Lawson, B.D.; Armitage, O.B. 2008. Weather guide for the Canadian Forest Fire Danger Rating System. Nat. Resour. Can., Can. For. Serv., North. For. Cent., Edmonton, AB.
- Ontario Ministry of Natural Resources. 2007. Sharpsand prescribed burn plan 2007. Ont. Minist. Nat. Resour., Aviation and For. Fire Manage., Sault-Ste. Marie, ON.
- Stocks, B.J. 1987. Fire behavior in immature jack pine. Can. J. For. Res. 17:80-86.

---

## APPENDIX 3

---

### ORDER AND SET OF PROMETHEUS FIRE GROWTH SIMULATION OPERATIONS



Note: See Appendix 1 for definitions of abbreviations.

**Simulate** {

Loop from simulation start time ( $t_0$ ) to end time ( $t_n$ ) {

For each display timestep ( $t_d$ ) {

Loop {

**Create a new calculation time step**

**Copy existing fires**

**Advance existing fires**

**Track existing fires**

**Untangle fire polygons**

**Add newly igniting fires**

**Resolve overlapping fires**

**Introduce new fire polygon vertices**

**Calculate fire polygon vertex statistics**

} until the calculation time step reaches the display time

}

Display fire perimeters and report statistics as required

}

}

**Create a new calculation time step** {

Start time is the current simulation time

End time is set to the end of the current display time step

For each ignition associated with the scenario {

If ignition time is between the start and end times, then

Set the end time to the ignition time

}

For each grid layer associated with the scenario {

If the grid defines an event between the start and end times, then

Set the end time to be the event time

}

For each weather stream associated with the scenario {

If the stream defines an event between the start and end times, then

Set the end time to be the event time

}

For each geographic vector layer associated with the scenario {

If the geographic vector layer defines an event between the start and end times, then:

tab twice flush with graphic

Set the end time to be the event time

}

If the scenario's burn condition for the simulated day is active, then {

If the burn condition starts between the start and end times, then

Set the end time to be the burn condition start time

If the burn condition ends between the start and end times, then

Set the end time to be the burn condition end time

}

Time step temporal threshold is set to  $t_{\tau_e}$

For each fire currently burning {

If the fire is burning in its acceleration phase, then

Time step temporal threshold is reset to  $t_{\tau_a}$

}

```

    If the time step duration exceeds the time step temporal threshold
      Set the end time so that the time step duration matches the time step
      temporal threshold
    Obtain the vertex with the fastest ROS
    If (ROS * time step duration) is greater than  $\Delta P_{\tau}$ 
      Set the end time so that  $\Delta P_{\tau}$  is not exceeded
  }
Copy existing fires {
  For each fire in the previous calculation time step  $t_{j-1}$ 
    Create a copy of the fire and add it to this calculation time step  $t_j$ 
  }
Advance existing fires {
  For each fire in the time step  $t_j$  {
    For each active (burning) vertex in that fire {
      Calculate a vertex-smoothed ROS based on
        this vertex's ROS
        the smoothing factor ( $\omega$ )
        neighboring vertex ROS values
      Move the vertex based on
        the vertex location
        the vertex-smoothed ROS
        the time step duration
    }
  }
}
Track existing fires {
  For each fire in the time step {
    For each active (burning) vertex in that fire {
      Ray-trace the vertex from its original location to its new location
      If the ray-tracing encounters a non-fuel grid cell, then {
        If breaching is enabled, then {
          Calculate distance travelled in the non-fuel cell(s)
          Calculate maximum distance the vertex can breach
          Determine if breaching can succeed or fail
        }
        If breaching fails or is disabled, then {
          Change the new location to the entry into the non-
            fuel grid cell
          Mark the vertex as inactive
        }
      }
      Ray-trace the vertex from its original location to its new location
      If the ray-tracing encounters a non-fuel grid cell, then {
        If breaching is enabled, then {
          Calculate distance travelled in the non-fuel vector break
          Calculate distance the vertex can breach
          Determine if breaching can succeed or fail
        }
        If breaching fails or is disabled, then {
          Change the new location to the entry into the non-
            fuel vector break
          Mark the vertex as inactive
        }
      }
    }
  }
}

```

```

    }
  }
}
Untangle fire polygons {
  For each fire in the time step  $t_j$  {
    Perform polygon untangling on the polygon fire perimeter
  }
}
Add newly igniting fires {
  For each ignition in the scenario {
    If the ignition is not already marked as burning, then
      If the ignition time occurs within the range of this time step, then
        If the ignition is not completely contained in another fire, or in a non-
        fuel area, then
          Introduce the ignition as a newly burning fire
  }
}
Resolve overlapping fires {
  For each fire( $i$ ) in the time step  $t_j$  {
    For each fire( $j$ ) in the time step  $t_j$  {
      If fire( $i$ ) overlaps with fire( $j$ ), then
        If fire( $i$ ) is smaller in area than fire( $j$ ), then {
          Remove the overlapping area from fire( $i$ )
          Mark the vertices on the shared perimeter of fire( $i$ )
          and fire( $j$ ) as inactive
        }
    }
  }
}
Introduce new fire polygon vertices {
  For each fire in the time step {
    For each active (burning) vertex in that fire {
      Calculate the  $\beta_j^i$ 
      Calculate the  $L_j^i$ 
      If a new point should be added, based on  $L_{\tau}$ ,  $L_j^i$ , and  $\beta_j^i$ , then {
        Introduce a new vertex at the midpoint of the edge
        Mark the vertex as active
      }
      Calculate  $L_j^{i+1}$ 
      If a new point should be added, based on  $L_{\tau}$ ,  $L_j^{i+1}$ , and  $\beta_j^i$ , then {
        Introduce a new vertex at the midpoint of the edge
        Mark the vertex as active
      }
    }
  }
}
Calculate fire polygon vertex statistics {
  For each fire in the time step {
    For each active (burning) vertex in that fire {
      Retrieve fuel data for the grid cell containing the vertex
    }
  }
}

```

```

If the vertex is in a nonfuel grid cell, then
  Mark the vertex as inactive
Else {
  Retrieve elevation and slope data
  Adjust the characteristics based on any fuel grid attribute
  layers (PC, PDF, etc.)
  Calculate FMC
  FMC may be provided as a scenario default, or a project
  default, or calculated from fuel type, time, location, and
  elevation.
  Retrieve weather data
  If the burning period settings will allow burning, then {
    Calculate FBP ROS values
    (RSS, ROS, ROSi, FRSS, FROS, FROSi, BRSS, BROS, BROSi,
    WSV, RAZ)
    Calculate partial differential equation values using
    ROSi, FROS, BROSi as inputs
    Partial different equations may be either two-dimensional or
    three-dimensional, depending on user selection
    Calculate CFB, CFC, SFC, TFC, FI statistics using
    partial differential equation output values
  }
}
}
}
}
}
}
}

```